1988

Experimental Studies in Dynamic and Elastic-Plastic Fracture

Himanshu Nigam
University of Rhode Island

EXPERIMENTAL STUDIES IN DYNAMIC AND ELASTIC-PLASTIC FRACTURE

BY

HIMANSHU NIGAM

A DISSERTATION SUBMITTED IN PARTIAL FULFILLMENT OF THE REQUIREMENT FOR THE DEGREE OF DOCTOR OF PHILOSOPHY IN MECHANICAL ENGINEERING AND APPLIED MECHANICS

UNIVERSITY OF RHODE ISLAND

1988

DOCTOR OF PHILOSOPHY DISSERTATION

OF

HIMANSHU NIGAM

APPROVED:

Dissertation Committee

Major Professor Arun Shukla

Thomas J. Kim

M.H. Sadd

Richard Bowman

Dean of Graduate School

UNIVERSITY OF RHODE ISLAND

1988

To my Parents

ABSTRACT

Dynamic fracture experiments have been conducted on a polymeric material Homalite-100 and heat treated 4340 steel and 7075-T6 aluminum using various specimen geometries. The experimental techniques of caustics, photoelasticity and strain gages have been used to evaluate the stress intensity factor describing the near tip stress field surrounding the dynamically moving crack. The data has been used to characterize dynamic fracture behavior of brittle and ductile materials as a stress intensity factor vs crack velocity relationship.

The results obtained from the three techniques used have been critically compared and the validity of each technique is discussed under the experimental conditions studied. Results show that the techniques of caustics in transmission when compared with photoelasticity under dynamic conditions give lower values for the stress intensity factor. For opaque materials the results from the three techniques compare well.

A direct method of evaluating J-integral in power law hardening materials using strain gages has been developed. The use of this new technique is demonstrated by obtaining an engineering estimate of the HRR singularity field size in annealed 4340 steel specimens.

ACKNOWLEDGEMENTS

I would like to express my thanks and appreciation for my advisor, Dr. Arun Shukla, for all the ideas he gave me at times when I got stuck and for helping me in every way throughout the course of this research.

I am thankful to my committee members, Prof. Thomas J. Kim, Prof. Martin H. Sadd and Prof. Richard Brown, who provided whatever help I needed. I am grateful to Dr. Ravindra Chona for his help in the analysis of the photoelastic data. I thank my fellow graduate students Rakesh Agarwal, Changyi Zhu, Vikas Prakash and Xu Yi in the photomechanics laboratory for their assistance in performing the experiments. The help of department staff Everett Cook, M. Merrill and Jim Byrnes in the project is acknowledged.

The work was supported by funds from the National Science Foundation under Grant No. MSM-8719567 and MEA-8415494 at the University of Rhode Island. I am grateful to the University of Rhode Island for awarding me the U.R.I. Graduate Fellowship.

Special thanks to the members of my family who have always provided what it takes to keep me going.

TABLE OF CONTENTS

LIST OF TABLES

LIST OF FIGURES

LIST OF BASIC SYMBOLS

Symbol	Name
a	crack length
K_I^d	Dynamic mode I stress intensity factor
$\dot{a}$	crack tip velocity
h	specimen thickness
σ_o	remote parallel stress
E	Modulus of elasticity
ν	Poisson's ratio
c_1	p wave speed
c_2	s wave speed
n	index of refraction
c	stress optic coefficient
f_σ	stress fringe value
r_o	initial curve radius
D	caustic diameter
z_o	distance to reference plane
σ, τ	stress components
N	fringe order
ϵ_g	strain along gage axis
K_{IC}^d	critical fracture toughness
K_{Ia}^d	crack arrest toughness
J	J integral value

CHAPTER 1

INTRODUCTION

The behavior of a dynamically moving crack is governed by the stress field surrounding it. A moving crack is considered dynamic when the inertial and strain rate effects have significant influence on the stress field. Such is considered the case when the crack speed is of the order of wave speed in the media. For linear-elastic, homogeneous materials it is possible to represent the stress field in the vicinity of a moving crack tip by a single parameter K_I^d, the dynamic stress intensity factor [1.1]. All the stresses in the singularity dominated zone[1.2] are proportional to the stress intensity factor. The singularity zone excludes a very small non-linear region at the crack tip itself.

It is believed by some investigators that the dynamic fracture toughness of a material can be characterized by a relationship between the stress intensity factor and the crack tip velocity i.e. such a relationship is unique for a material and can be treated as a material property[1.3,1.4]. Thus the measurement of stress intensity factor and crack velocity are of vital importance in the study of the fracture behavior of materials and in the establishment of a fracture criteria.

There are many techniques currently being used to estimate the value of stress intensity factor. Among these techniques are included the experimental methods of photoelasticity[1.5,1.6], caustics[1.7,1.8] and strain gages[1.9,1.10] and numerical method of finite elements[1.11,1.12].

In contrast, for power-law hardening materials the stress intensity factor is not a valid parameter to describe the state of stress around the crack tip because there is significant amount of non-linearity and plastic deformation. Hutchinson, Rice and

Rosengren[1.13,1.14] suggested the existence of HRR singularity the intensity of which is governed by the value of the J integral evaluated around the crack tip. Thus the measurement of J has the same importance for power law hardening materials as the measurement of stress intensity factor has for linear elastic materials.

A considerable amount of stress field data has been generated from various experimental techniques over the years but the results have never been critically compared. In recent years, there has been some controversy over the results obtained by different researchers using the techniques of caustics and photoelasticity. In particular, the results using photoelasticity[1.15] show that the relationship between the crack tip stress intensity factor and the crack tip velocity is unique for a given material in low velocity regions whereas the results from caustics[1.16] show no such relationship. This has lead the researcher to question the accuracy of the results obtained using different methods.

In this research the technique of caustics and photoelasticity have been used to evaluate stress intensity factor in a polyester material Homalite-100. The results from the two techniques are compared with each other to look for any discrepancies in the techniques. Next, heat treated 4340 steel specimens have been tested using the technique of caustics and strain gages. The stress intensity factor values are evaluated and compared for different methods.

The analysis technique is developed to use strain gages for the evaluation of J integral value in power-law hardening materials. This technique is then used to determine J in 4340 steel specimens. Also the region of validity of HRR field is investigated.

Figure 1.1 shows schematically the various studies conducted in this research and how they relate with each other. Chapter two reviews the past work done in development of the three techniques used in this work. Review of work done in dynamic fracture of metals and non-metals, in $K_I^d - \dot{a}$ characterization and in the

study of power law hardening materials are given in the appropriate chapters. In chapter three the details of analysis used for these methods are provided. Next two chapters give the experimental procedure and results of dynamic stress intensity factor evaluation in polyester and metals respectively. Stress intensity factor and crack tip velocity data is analyzed in the light of $K_I^d - \dot{a}$ relationship in chapter six. Studies related to J integral evaluation in power law hardening materials are discussed in chapter seven.

REFERENCES:

[1.1] Irwin,G.R., "Series Representation of the Stress Field Around Constant Speed Cracks," Univ. of Maryland Lecture Notes, 1980.

[1.2] Chona,R., Irwin,G.R. and Sanford,R.J., "Influence of Specimen Size and Shape on the Singularity-Dominated Zone," Fracture Mechanics: Fourteenth Symposium, vol. 1: Theory and Analysis, ASTM STP 791, J.C.Lewis and G.Sines eds., ASTM, 1983, pp. I-3-I-23.

[1.3] Irwin,G.R., Dally,J.W, Kobayashi,T., Fourney,W.L., Etheridge,M.J. and Rossmanith,H.P., "On he Determination of the $\dot{a}$ -K Relationship for Birefringent Polymers," Experimental Mechanics, vol. 19, No. 4, April 1979, pp. 121-128.

[1.4] Irwin,G.R., Dally,J.W. and Fourney,W.L., "On the Uniqueness of the Stress Intensity Factor-Crack Velocity Relationship," International Journal of Fracture, 27, 1985, pp. 159-168.

[1.5] Dally,J.W., "Dynamic Photoelastic Studies of Fracture," Experimental Mechanics, vol. 19, No. 10, October 1979. pp. 349-361.

[1.6] Bradley,W.B. and Kobayashi,A.S., "An Investigation of Propagating Crack by Dynamic Photoelasticity," Experimental Mechanics, 10(3), 1970, pp. 106-113.

[1.7] Beinert,J. and Kalthoff,J.F., "Experimental determination of dynamic stress intensity factors by shadow patterns," Mechanics of Fracture, vol. VII, G.C.Sih, ed., Noordhoff Int. Publishing, London, The Netherlands, 1981.

[1.8] Theocaris,P.S., "Elastic Stress Intensity Factors Evaluated by Caustics," Mechanics of Fracture, vol. VII, G.C.Sih, ed., Noordhoff Int. Publishing, London, The Netherlands, 1981.

[1.9] Dally,J.W. and Sanford,R.J., "Strain Gage Methods for Measuring the Opening Mode Stress Intensity Factor," SEM Spring Conference Proceedings 1985, Las Vegas, pp. 851-860.

[1.10] Dally,J.W. and Berger,J.R., "A Strain Gage Method for Determining KI and KII in a Mixed Mode Stress Field," Proceedings of the 1986 SEM Spring Conference on Experimental Mechanics, New Orleans, June 8-13, 1986, pp. 603-612.

[1.11] Atluri,S.N. and Nishioka,T., "Numerical Studies in Dynamic Fracture Mechanics," International Journal of Fracture, vol. 27, 1985, pp. 245-261.

[1.12] Nishioka,T., and Atluri,S.N., "Path Independent Integrals, Energy Release Rates, and General Solutions of Near Tip Fields in Mixed Mode Dynamic Fracture Mechanics," Engr. Frac. Mech., Vol. 18, No. 1, 1983, pp. 1-22.

[1.13] Hutchinson,J.W., "Singular Behavior at the End of a Tensile Crack in a Hardening Material," J Mech. Phys. Solids, vol. 16, 1968, pp. 13-31.

[1.14] Rice,J.R. and Rosengren,G.F., "Plane Strain Deformation Near a Crack Tip in a Power Law Hardening Material," J of the Mech. and Phy. of Solids, vol. 16, 1968, pp. 1-12.

[1.15] Dally,J.W., Kobayashi,T. and Fourney,W.L., "Influences of Specimen Geometry on Crack Propagation and Arrest Behavior," VIth International Conference of Experimental Stress Analysis, Society for Experimental Stress Analysis, Munich, West Germany, September 1978, pp. 18-22.

[1.16] Kalthoff,J.F., "On some Current problems in Experimental Fracture Dynamics," Workshop on Dynamic Fracture, Caltech, Feb. 11-25, 1983.

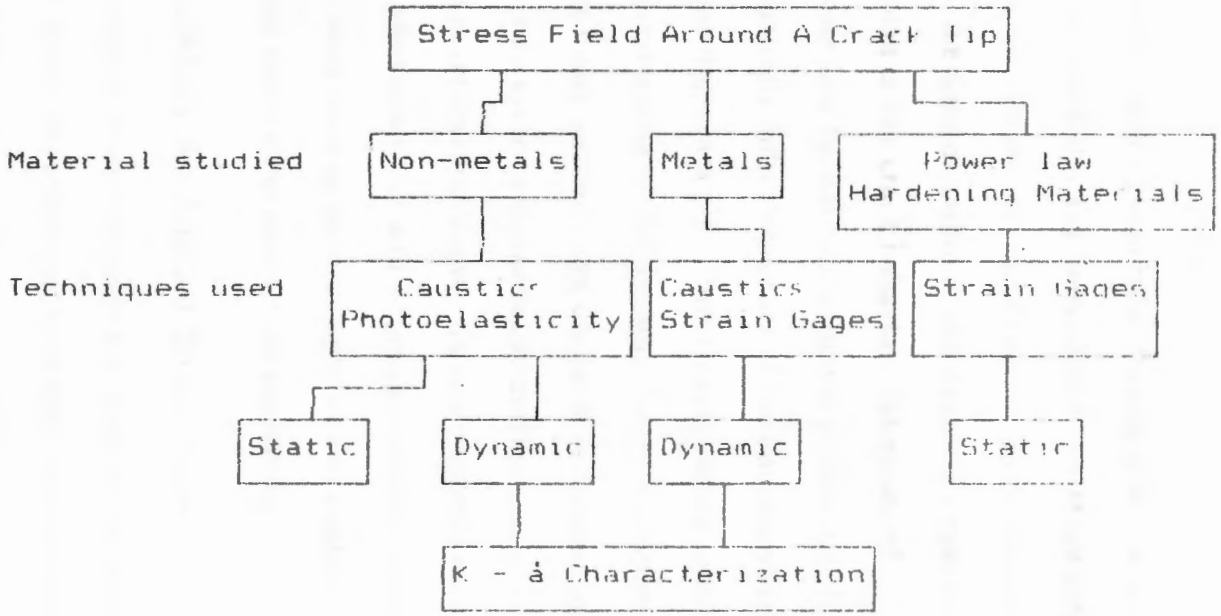

Figure 1.1 Correlation of the various aspects studied.

CHAPTER 2

REVIEW OF PAST WORK IN THE THREE TECHNIQUES

The behavior of a dynamically moving crack is governed by the stress field surrounding the crack tip. For linear-elastic materials the stress field near a moving crack tip can be defined by the dynamic stress intensity factor K_I^d. It is thus believed that the determination of the dynamic stress intensity factor would assist in the prediction of the crack behavior. Estimates of K_I^d can be made on a totally theoretical basis only for extremely simple geometries. In finite bodies the problem becomes analytically difficult because of the boundary reflected stress waves coming back to the moving crack tip. Direct experimental observations are necessary for complete understanding of the dynamic fracture process.

There are many methods now available to an experimentalist for evaluating the stress intensity factor for a dynamically moving crack. These methods include both optical and non-optical techniques. In this research work the optical techniques of caustics and photoelasticity and a non-optical technique of strain gages have been used. Recent work done in the development and analysis of these is discussed below in light of their application to fracture mechanics.

2.1 Photoelasticity As Applied To Fracture:

The method of photoelasticity has been in use for almost 20 years by many investigators. Many improvements have been incorporated in the analysis technique to allow full field evaluation of the stresses around the crack tip.

The application of photoelasticity to fracture mechanics was first demonstrated by Post[2.1] and Wells and Post[2.2] and in the discussion of the latter paper by Irwin[2.3]. Irwin showed that for the mode$-I$ conditions the stress intensity factor

could be determined from a single isochromatic fringe loop at the crack tip. The accuracy of his method is very sensitive to the precision of locating points on the fringe[2.4].

Bradley and Kobayashi [2.5] and Schroedl and Smith[2.6] modified his approach and employed a differencing technique to obtain K_I and σ_{ox}. Etheridge and Dally [2.7] introduced a third parameter into the analysis by modifying the Westergaard stress function to more closely account for stress field variations near the crack tip. These methods are based on measurements taken from specific points and there is no way to minimize the errors.

Sanford and Dally[2.8] suggested a multi-point method which uses more number of data points from the fringe pattern than the number of unknowns to be determined. Their technique uses the method of least squares coupled with Newton-Raphson method to minimize error in obtaining the solution. It is global in nature and the use of full field data permits a significant improvement in the accuracy of determining the stress field coefficients.

C.W.Smith and his associates[2.9] have applied stress freezing photoelastic techniques to determine the stress intensity factor for a number of three dimensional crack problems. A.S.Kobayashi and his associates[2.10] have used dynamic photoelasticity to study the stress field around a propagating crack. They have also developed hybrid techniques to solve fracture mechanics problems by combining photoelasticity with numerical methods.

J.W.Dally and his associates [2.11] have employed photoelasticity to study the range of dynamic fracture behaviors from crack initiation and propagation to crack arrest and crack branching. They have also employed photoelasticity to study crack-wave interaction problems in rock mechanics applications. Kobayashi and Dally[2.12] have demonstrated successful use of photoelastic coatings on metals using diffused light setups.

2.2 Caustics As Applied To Fracture:

The method of caustics, developed by Manogg[2.13] is in current use by many researchers[2.14-2.16]. The great advantage of this method over other experimental techniques is that it provides a direct measure of the crack tip stress field and the corresponding crack speed without concern for the geometry of the specimen, the boundary conditions or the complex stress wave pattern in the bulk of the specimen. This technique gives the first term of the series representing the stress field around the crack tip which is related to the stress intensity factor.

Theocaris and co-workers[2.17] generalized the method of caustics to non-transparent materials by using reflection and applied it to fracture problems of general interest in various branches of engineering science. Theocaris and Gdoutos [2.18] applied this method to examine the deformation fields near the tips of stationary crack in metal plates. Kalthoff and his associates[2.15,2.19] in Germany have also employed caustics to study dynamic fracture in both transparent as well as opaque materials.

Kalthoff et al.[2.20] introduced an approximate correction factor to account for the error introduced by assuming static local field in data analysis. The exact equations of the caustic envelope formed by the reflection of parallel incident light from the surface of the specimen containing a rapidly growing crack were obtained by Rosakis[2.21] for mixed mode plane stress crack growth. It was found that, for some typical laboratory materials used in crack propagation studies, the neglect of the influence of inertia on the crack tip stress field could lead to errors of up to 30-40 percent in the value of the elastic stress intensity factor evaluated from the measured caustic diameter.

Rossmanith[2.22] included the higher order terms of the Westergaard type stress functions and discussed their effect on the shape and extension of the highly constrained zone surrounding a crack tip. For a singular solution it was found that

the K_I^d values associated with larger shadow spots are lower than their static counterparts. Higher order terms induce a generalized evaluation formula for the stress intensity factor where powers of the order $n + 5/2(n = 0, 1, ...)$ of the caustic diameter appear. The dynamic correction is negligible for small and moderate crack velocities justifying the use of static equations for practical purposes.

In a detailed report on crack tip stress state, Rosakis and Ravi Chander[2.23] discussed the effect of three dimensional stress state on the evaluated results which are based on two dimensional analysis. They tried to identify the regions in which local experimental measurements based on two dimensional theory can be performed with confidence. They concluded that the three dimensional nature of the crack tip field scales with thickness. Extremely small plane strain region exists around the crack tip.

Rosakis with Freund[2.24] also studied the effect of the crack tip plasticity on the determination of dynamic stress intensity factors and found that the error introduced by neglecting plasticity in the analysis of data are small as long as the distance from the crack tip to the initial curve ahead of the tip is more than about twice the plastic zone size. They also found that the error introduced by neglecting inertial effects are small as long as the crack speed is less than about 20 percent of the longitudinal wave speed.

Effect of higher order stress terms on mode$-I$ caustics in birefringent materials has been recently studied by Phillips and Sanford[2.25]. They developed a theory to determine the sizes, shapes and location of the double caustics produced in statically loaded birefringent plates containing mode$-I$ cracks. It was found that the transverse diameters of the inner and outer parts of the double caustic have an average value essentially equal to the transverse diameter of the single caustic produced by optically isotropic material having the same optical constant. They also observed that with the superposition of a constant tensile or compressive stress

parallel to the crack, each part of the double caustic deforms independently but in such a way as to maintain this average transverse diameter.

More recently, Ravi Chander and Knauss[2.26-2.28] have used the technique of caustics to investigate dynamic fracture in a birefringent polyester material, Homalite-100, which was also used extensively by both Kobayashi and Dally with photoelasticity. The use of the method of caustics has recently been extended to the study of elastic-plastic fracture of power law hardening materials[2.16].

2.3 Strain Gages As Applied To Fracture:

Electrical resistance strain gage technique suggested by Irwin[2.29] in 1957 for the evaluation of stress intensity factor, is one of the lesser used methods for fracture studies. The primary hesitation in the use of resistance strain gages for fracture studies was their finite size. Since the crack tip strain field has steep gradients the averaging effects can be large if the strain gages are not small enough. With the use of extremely small strain gages of sizes less than a millimeter square, it is possible to accurately measure strains at any point.

Dally and Sanford[2.30] demonstrated the evaluation of stress intensity factor using strain gages under static loading. Further, Dally and Berger[2.31] have used the technique to evaluate stress intensity factor in 6061-T6 aluminum for stationary cracks.

In a recent paper Shukla et al.[2.32] have shown the applicability of strain gages to the study of dynamic fracture of a polyester material Homalite 100. The effect of various parameters on the accuracy and applicability of results is studied in detail. In this work the applicability of strain gages is extended to power law hardening materials.

References:

[2.1] Post,D., "Photoelastic Stress Analysis for an Edge Crack in a Tensile Field,"

Proceedings of SESA, 12(1), 1954, pp. 99-116.

[2.2] Wells,A. and Post,D, "The Dynamic Stress Distribution Surrounding a Running Crack- A Photoelastic Analysis," Proc. of SESA, 16(1), 1958, pp. 69-92.

[2.3] Irwin,G.R., "Discussion of Wells and Post Paper (in Proceedings of SESA, 16(1))," Proceedings of SESA, 16(1), 1958, pp. 93-96.

[2.4] Etheridge,J.M. and Dally,J.W., "A Critical Review of Methods for Determining Stress Intensity Factors from Isochromatic Fringes," Experimental Mechanics, 17(7), 1977, pp. 248-254.

[2.5] Bradley,W.B. and Kobayashi,A.S., "An Investigation of Propagating Crack by Dynamic Photoelasticity," Experimental Mechanics, 10(3), 1970, pp. 106-113.

[2.6] Schroedl,M.A. and Smith,C.W., "Local Stresses near Deep Surface Flaws Under Cylindrical Bending Fields," Progress in Flaw Growth and Fracture Toughness Testing, ASTM STP 536, 1973, pp.45-63.

[2.7] Etheridge,J.M. and Dally,J.W., "A Three Parameter Method for Determining Stress Intensity Factor from Isochromatic Fringe Loops," Journal Strain Analysis, 13(2), 1978, pp. 91-94.

[2.8] Sanford,R.J. and Dally,J.W., "A General Method for Determining Mixed-mode Stress Intensity Factor from Isochromatic Fringe Patterns, Journal of Engineering Fracture Mechanics, 11, 1979, pp. 621-633.

[2.9] Schroedl,M.A., McGowen,J.J. and Smith,C.W., "Assessment of Factors Influencing Data Obtained by the Photoelastic Stress Freezing Technique for Stress Fields Near Crack Tips," J. of Engr. Fract. Mech., 4(4), 801-809, 1972.

[2.10] Kobayashi,A.S., Wade,B.G. and Bradley, W.B., "Fracture Dynamics of Homalite 100," Deformation and Fracture of High Polymers, H.H.Kausch, J.A.Hassell and R.I.Jaffee, eds., Plenum Press, New York, 487-500, 1973.

[2.11] Kobayashi, T. and Dally,J.W., "The Relation Between Crack Velocity and the Stress Intensity Factor in Birefringent Polymers," ASTM STP 627, 257-273

(1977).

[2.12] Kobayashi,T., and Dally,J.W., "Dynamic Photoelastic Determination of the $\dot{a}-K$ Relation for 4340 Alloy Steel," Crack Arrest Methodology and Applications, ASTM STP 711, G.T.Hahn and M.F.Kanninen, Eds., American Society for Testing Materials, 1980, pp. 189-210.

[2.13] Manogg,P., "Investigation of the rupture of a Plexiglas Plate by means of an Optical Method Involving High-speed Filming of the Shadows Originating Around Holes Drilling in the Plate," Int. J Frac. Mech., 2, 1966, pp. 604-613.

[2.14] Theocaris,P.S., "Caustics for the Determination of Singularities in Cracked Plates," Proceedings of IUT Symposium on Optical Methods in Mechanics of Solids, Univ. of Poitires, (1979).

[2.15] Beinert,J. and Kalthoff,J.F., "Experimental determination of dynamic stress intensity factors by shadow patterns," Mechanics of Fracture, vol. VII, G.C.Sih, ed., Noordhoff Int. Publishing, London, The Netherlands, 1981.

[2.16] Rosakis,A.J., Ma,C.C. and Freund,L.B., "Analysis of the Optical Shadow Spot Method for a Tensile Crack in a Power-Law Hardening Material," Journal of Applied Mechanics, vol. 105, December 1983, pp. 777-782.

[2.17] Theocaris,P.S. and Gdoutos,E., "An optical Method for Determining Opening Mode and Edge Sliding Mode Stress Intensity Factors," Journal of Applied Mechanics, Vol. 39, No. 1, March 1972, 91-97.

[2.18] Theocaris,P.S. and Gdoutos,E.E., "The Modified Dugdale-Barenblatt Model Adapted to Various Fracture Configurations in Metals," International Journal of Fracture, vol. 10, 1974, pp. 549-564.

[2.19] Kalthoff,J.F., "Stress Intensity Factor Determination by Caustics," Intl. Conf. Experimental Mechanics, Society for Exptl. Stress Analysis and Japan Society of Mech. Engrs., Honolulu, Hawaii, USA, May 23-28, 1982.

[2.20] Kalthoff,J.F., Beinert,J. and Winkler,S., "Influence of Dynamic Effects on

Crack Arrest," EPRI 1022-1, First Semi-annual Progress Report, Report V9/78, Institut fur Festkopermechanik, Freiburg, Germany, Aug (1978).

[2.21] Rosakis,A.J., "Analysis of the Optical Method of Caustics for Dynamic Crack Propagation," Report ONR-79-1 Division of Engineering Brown Univ., Mar.1979, Engineering Fracture Mechanics, vol.13, 1980, pp. 331-347.

[2.22] Rossmanith, H.P., "General Mode - I Caustic Evaluation for Optically Anisotropic Materials," Ingenieur-Archiv, 50(1981), pp. 73-83.

[2.23] Rosakis,A.J. and Ravi Chander,K., "On Crack Tip Stress State: An Experimental Evaluation of Three Dimensional Effects," Caltech Report, SM84-2, March 1984.

[2.24] Rosakis,A.J. and Freund,L.B., "The Effect of Crack Tip Plasticity on the Determination of Dynamic Stress Intensity Factors by the Optical Method of Caustics," Trans. ASME, J Appl. Mech., vol. 48, June 1981, pp. 302-308.

[2.25] Phillips,J.W. and Sanford,R.J., "Effect of Higher-order Stress Terms on Mode-1 Caustics in Birefringent Materials," Special Technical Publication 743, ASTM.

[2.26] Ravi-Chander,K. and Knauss,W.G., "An Experimental Investigation into Dynamic Fracture: I Crack Initiation and Arrest," International Journal of Fracture, 25, 1984, 247-262.

[2.27] Ravi-Chander,K. and Knauss,W.G., "An Experimental Investigation into Dynamic Fracture: III On Steady-State Crack Propagation and Crack Branching," International Journal of Fracture, 26, 1984, 141-154.

[2.28] Ravi-Chander,K. and Knauss,W.G., "An Experimental Investigation into Dynamic Fracture: IV On the Interaction of Stress Waves with propagating Cracks," International Journal of Fracture, 26, 1984, 189-200.

[2.29] Irwin,G.R., "Analysis of Stresses and Strains Near the End of a Crack Traversing a Plate," Journal of Applied Mechanics, vol. 24, No. 3, 1957.

[2.30] Dally,J.W. and Sanford,R.J., "Strain Gage Methods for Measuring the Opening

Mode Stress Intensity Factor," SEM Spring Conference Proceedings 1985, Las Vegas, pp. 851-860.

[2.31] Dally,J.W. and Berger,J.R., "A Strain Gage Method for Determining KI and KII in a Mixed Mode Stress Field," Proceedings of the 1986 SEM Spring Conference on Experimental Mechanics, New Orleans, June 8-13, 1986, pp. 603-612.

[2.32] Shukla,A., Chona,R., and Agarwal,R.K., "Investigation of Dynamic Fracture Using Strain Gages," Soc. Exptl. Mech., Fall meeting, Houston 1987.

CHAPTER 3

METHOD OF ANALYSIS

In this research three different experimental techniques have been used for obtaining the stress field data around the dynamically moving crack tip. The techniques are **a:** The method of photoelasticity **b:** The method of caustics and **c:** The method of strain gages.

A detailed review of the past work done in the development and use of the three techniques was given in chapter 2. The three techniques depend on different phenomenon to extract the information regarding the stress field. The method of photoelasticity depends on the change in the optical properties of the birefringent material. The method of caustics is primarily based on the out of plane displacements caused by the existing stresses. In contrast, the strain gages measure the in plane strains on the surface of the material being studied. Hence, the three techniques are very different in their analysis procedure and it is of extreme importance to understand the underlying assumptions and derivations to be able to interpret the results correctly.

3.1 Method Of Photoelasticity:

When circularly polarized light passes through a stressed birefringent material and then through a circular analyzer, an optical interference pattern of light is produced. These bands are referred to as the isochromatic fringes. These fringes are lines of constant maximum in-plane shear stress and are related to the fringe order by the stress optic law, namely

$$2\tau_m = \sigma_1 - \sigma_2 = \frac{N f_\sigma}{h} \tag{3.1}$$

where σ_1 and σ_2 are the in-plane principal stresses, τ_m is the maximum in-plane shear stress, N is the fringe order, f_σ is the material fringe value and h is the thickness of the material[3.1]. The isochromatic fringe pattern which is obtained can then be used in combination with the appropriate stress field model to obtain the parameters of interest. The optical setup used is shown in figure(3.1) and a typical isochromatic fringe pattern is shown in figure(3.2).

The cartesian stress components for a constant speed crack propagating in a finite body can be expressed as[3.2,3.3]

$$\begin{aligned}
\sigma_{xx} &= \Omega\Big[(1+2\alpha_1^2-\alpha_2^2)ReZ_1 - \Omega_1 ReZ_2 + (1+2\alpha_1^2-\alpha_2^2)ReY_1 \\
&\qquad - (1+\alpha_2^2)ReY_2\Big] \\
\sigma_{yy} &= \Omega\Big[-(1+\alpha_2^2)ReZ_1 + \Omega_1 ReZ_2 - (1+\alpha_2^2)ReY_1 \\
&\qquad + (1+\alpha_2^2)ReY_2\Big] \\
\tau_{xy} &= \Omega\Big[-2\alpha_1 ImZ_1 + 2\alpha_1 ImZ_2 - 2\alpha_1 ImY_1 + \Omega_2 ImY_2\Big]
\end{aligned} \tag{3.2 - 3.4}$$

where,

$$\begin{aligned}
\Omega &= \frac{(1+\alpha_2^2)}{(4\alpha_1\alpha_2 - (1+\alpha_2^2)^2)} \\
\Omega_1 &= \frac{4\alpha_1\alpha_2}{(1+\alpha_2^2)} \\
\Omega_2 &= \frac{(1+\alpha_2^2)^2}{2\alpha_2}
\end{aligned} \tag{3.5}$$

$$Z_1 = \sum_{n=0}^{\infty} A_n z_1^{n-1/2} \qquad Z_2 = \sum_{n=0}^{\infty} A_n z_2^{n-1/2} \tag{3.6}$$

$$Y_1 = \sum_{m=0}^{\infty} B_m z_1^m \qquad Y_2 = \sum_{m=0}^{\infty} B_m z_2^m \tag{3.7}$$

$$z_1 = x + i\alpha_1 y \qquad z_2 = x + i\alpha_2 y \tag{3.8}$$

$$\begin{aligned} \alpha_1^2 &= 1 - \left[\frac{\dot{a}}{c_1}\right]^2 \\ \alpha_2^2 &= 1 - \left[\frac{\dot{a}}{c_2}\right]^2 \end{aligned} \tag{3.9}$$

where $\dot{a}$ is the crack velocity, c_1 is the longitudinal wave speed and c_2 is the shear wave speed in the material. The crack tip coordinates, x and y, are oriented such that the negative branch of the x-axis coincides with the crack faces (see fig3.3), and A_n , B_m are unknown real coefficients to be determined for the problem of interest.

A_o is related to K_I by the relation $K_I = A_o\sqrt{2\pi}$. Equations (3.2)-(3.4) can be combined with (3.1) to relate the fringe order and position coordinates at any point in the isochromatic field with the unknown real coefficients A_n and B_m through the stress transformation expression

$$\left(\frac{N f_\sigma}{2h}\right)^2 = \tau_m^2 = \frac{(\sigma_{yy} - \sigma_{xx})^2}{4} + \tau_{xy}^2 \tag{3.10}$$

The first step in the analysis of an isochromatic fringe pattern obtained experimentally is to take a region around the crack tip from the experimental pattern being analyzed, extract a large number of individual data points, generally 40-60 points, and determine the coordinates and fringe order at each point. These data points are then used as inputs to an over-deterministic system of non-linear equations of the form of equation (3.10) and solved in a least-squares sense for the unknown coefficients by the method of Sanford and Dally[3.4]. It should be noted that the region surrounding the crack tip for which data points would lie less than one-half the plate thickness away from the crack tip is likely to be strongly influenced by triaxial and nonlinear effects, and should therefore be avoided. Once the

coefficients are determined the complete stress and strain field around the crack tip is established.

When analyzing dynamic stress patterns, the data acquisition region is usually restricted to that portion of the stress pattern which can be seen to translate with moderate changes in the pattern because of the constant crack-speed assumption in the analytical representation being used. The number of coefficients necessary for an adequate representation of the stress field over the data acquisition region is estimated by examining the average fringe order error, the values of the leading coefficients and the reconstructed fringe patterns corresponding to a given set of coefficients[3.5].

It is seen that as the number of parameters increases the average fringe order error generally falls but it does not necessarily mean that the solution is approaching the actual stress field. As can be seen in fig(3.4), the average fringe order error $n(\%)$ falls from 5.8% for two parameter analysis to 2.3% for six parameter analysis but the reconstructed fringe pattern from a six parameter analysis does not match with the actual experimental pattern. Thus it is important to look at both the fringe order error as well as the fringe replot before deciding on a solution. In general it is found that three to five parameters are sufficient to represent the stress field surrounding the crack tip but when the crack is close to the boundary up to 10 parameters are required to get a satisfactory reconstructed fringe pattern. Hence no set rule can be provided as to how many parameters are sufficient. The choice is dependent on the location of the crack tip with respect to the boundary among other factors.

3.2 Method Of Caustics:

Unlike the method of photoelasticity, which is based on the interference of light, the method of caustics is based on geometric optics governed by Fermat's principle. When a material with a crack in it is loaded in tension, the high stresses near the

crack tip cause the deformation of the body leading to a non-uniform change in the optical path length of the light transmitted through it, or reflected from its surface. For an opaque material the change in optical path is due to non-uniform changes in thickness of the body and for transparent material there is an additional contribution due to changes in the refractive index of the material.

If light from a point source falls on the crack tip region, the image of the crack tip on a reference plane appears as a dark spot surrounded by a bright curve, called the caustic curve. An experimentally obtained shadow pattern is shown in figure(3.5).

To determine the stress intensity factor K_I^d from the experimentally obtained diameter of the caustic, consider an initially planar body lying in the x, y plane at $z = 0$. Consider light falling normally on the surface $z = -f(x, y)$ of the opaque material as illustrated in figure(3.6). Let a reference plane (screen) be located behind the reflecting surface at $z = -z_o$. An incident light ray falling at a point $p(x, y)$ denoted by $\vec{x}$ of the reflecting surface will be projected to point $P(X, Y)$ denoted by $\vec{X}$. The mapping of points $p(x, y)$ of the body surface on to points $P(X, Y)$ of the reference plane is given by the following expression[3.6].

$$\vec{X} = \vec{x} - 2(z_o - f) \cdot \left[\frac{\vec{\nabla} f}{1 - (\vec{\nabla} f)^2} \right] \tag{3.11}$$

The choice of the sign of z_o depends on whether the image is real or virtual.

The optical arrangements used in this study are shown in figure(3.7a,b). The light from the point source was collected by the concave mirror and focused on the 20-lens camera. The specimen was placed in the path of the light between the concave mirror and the camera, and the camera was focused at the reference plane, located at a distance z_o from the specimen, as shown. For transparent material the image is real (fig3.7a) and z_o is negative. For opaque materials the image on the reference plane is virtual i.e. z_o is positive (fig3.7b). When $z_o \gg f$, as is usually

the case, the above relationship simplifies to

$$\vec{X} = \vec{x} - 2z_o\vec{\nabla}f \tag{3.12}$$

The deformed shape of the specimen surface reflects the light in such a way that the virtual extension of reflected light rays forms an envelope in space as illustrated in fig(3.6). This surface, called the caustic surface, is the locus of points of maximum luminosity. The intersection of the caustic surface with the reference plane is called the caustic curve. The caustic exists if and only if the Jacobian determinant J of the mapping[3.6] vanishes, i.e.,

$$J(x, y, z_o) = det\left[\frac{X_i}{x_i}\right] = 0 \tag{3.13}$$

The locus of points on the specimen surface for which $J = 0$ is called the initial curve, the points of which map onto the caustic. All points inside and outside the initial curve map outside the caustic. Since the light from the initial curve is mapped on the caustic the interpretation of the results will depend on the location of the initial curve. It should be noted that the initial curve position is dependent on the experimental setup parameter z_o and hence can be varied by varying z_o.

The shape of the caustic will depend on the out of plane displacement of the specimen which in turn depends on the stress field given by equations (3.2-3.4). In caustic analysis only the first term of the Z_1 series is used. The stress field equations thus simplify to:

$$\begin{aligned}
\sigma_{xx} &= \frac{K_I}{\sqrt{2\pi}}\Omega\left[(1 + 2\alpha_1^2 + \alpha_2^2)\cdot\frac{1}{\sqrt{r_1}}\cdot\cos(\frac{\phi_1}{2}) - \Omega_1\cdot\frac{1}{\sqrt{r_2}}\cdot\cos(\frac{\phi_2}{2})\right] \\
\sigma_{yy} &= \frac{K_I}{\sqrt{2\pi}}\Omega\left[-(1 + \alpha_2^2)\cdot\frac{1}{\sqrt{r_1}}\cdot\cos(\frac{\phi_1}{2}) + \Omega_1\cdot\frac{1}{\sqrt{r_2}}\cdot\cos(\frac{\phi_2}{2})\right] \qquad (3.14 - 3.16) \\
\tau_{xy} &= \frac{K_I}{\sqrt{2\pi}}\Omega\left[2\alpha_1\left(\frac{1}{\sqrt{r_1}}\cdot\sin(\frac{\phi_1}{2}) - \frac{1}{\sqrt{r_2}}\cdot\sin(\frac{\phi_2}{2})\right)\right]
\end{aligned}$$

The out of plane displacement is given by the following relationship:

$$z = -\frac{\nu h}{E}(\sigma_1 + \sigma_2) = -\frac{\nu h}{E}(\sigma_{xx} + \sigma_{yy}) \tag{3.17}$$

combining equations (3.14)-(3.16) with the above equation gives:

$$z = \frac{\nu h}{E} \cdot \frac{K_I^d}{\sqrt{2\pi r_1}} \cdot \cos\frac{\theta_1}{2} \cdot \frac{1}{F(\dot{a})} \tag{3.18}$$

with

$$F(\dot{a}) = \frac{4\alpha_1\alpha_2 - (1+\alpha_2^2)^2}{(1+\alpha_2^2)(\alpha_1^2 - \alpha_2^2)}$$

Substituting equation (3.18) into equations (3.12) and (3.13) one can determine the shape of the caustic and can obtain the expression defining the relationship between the stress intensity factor K_I^d, and the caustic diameter D,

$$K_I^d = \frac{2\sqrt{2\pi}}{3f^{5/2}z_o ch} \cdot F(\dot{a}) \cdot C(\alpha_1) \cdot D^{5/2} \tag{3.19}$$

where $f = 3.17$ and $c = \nu/E$ for opaque materials and the expression for C is given as:

$$C(\alpha_1) = \frac{(6.8 + 14.4\alpha_1 - 2.6\alpha_1^2)}{18.6} \tag{3.20}$$

For anisotropic transparent materials the equation is very similar and takes into account the optical path length changes due to refractive index gradients:

$$K_I^d = \frac{2\sqrt{2\pi}}{3f_{o,i}^{5/2}z_o ch} \cdot F'_{o,i} \cdot F(\dot{a}) \cdot C(\alpha_1) \cdot D_{o,i}^{5/2} \tag{3.21}$$

where the subscripts o, i refer to the outer and inner caustics that are obtained for materials which display significant optical anisotropy. $F'_{o,i}$, the additional correction factor is very close to 1.0 for Homalite 100[3.7]. The initial curve is very nearly circular and its size is closely approximated by[3.7]

$$r_o = \left[\frac{3}{2\sqrt{2\pi}} K_I^d ch z_o\right]^{5/2} \cdot F(\dot{a})^{-2/5} \tag{3.22}$$

It should be noted that the term $F(\dot{a})$ only accounts for the in-plane inertia effects caused by the dynamic nature of the problem. Out of plane inertia effects, which influence the surface displacements and hence the caustic evaluation, are not accounted for in the correction factor.

Since the intensity of light is a maximum at the boundary of the caustic[3.8], the measurement of the diameter should be made at a point where the steepest gradient in the light intensity is observed. Some investigators [3.8,3.9] measure the diameter at the outer edges of the shadow spot where as others [3.7] contend that because of diffraction effects and because of an imperfect point light source the boundary is not defined properly and the use of the surrounding bright rim for measurement purposes gives more accurate values. The difference in the two diameters is about 5%, which can in turn lead to difference of about 13% in the calculated stress intensity factor values. In this work the diameter of the caustic has been taken as the diameter of the dark spot.

The caustic is a mapping of points on the initial curve on the specimen. It is thus important to know the radius, r_o, of the initial curve. It has been demonstrated here and also in [3.10] that if r_o is not large enough in comparison to the thickness of the specimen, three dimensional effects in the vicinity of the crack tip can produce significant errors. Since r_o depends on z_o and K_I^d (equation 3.22) its value can be adjusted appropriately.

Figure(3.8) shows the effect of the initial curve size on the stress intensity factor. K_I/K_{th} is plotted as a function of r_o/h. It is seen that when r_o is less than 0.4 the thickness, the stress intensity factor value calculated is influenced by the three dimensional effects existing close to the crack tip. Hence all the data should be taken from outside this region.

The anisotropy parameter [3.7], which determines the splitting of the caustic into an inner and an outer one, depends on the birefringence of the material and also on its elastic constants. For Homalite-100 the elastic and optical constants combine to give a small amount of separation of the two caustics, which is largely masked by the blurring of the caustic boundary[3.11]. The outer caustic, where it is visible is not very well defined at the points of measurement. Hence, the inner caustic, with a relatively well defined boundary, has been used throughout this work.

3.3 Strain Gage Analysis:

The analysis of the strain gage data involves the evaluation of the stress intensity factor from the strain profiles recorded by each gage. The experimental setup used for recording the strain profiles from six strain gages placed along the crack propagation path is shown in figure(3.9). Using the dynamic stress field representation given by equations (3.2)-(3.4) dynamic strain field representation can be derived in a rotated coordinate system by using Hooke's law and appropriate transformation laws[3.12].

Two coordinate frames are introduced G_{xGyG} and L_{xLyL}, as shown in Fig(3.10). The rotated coordinate system G_{xGyG} is fixed to the strain gage and orients itself with it. The coordinate system L_{xLyL} is fixed to the model and is located right below the strain gage on the crack propagation path. In this coordinate frame the crack tip position x_L will be given. The strain gage is considered to be located at an arbitrary point, $G(x, y)$ which is coincident with the strain gage grid center, and rotated at an angle with respect to coordinate system, O_{xy}. The strain at point G can be determined from the complex strain transformation equation

$$(\epsilon_{yG} - \epsilon_{xG}) + i\gamma_{xGyG} = (\epsilon_{yy} - \epsilon_{xx} + i\gamma_{xy})e^{2i\alpha} \tag{3.23}$$

and the first strain invariant

$$\epsilon_{xG} + \epsilon_{yG} = \epsilon_x + \epsilon_y \tag{3.24}$$

Using Hooke's law along with eq.(3.23) and eq.(3.24), we get

$$\begin{aligned} 2\epsilon_{xG} = \frac{1}{E}\big[&(1-\nu)(\sigma_y + \sigma_x) - (1+\nu)(\sigma_y - \sigma_x)\cos(2\alpha) \\ &+ 2(1+\nu)\tau_{xy}\sin(2\alpha)\big] \end{aligned} \tag{3.25}$$

Substituting eq.(3.2), eq.(3.3) and eq.(3.4) into eq.(3.25) leads to

$$\begin{aligned} \epsilon_{xG} = \Omega\frac{(1+\nu)}{E}\big[&\frac{(1-\nu)}{(1+\nu)} \cdot (\alpha_1^2 - \alpha_2^2)(ReZ_1(z_1) + ReY_1(z_1)) \\ &+ (1+\alpha_1^2)(ReZ_1(z_1) + ReY_1(z_1))\cos(2\alpha) \\ &- \Omega_1 ReZ_2(z_2)\cos(2\alpha) - (1+\alpha_2^2)ReY_2(z_2)\cos(2\alpha) \\ &- (1+\alpha_2^2)ReY_2(z_2)\cos(2\alpha) \\ &+ 2\alpha_1(ImZ_2(z_2) - ImZ_1(z_1) - ImY_1(z_1))\sin(2\alpha) \\ &+ \Omega_2 ImY_2(z_2)\sin(2\alpha)\big] \end{aligned} \tag{3.26}$$

Also the strain in the y_G direction is obtained by replacing α by $\alpha + 90^\circ$ in equation (3.26)

$$\epsilon_{yG} = \epsilon_{xG}(\alpha + 90^\circ) \tag{3.27}$$

Setting $n = 0$ and $m = 0$ in eq.(3.6) and eq.(3.7) and substituting them in eq.(3.26) yields a two parameter representation of the strain field

$$
\begin{aligned}
\epsilon_{xG} = \Omega\frac{(1+\nu)}{E}\Big[A_o\Big[\frac{(1-\nu)}{(1+\nu)}(\alpha_1^2-\alpha_2^2)\frac{1}{\sqrt{r_1}}\cos(\frac{\phi_1}{2}) \\
+ (1+\alpha_1^2)\frac{1}{\sqrt{r_1}}\cos(\frac{\phi_1}{2})\cos(2\alpha) \\
- \Omega_1\frac{1}{\sqrt{r_2}}\cos(\frac{\phi_2}{2})\cos(2\alpha) \\
+ 2\alpha_1\sin(2\alpha)\Big(\frac{1}{\sqrt{r_1}}\sin(\frac{\phi_1}{2}) \\
- \frac{1}{\sqrt{r_2}}\sin(\frac{\phi_2}{2})\Big)\Big] \\
+ B_o\Big[(\alpha_1^2-\alpha_2^2)(\frac{(1-\nu)}{(1+\nu)}+\cos(2\alpha))\Big]\Big]
\end{aligned}
\tag{3.28}
$$

Inspection of eq.(3.28) suggests that the contribution of B_o term can be set to zero if[3.13]

$$
\cos(2\alpha) = -\left(\frac{1-\nu}{1+\nu}\right) \tag{3.29}
$$

For a range of values of Poisson's ratio, ν, the angles, α, which remove the contribution of B_o term are shown in Fig(3.11). Note for 4340 steel which has a Poisson's ratio ν, of 0.3 the corresponding α is 118.7° and for 7075 aluminum having Poisson's ratio 1/3, it is 120.0°. Accordingly, the strain gages were placed at orientation angle, α, equal to 118.7° and 120.0° on steel and aluminum specimens respectively.

Theoretical strain at orientation, $\alpha = 118.7°$ for steel, ϵ_G^S, and $\alpha = 120°$ for aluminum, ϵ_G^A, evaluated using eq.(3.28) are plotted as a function of the crack tip position, x_L, in Fig(3.12). The plots show that the peak strain for these orientations for steel and aluminum occur when the crack tip is right below the strain gage, i.e., x_L is equal to zero. Assuring, that the strain gage grid lies inside the K_I^d dominated zone, K_I^d can be evaluated from the peak strain recorded by a strain gage knowing that the crack tip is located right below the strain gage grid at that instant. A detailed study of the effect of strain gage grid size, orientation etc. can be found in

reference[3.14].

Using peak strain from the dynamic strain profile leads to ($\theta = \phi 1 = \phi 2 = 90°$ and $\rho 1 = \rho 2 = y = h_g$) where h_g is the height of the strain gage above the crack propagation path. Substituting these values in eq.(3.28) and using the relation $K_I^d = A_o\sqrt{2\pi}$ yields peak strain, $(\epsilon_{xG})^P$, as a function of K_I^d

$$(\epsilon_{xG})^P = K_I^d \Omega \frac{(1+\nu)}{2E} \frac{1}{\sqrt{h_g}} \left[\frac{(1-\nu)}{(1+\nu)} (\alpha_1^2 - \alpha_2^2) + \cos(2\alpha) \left((1+\alpha_1^2) - \Omega_1 \right) \right] \quad (3.30)$$

Knowing peak strain from the strain profile, $(\epsilon_{xG})^P$, the crack velocity, $\dot{a}$, and measuring the gage orientation, α, and the gage height, h_g, the value of the stress intensity factor, K_I^d is evaluated.

References:

[3.1] Dally,J.W. and Riley,W.F., Experimental Stress Analysis, Mc Graw- Hill, (1978).

[3.2] Irwin,G.R., "Series Representation of the Stress Field Around Constant Speed Cracks," Univ. of Maryland Lecture Notes, 1980.

[3.3] Nishioka,T., and Atluri,S.N., "Path Independent Integrals, Energy Release Rates, and General Solutions of Near Tip Fields in Mixed Mode Dynamic Fracture Mechanics," Engineering Fracture Mechanics, Vol. 18, No. 1, 1983, pp. 1-22.

[3.4] Sanford,R.J. and Dally,J.W., "A General Method for Determining Mixed-mode Stress Intensity Factor from Isochromatic Fringe Patterns, Journal of Engineering Fracture Mechanics, 11, 1979, pp. 621-633.

[3.5] Chona,R., Irwin,G.R. and Sanford,R.J., "Influence of Specimen Size and Shape on the Singularity-Dominated Zone," Fracture Mechanics: Fourteenth Symposium, vol. 1: Theory and Analysis, ASTM STP 791, J.C.Lewis and G.Sines eds., ASTM, 1983, pp. I-3-I-23.

[3.6] Rosakis,A.J., and Aehnder,A.T., "On the Method of Caustics: An Exact Analysis Based on Geometrical Optics," Journal of Elasticity, vol. 15, 1985, pp. 347-367.

[3.7] Beinert,J. and Kalthoff,J.F., "Experimental determination of dynamic stress intensity factors by shadow patterns," Mechanics of Fracture, vol. VII, G.C.Sih, ed., Noordhoff Int. Publishing, London, The Netherlands, 1981.

[3.8] Rosakis,A.J., "Experimental Determination of the Fracture Initiation and Dynamic Crack Propagation Resistance of Structural Steels by the Optical Method of Caustics," PhD Thesis, Brown University, June 1982.

[3.9] Ravi-Chander,K. and Knauss,W.G., "An Experimental Investigation into Dynamic Fracture: III On Steady-State Crack Propagation and Crack Branching," International Journal of Fracture, 26, 1984, 141-154.

[3.10] Rosakis,A.J. and Ravi Chander,K., "On Crack Tip Stress State: An Experimental Evaluation of Three Dimensional Effects," Caltech Report, SM84-2, March 1984.

[3.11] Ravi-Chandar,K., "An Experimental Investigation into the Mechanics of Dynamic Fracture," PhD Thesis, California Institute of Technology, 1982.

[3.12] Shukla,A., Agarwal,R.K. and Nigam,H., "Dynamic Fracture Studies on 7075-T6 Aluminum and 4340 Steel Using Strain Gages and Photoelastic Coatings," Submitted for Publication.

[3.13] Dally,J.W. and Sanford,R.J., "Strain Gage Methods for Measuring the Opening Mode Stress Intensity Factor," SEM Spring Conference Proceedings 1985, Las Vegas, pp. 851-860.

[3.14] Shukla,A., Chona,R., and Agarwal,R.K., "Investigation of Dynamic Fracture Using Strain Gages," Society for Experimental Mechanics, Fall meeting, Houston 1987.

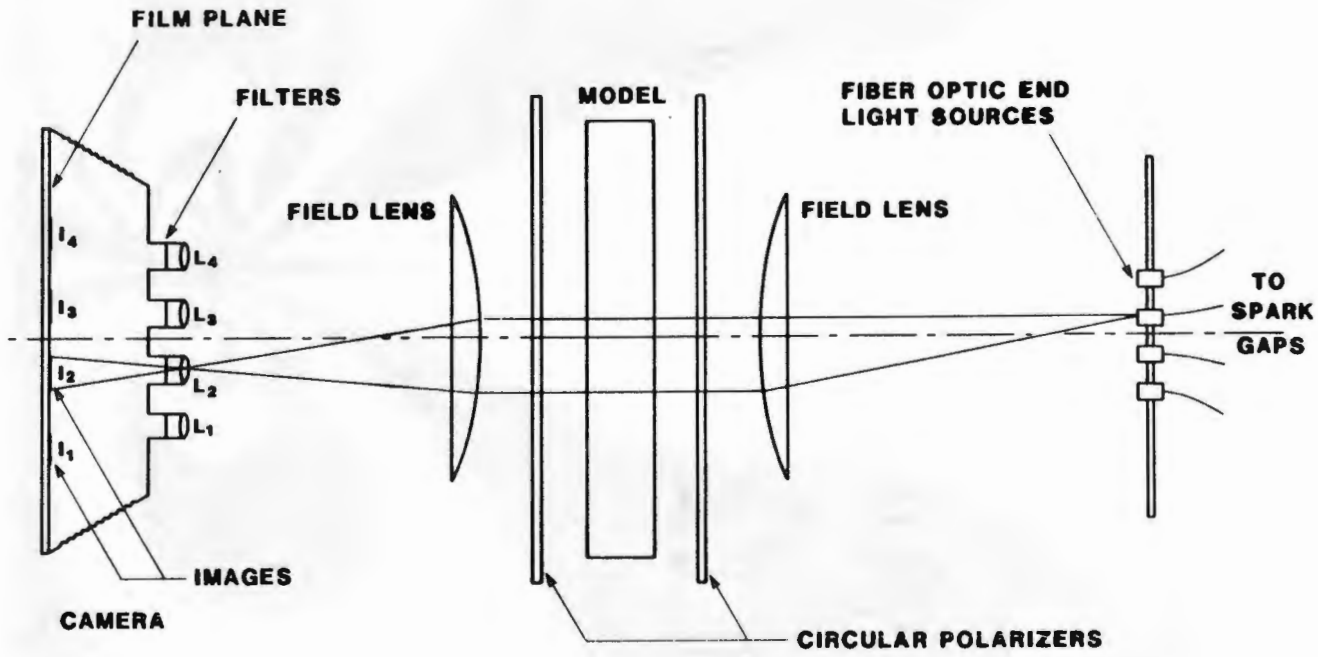

Figure 3.1 Optical arrangement of the camera for obtaining isochromatics.

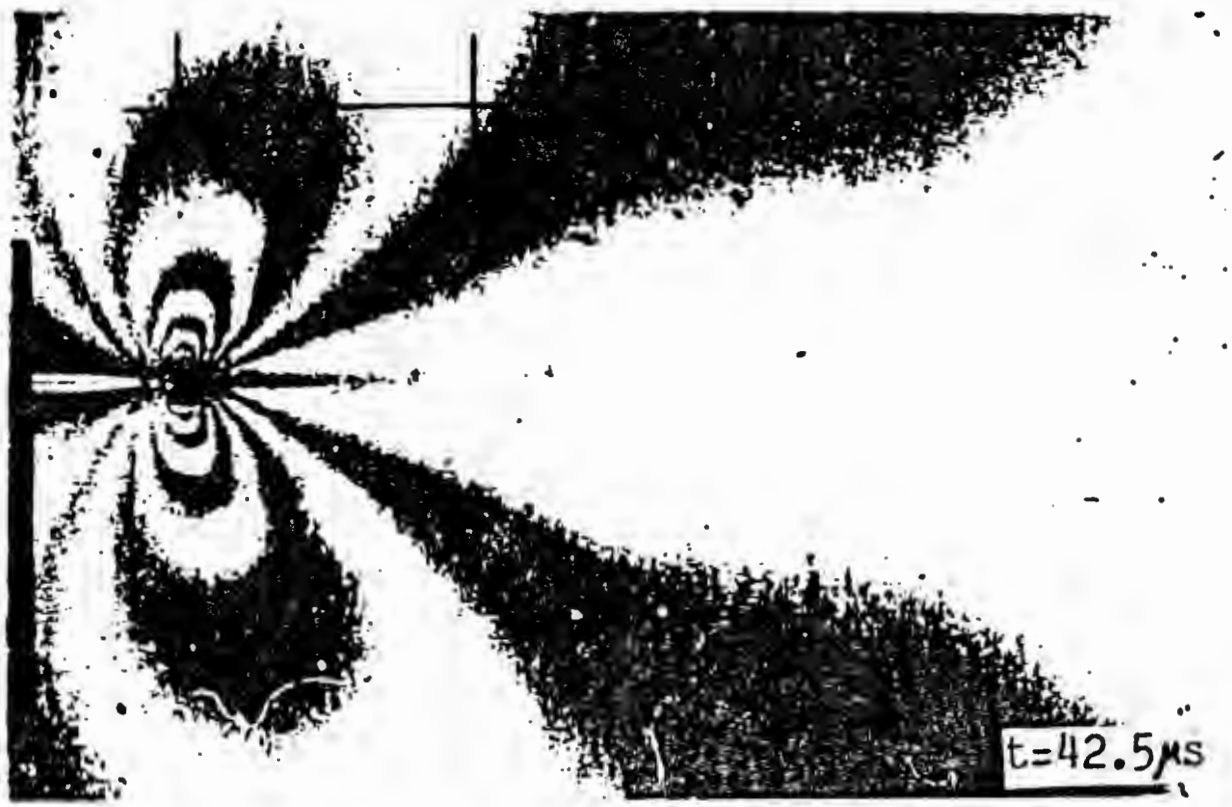

Figure 3.2 Typical photoelastic pattern around a crack tip.

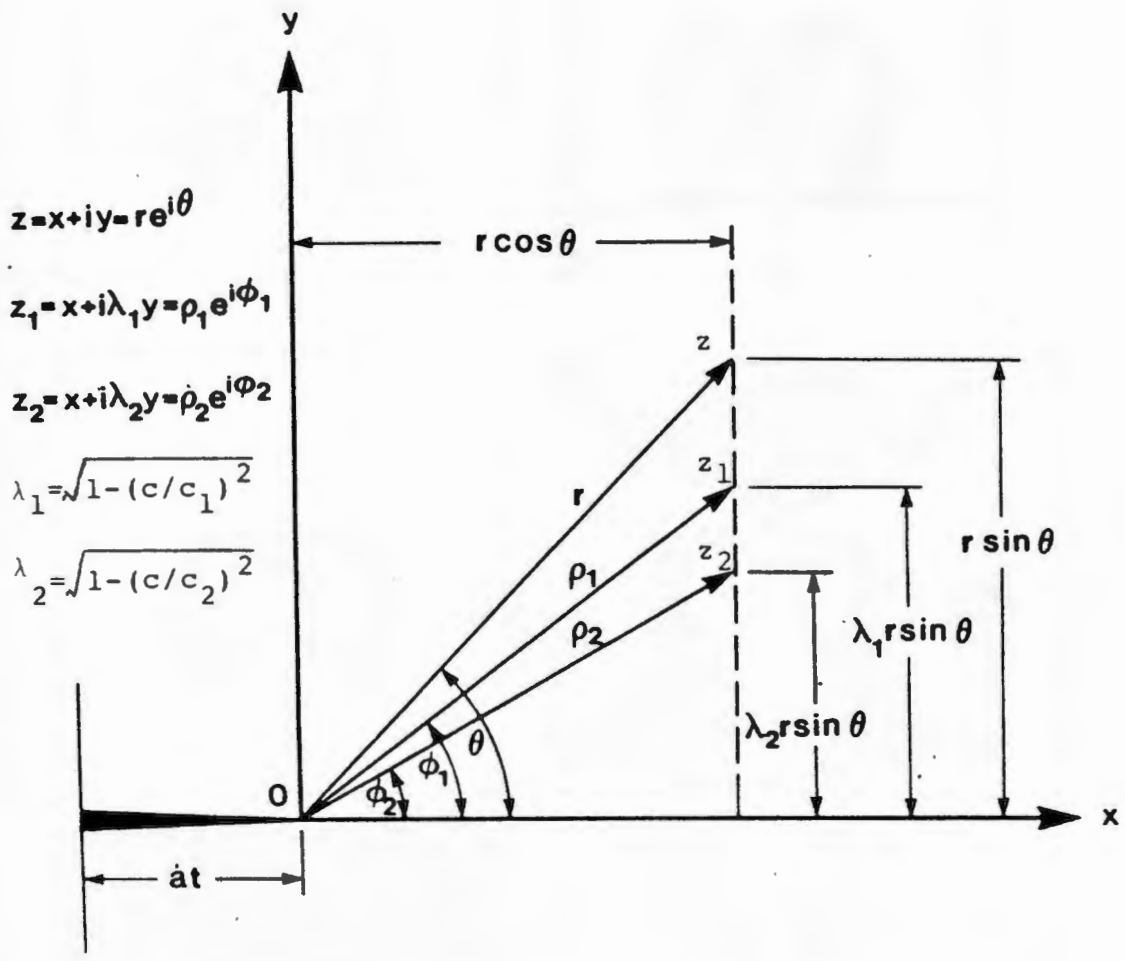

Figure 3.3 Coordinate systems and transformation relations used for constant crack speed analysis.

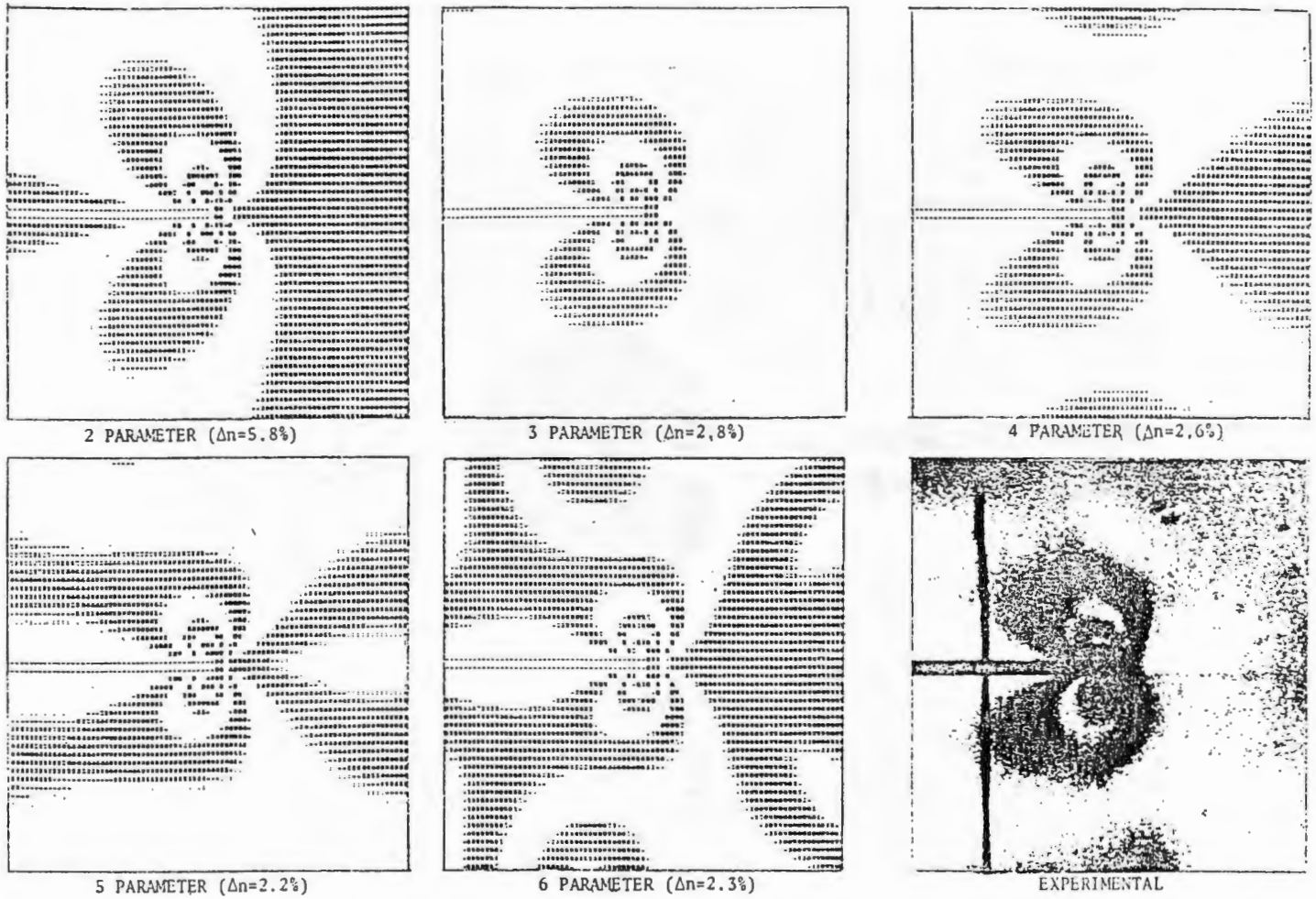

Figure 3.4 Reconstructed fringe patterns as obtained by different number of parameters and the actual pattern for a frame in DCB experiment.

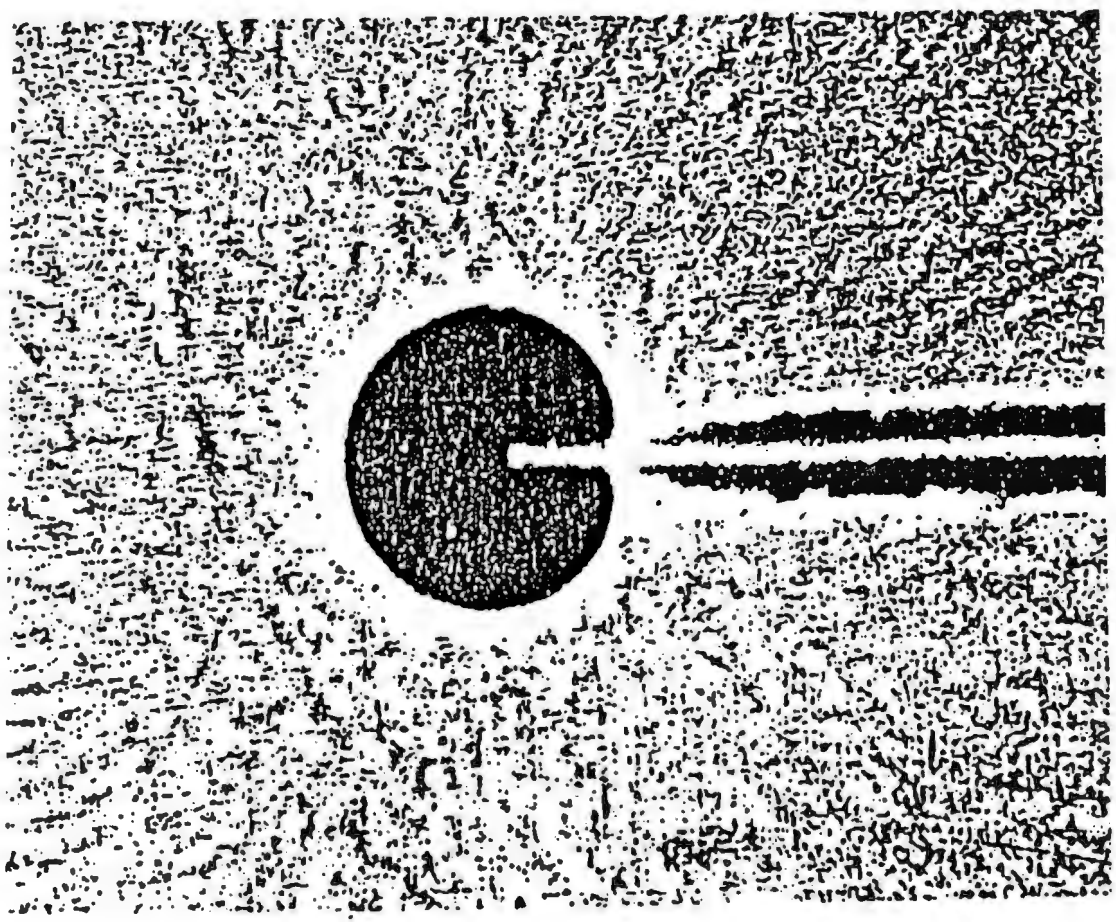

Figure 3.5 Typical caustic obtained for stress field around a crack tip.

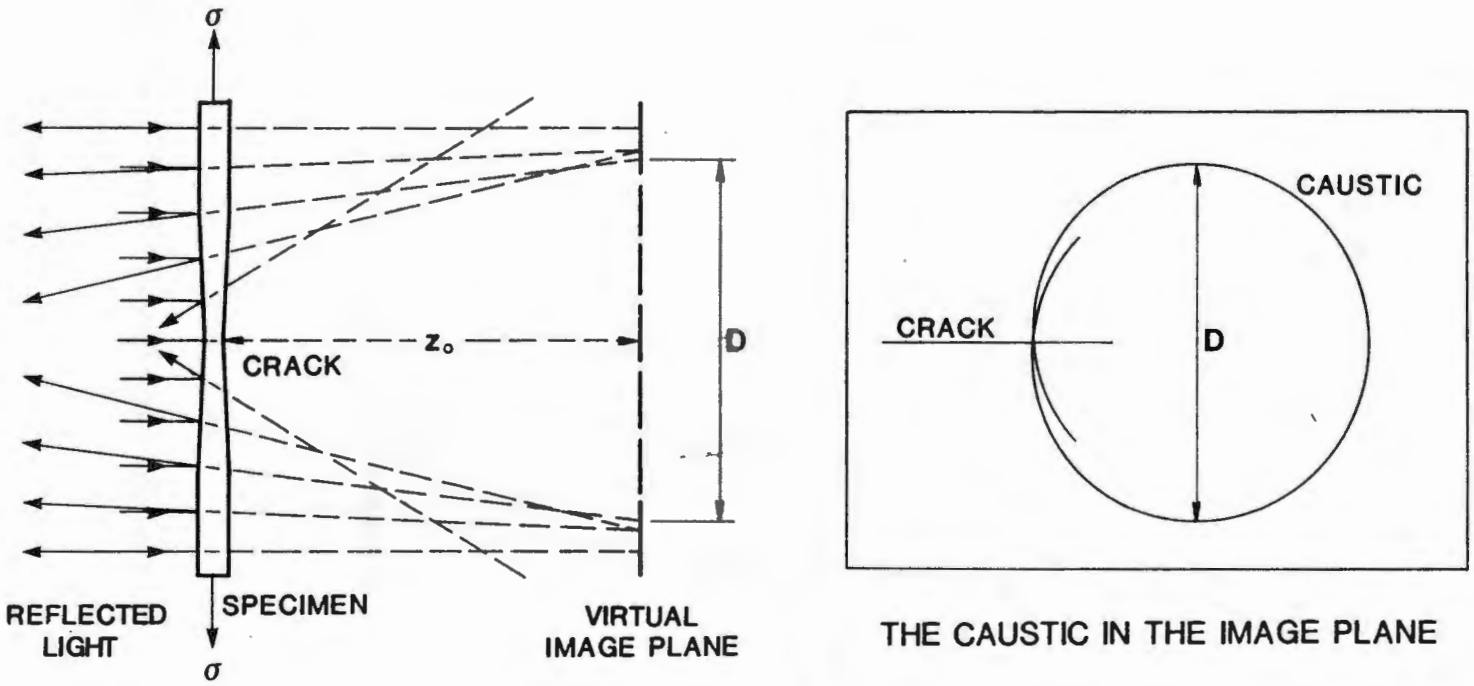

Figure 3.6 Formation of caustic due to reflection of light from the polished, deformed specimen surface near the crack tip.

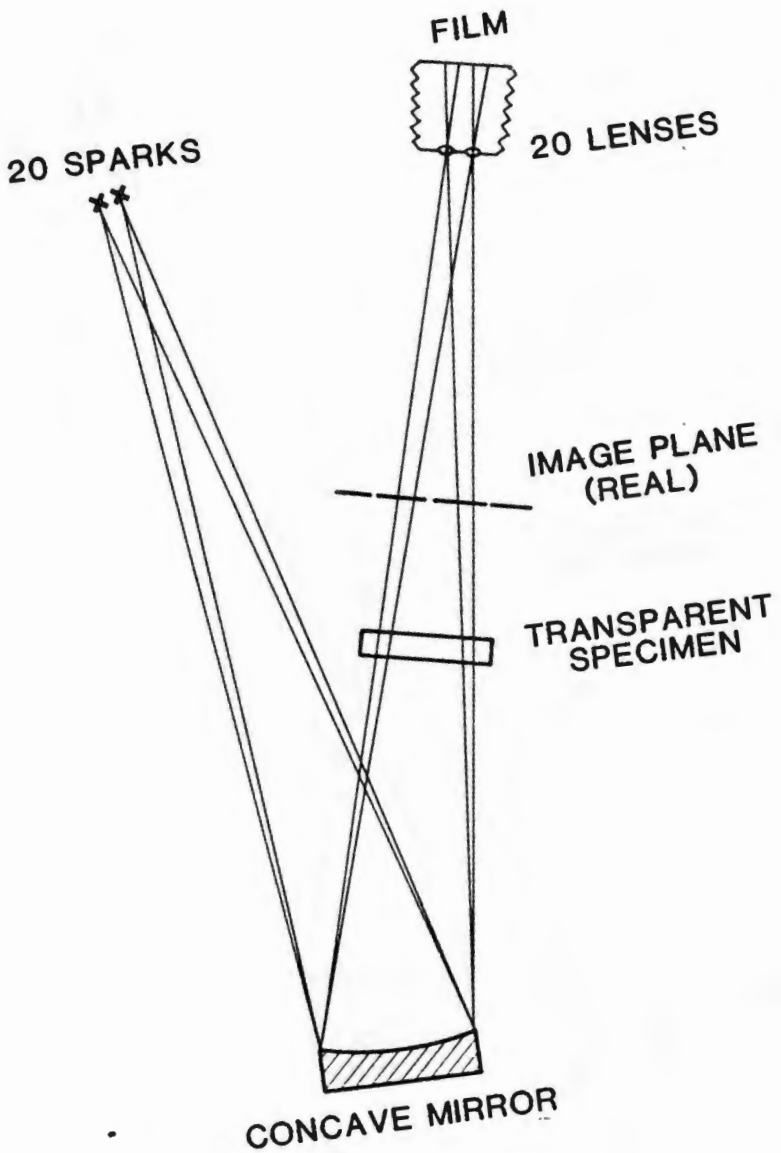

Figure 3.7a Optical setup for the method of caustic used in transmission mode.

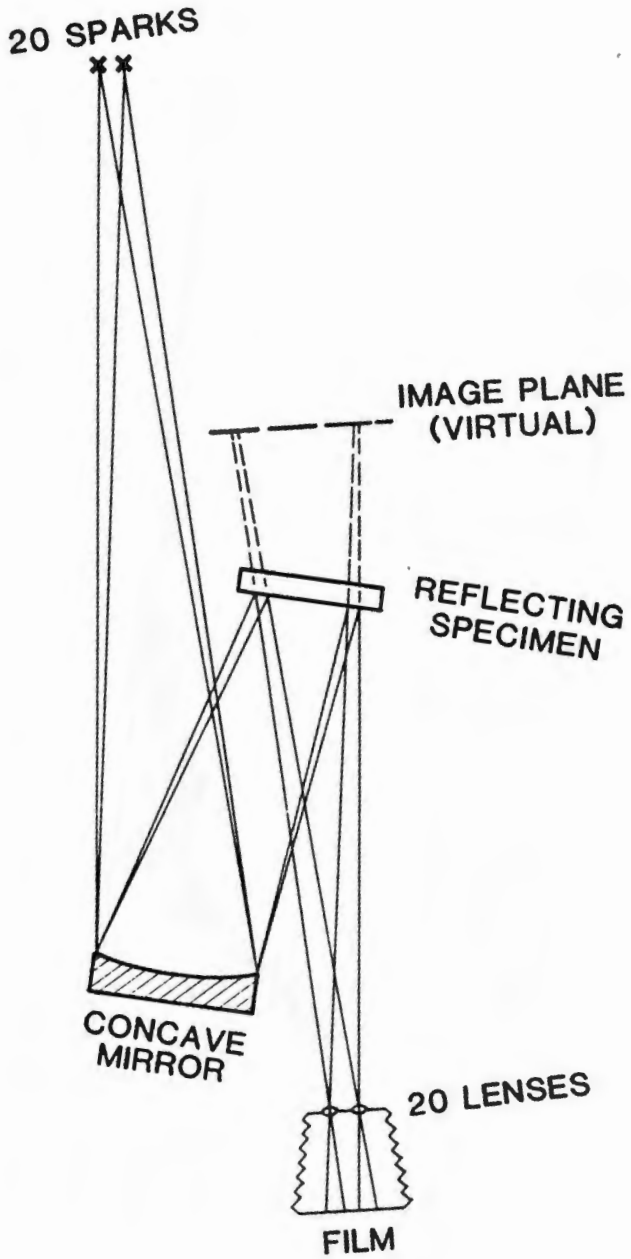

Figure 3.7b Optical setup for the method of caustic used in reflection mode.

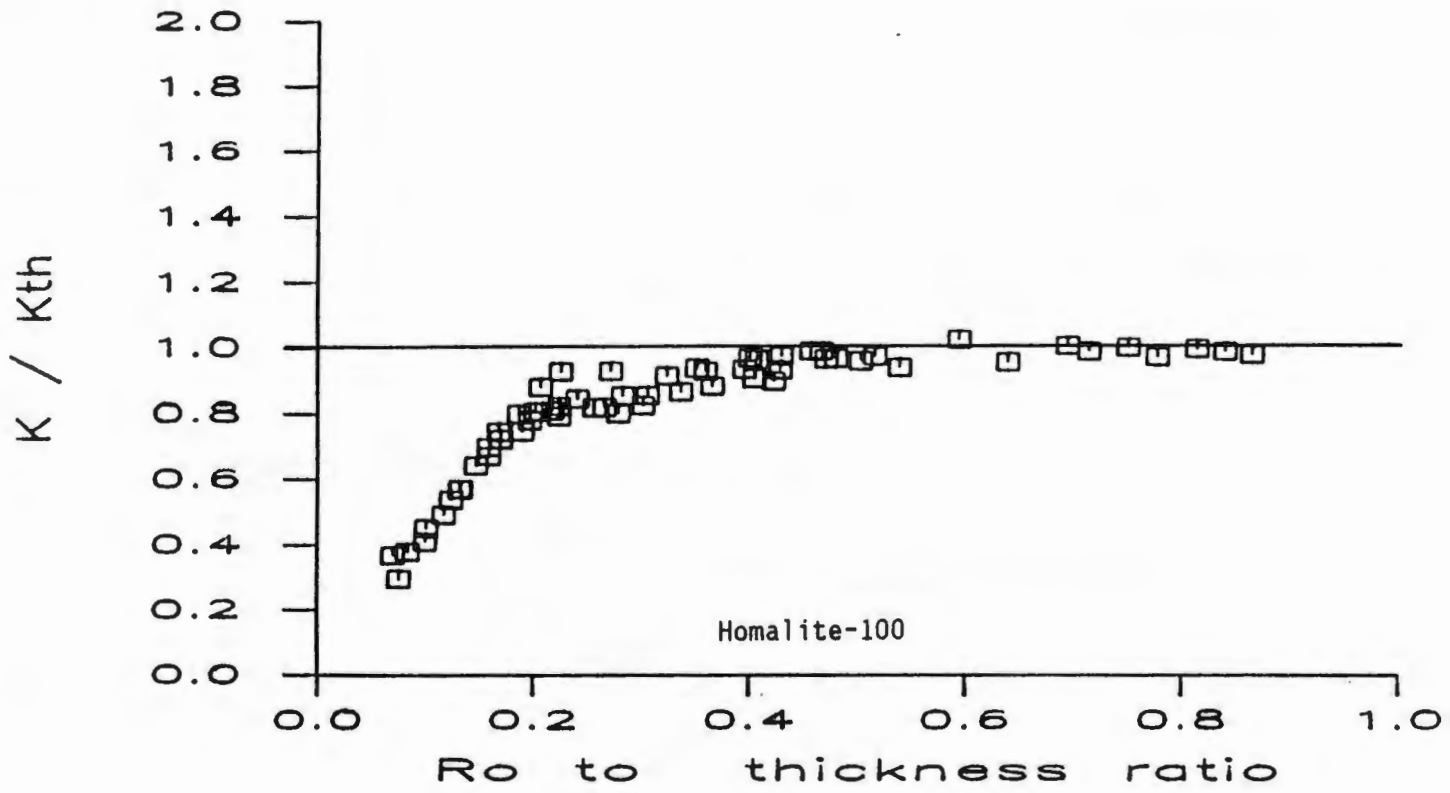

Figure 3.8 Influence of the initial curve radius on stress intensity factor for Homalite-100.

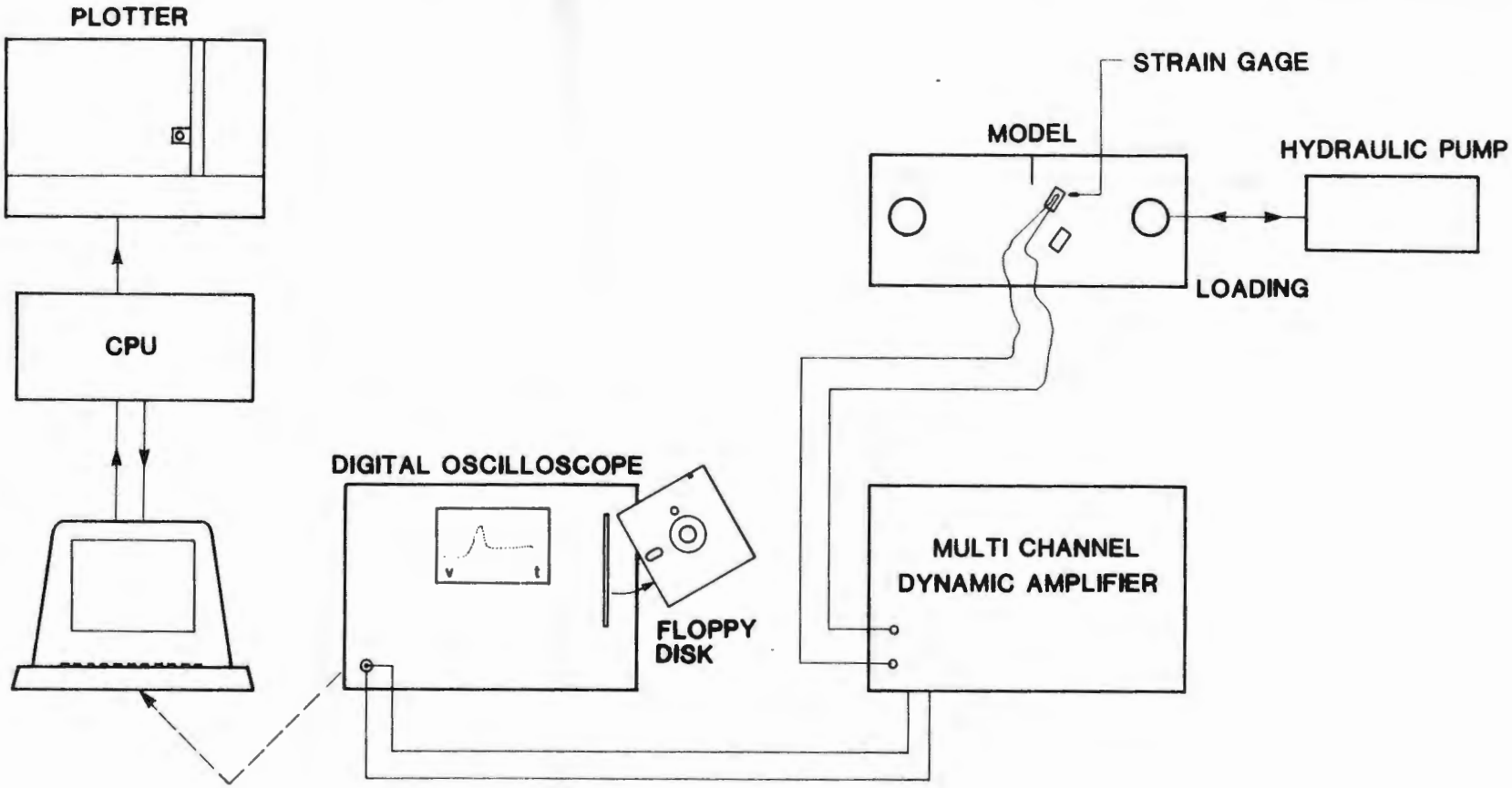

Figure 3.9 Schematic of the experimental setup used for strain gage experiments.

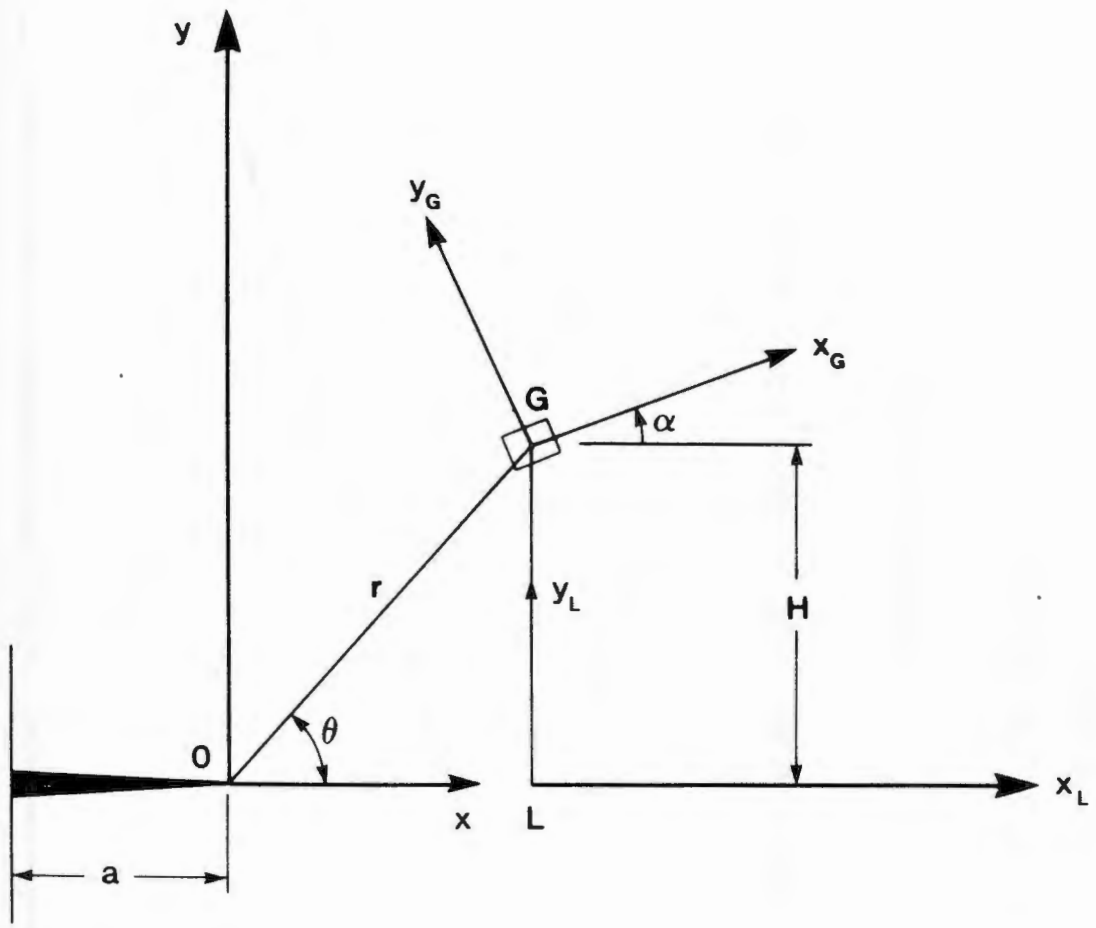

Figure 3.10 Coordinate system used for strain gage analysis.

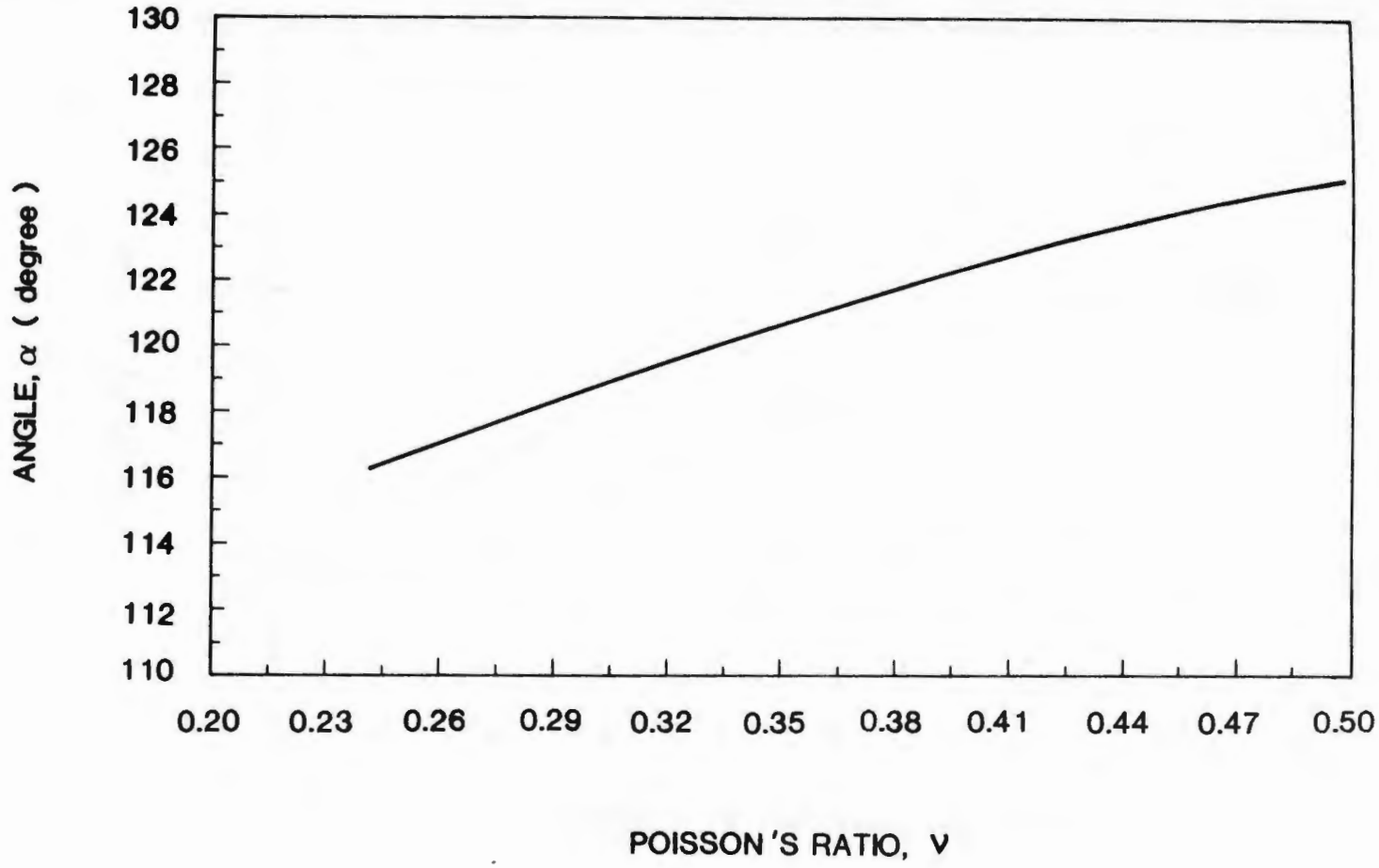

Figure 3.11 Variation of strain gage orientation angle α with the poisson's ratio of the material.

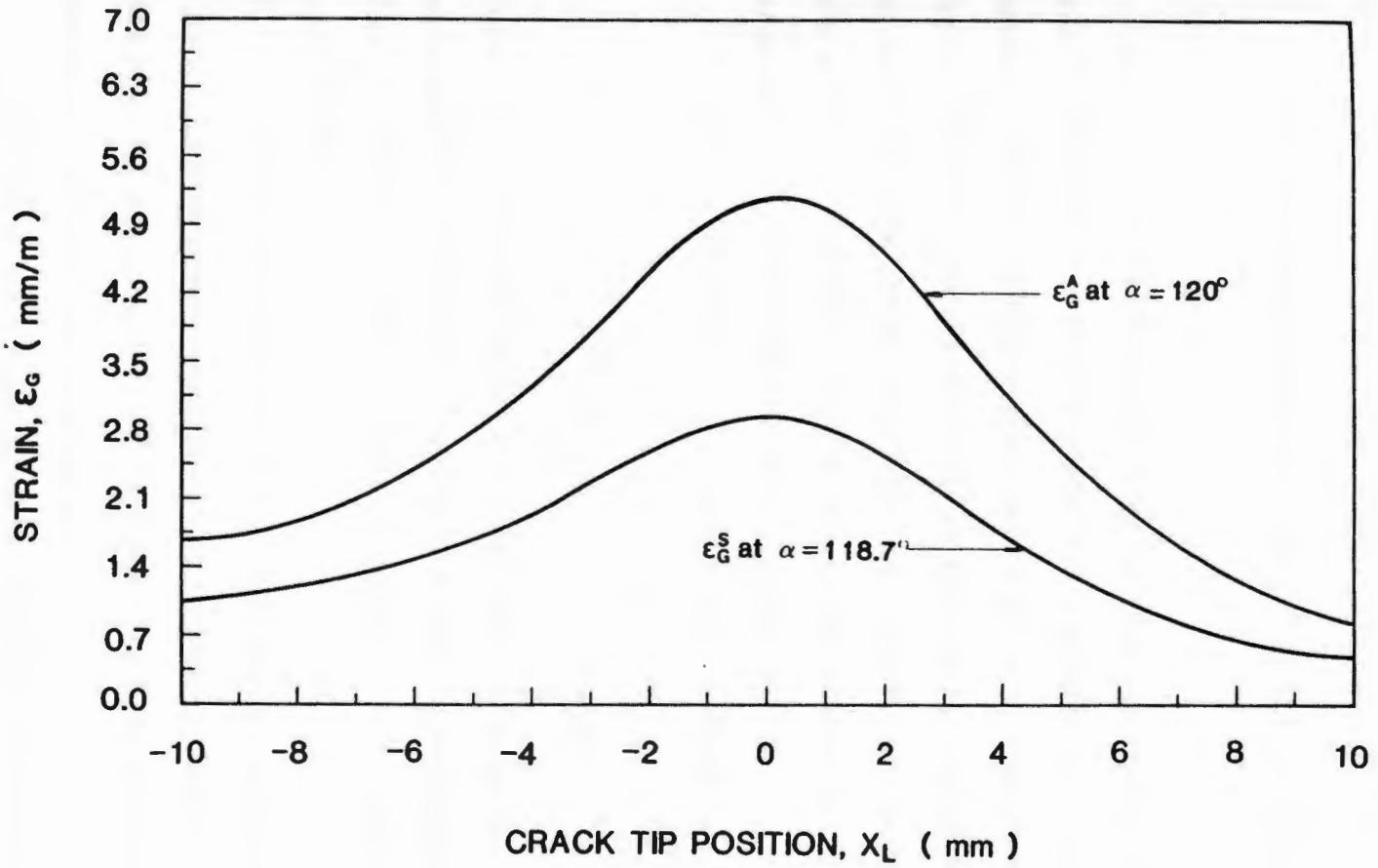

Figure 3.12 Theoretical strains at the strain gage location for varying crack tip position.

CHAPTER 4

DYNAMIC FRACTURE OF HOMALITE-100

Dynamic fracture studies are concerned with the determination of a fracture criteria which would enable the prediction of the behavior of a crack in dynamic conditions. For dynamically moving crack under mode I small scale yielding conditions a fracture criterion is postulated by equating the amplitude K_I^d of the crack tip stress field to a critical value K_{IC}^d. K_{IC}^d is considered to be a material property and it is a measure of the resistance of the material to crack growth and its magnitude is expected to depend on crack speed.

The fracture criterion can be expressed mathematically as

$$K_I^d\left(a(t), \dot{a}(t), P(t)\right) = K_{IC}^d\left(\dot{a}(t)\right) \tag{4.1}$$

where $a(t)$ is the crack length, $\dot{a}(t)$ is the crack tip speed and $P(t)$ is dynamic generalized load. The above equation is the equation of motion for the crack tip[4.1]. If at any time $K_I^d(t) < K_{Ia}^d$, where K_{Ia}^d is the minimum value of K_{IC}^d, then the crack will arrest.

Since K_I^d is a stress field related term, it in principle can be calculated through a purely elastodynamic analysis. K_{IC}^d being a material property cannot be determined by pure analysis and it must be obtained experimentally or by micromechanical modelling of the fracture process[4.2].

In practice, for complex geometries K_I^d cannot be determined from analytical solutions and as such its value at any time is estimated directly using experimental techniques. In this chapter dynamic fracture studies of Homalite-100 have been performed using the two optical techniques- photoelasticity and caustics. In the next

chapter fracture behavior of heat treated 4340 steel is studied using the techniques of caustics and strain gages.

Homalite-100 is a brittle polyester material which behaves very much in a linear elastic manner. Its fracture behavior is typical of linear elastic brittle materials. The reason for using this material is the fact that it is birefringent and as such can be used with both- the technique of photoelasticity and the technique of caustics.

Details of the two techniques and their analysis is given in chapter 3. The camera used and the experimental procedure is briefly described below. Detail discussion of the experimental results is given in the section that follows.

4.1 Experimental Procedure:

High Speed Camera:

For dynamic applications, both techniques require a high-speed recording system, usually a multiple spark camera. Approximately one hundred times more light energy is needed for photoelastic applications than for caustics work because the light has to pass through at least three different filters before reaching the film plane. On the other hand, the method of caustics requires the light to emanate from a point light source to ensure a clearly defined shadow spot. These conflicting requirements for the light source in the two methods are met by using different fiber optic light guides for each technique[4.3]. A specially designed fiber optic guide is used for recording caustics. This light guide contains a step index of refraction fiber 200 μm in diameter with the fiber optic end adjacent to the spark positioned at the focal point of a micro lens. The micro lens picks up light at a diverging angle of 5 degrees from the spark gap and concentrates it on the end of the fibers. Such an arrangement provides both the desired point light source and sufficient light intensity. The light guide used for photoelastic applications is $6.3mm$ thick bundle of fibers. Thus the same multiple spark camera has been used for both caustics and photoelasticity, by simply using the appropriate fiber optic light guide.

Specimen and Loading:

Dynamic experiments were performed with the three different specimen geometries shown in figure(4.1). Identical specimens were machined from the same shipment of material to avoid variation in material properties. The material used had a thickness of half an inch.

The loading for the single edge notch specimen was provided by pulling apart the two pins inserted in the two holes in the specimen. The load was recorded by a load cell placed inline with the loading arms[4.4]. The double cantilevered beam specimen and the eccentric pin loaded SEN specimens were not loaded by pulling the two pins but by pushing them apart by inserting a wedge in between them. While loading these specimens the displacement of the two pins (increase in the opening) was recorded. The specimens were loaded to the required load and the crack was initiated with the help of a solenoid operated knife. The timings of sparks were recorded on the oscilloscope with a high frequency response diode. The electronic circuitry of the camera was triggered by breaking the continuity of a conducting silver paint placed just below the crack.

The stress intensity factor variation with time was obtained for each photoelastic experiment and compared with the corresponding caustics experiment. The fracture surfaces from each test were compared to confirm that the experiments had been performed under similar conditions. The elastic and optical properties of Homalite 100 used in the evaluation of experimental results are shown in table(4.1).

4.2 Results Of The Experiments:

Single Edge Notch Specimen:

Experiments were performed under two different loading conditions for this geometry. In the first experiment the specimen was loaded to $4.8kN$ and the crack was initiated with a sharp knife. Typical isochromatic and caustic photographs obtained during the experiment are shown in figure(4.2) and figure(4.3) respectively.

For this loading two different caustics experiments were performed using different optical setups. In the first experiment a single lens [4.5] setup was used whereas in the second a mirror arrangement was used (see chapter 3 for details). The result for the photoelastic experiment as well as the two caustic experiments are shown in figure(4.4). It is seen that substantially lower values of K_I^d are obtained by the method of caustics. The initial values differ by about $30 - 40\%$. The value of r_o/h in both the caustic experiments were in the range of $0.4 < r_o/h < 0.65$. The crack velocity data in all the three experiments was consistent and gave a constant velocity of $360m/s$.

In the second experiment the specimens were loaded to $5.8kN$ before the crack was initiated. The stress intensity factor as a function of time results are shown for both the experiments in fig(4.5). In the photoelastic experiment K_I^d increases steadily from $1.37MPa\sqrt{m}$ to $1.7MPa\sqrt{m}$ as the crack propagates through the model. For caustic experiment K_I^d starts at $1.00MPa\sqrt{m}$ and shows little changes with crack propagation till the crack comes closer to the outer boundary ($a/w = 0.85$). At this point the stress intensity factor shows a steep fall. This can be explained by the fact that the current caustics analysis involves the use of only one stress field parameter (K_I^d) where as close to the boundary many more (8-10) parameters are needed to define the stress field accurately as was found in the isochromatic analysis with fringe pattern replots. The shape of the caustics distorts and the diametral size diminishes as the crack approaches the boundary as shown in figure(4.6). Shape distortions also renders crack length measurements impossible. In this case r_o/h was in the range of $0.6 < r_o/h < 0.85$. Fracture surfaces of the broken specimens were examined as an additional check to make sure that the experimental conditions for the two methods remained the same. The fracture surfaces for the caustic and the photoelastic specimens are shown in figure(4.7). The roughness is seen to increase with crack length showing an increase in stress

intensity factor values.

Double Cantilever Beam Specimen:

The specimen geometry is shown in figure(4.1). The models were loaded by inserting a wedge between the loading pins and thus pushing them apart. The displacement between the loading pins was recorded with an eddy current transducer. Two sets of experiments were performed with this geometry under different loading conditions. The results for the first set of experiments are shown in figure(4.8). Both the techniques show similar trends but the values for caustic experiment are again $20 - 30\%$ lower than the photoelastic experiment. The value of r_o/h for this experiment were in the range $0.65 < r_o/h < 1.0$.

For the second set of experiments the crack was initiated at a much higher load to give even higher r_o/h values ($0.6 < r_o/h < 1.3$). Again the trend of the results was similar to the previous set of experiments. The photoelastic values are higher than the values obtained by the caustic method as shown in figure(4.9).

Eccentric Pin Loaded SEN Specimen:

The geometry of these specimens is also shown in figure(4.1). The specimens were again loaded with a wedge and the displacements of the loading pins were monitored with an eddy current transducer. The results for the two experiments are shown in figure(4.10). The photoelastic results show that the K_I^d value decreases monotonically from $1.2MPa\sqrt{m}$ to about $0.5MPa\sqrt{m}$. The caustic data shows large fluctuations in the K_I^d values which vary between $0.6MPa\sqrt{m}$ and $0.2MPa\sqrt{m}$. The value of r_o/h varied between 0.65 and 0.90.

4.3 Discussion And Conclusions:

A comparison of the techniques of caustics and photoelasticity as applied to dynamic fracture has been made. The experiments show large differences in the results obtained from the two techniques. The caustics results are always smaller

than the photoelastic values by about thirty percent. Since the two techniques match well under static conditions[4.4] it is believed that most of the differences arise due to the dynamic effects. A brief discussion is presented to point out the possible sources of errors in both the techniques and any advantage of one technique over the other.

For dynamic crack growth strain rate effects can be very high near the propagating crack tip. These strain rates are expected to vary with the radial distance from the crack tip and with crack velocity. As a result in dynamic experiments the Young's modulus E, the photoelastic fringe value f_σ and the stress optical coefficient in caustics c, all vary with distance from the tip. Thus for Homalite 100 which is a viscoelastic material these properties are field quantities and should not be characterized by a single number. Since single numbers have been used in current analysis this error exists in both the techniques.

One source for the difference in dynamic K_I^d values can be the different analysis procedures employed in the two techniques. In the method of caustics a one parameter stress field representation is used (the second term σ_{ox} does not influence the caustic diameter) where as in photoelasticity a multi-parameter characterization is incorporated where the number of parameter depends on the region of data acquisition. This can be important as in both the techniques the data for the computation of K_I^d is taken at least half the plate thickness away from the crack tip and as we move further and further away from the crack tip a single parameter characterization may not be sufficient.

Both the techniques require location measurements to be made from photographs for the evaluation of K_I^d. In the method of photoelasticity there is some uncertainty in locating the exact positions of fringe order because of the finite fringe thickness and the restricted ability of the available films to record varying light intensities. But the use of multipoint method to evaluate the stress field coefficients

using a numerical scheme minimizes this error in a least square sense. The method of caustics uses a single measurement, the diameter of the caustic, to evaluate the stress intensity factor. Any mistake in the measurement of this diameter would reflect directly in the result. It is worth noting at this point that K_I^d varies as a 5/2 power of the caustic diameter and only linearly with the fringe order. There is currently a difference of opinion as to how the caustic diameter should be measured. Theoretically the caustic formulas are derived from geometrical optics which show that the light intensity along the caustic curve is infinite and thus the diameter is well defined. However, in practice the actual light intensity at the caustic is bounded and the diffraction effects make the measurement of diameter ambiguous. The detailed discussion of these effects is provided by Kamath and Kim in [4.6]. One school of thought [4.7,4.8] suggests to measure the diameter as the outside edge of the black spot where as the other group [4.5] suggests that the center of the bright rim around the black spot should be considered as the correct diameter. The diameter measured from the center of the bright rim is on the average 5% larger giving 13% higher values of K_I^d.

The difference in the results from the two techniques becomes even larger as the crack length increases ($a/w > 0.8$) and approaches the outer boundary. This was observed in all the experiments with the SEN geometry. It was seen that the caustic shape distorts and the diameter shrinks considerably as the crack approaches the outer boundary. This decrease in the diameter means a decrease in the K_I^d value. This is in contradiction to the pevious results which have shown that a single edge notch geometry is an increasing K_I^d geometry under dynamic crack propagation conditions. The photoelastic data in this region itself required more than 10 higher order terms in the analysis to give the stress field which matched well with the experimental pattern. The photoelastic results did show an increasing trend in the K_I^d values.

One other factor which might influence our caustic results is the value of the calibration constant c. The static value of this constant was obtained by using the values of the direct and transverse stress optic coefficient from ref[4.9] and using the values of Poisson's ratio ν and elastic modulus E obtained in our laboratory. The constant thus obtained gave accurate results for the static experiments. This value of c was corrected for dynamic effects by using dynamic values of ν and E and using the shadow optical function relation given by Kim et.al.[4.10]. The dynamic value of c thus obtained was 25 percent lower than the static value. It must be mentioned here that if the dynaimc value of c was computed using stress optic coefficients c_1 and c_2 from reference [4.9] and dynamic values of ν and E a value of c only 10 percent lower than the static value is obtained. This will give even larger differences between the dynamic results from the two techniques.

Finally it must be mentioned that in both the techniques since the data is taken from a region away from the crack tip, a time averaging effect of the crack tip information occurs and the true time history of the crack tip deformation field becomes less precise[4.11]. A complete quantitative analysis of this time averaging effect has yet to be developed although Freund[4.12] has performed some computations for the time it takes to establish a two dimensional singular stress field in a region around a moving crack from which the stress intensity factor can be determined.

It is believed that a detailed quantitative study of the possible causes for the differences (for example, the out of plane inertia effects and the variation of material properties with strain rate) is needed. Both the techniques have their own advantages but require a better understanding to give consistent results.

References:

[4.1] Freund,L.B., "The Mechanics of Dynamic Fracture," Proceedings of the Tenth U.S. National Congress of Applied Mechanics, Austin, TX, 1986.

[4.2] Lam,P.S. and Freund,L.B., "Analysis of Dynamic Crack Growth of a Tensile

Crack in an Elastic Plastic Material," Journal of Mechanics and Physics of Solids, vol. 33, 1985, pp. 153-167.

[4.3] Shukla,A. and Nigam,H., "Multiple Spark Camera for Dynamic Photoelastic and Caustic Studies," Experimental Techniques, August 1984, pp. 17-19.

[4.4] Nigam,H., "Comparison of the Optical Techniques of Caustic and Photoelasticity as applied to Fracture," M.S. Thesis, University of Rhode Island, 1985.

[4.5] Beinert,J. and Kalthoff,J.F., "Experimental determination of dynamic stress intensity factors by shadow patterns," Mechanics of Fracture, vol. VII, G.C.Sih, ed., Noordhoff Int. Publishing, London, The Netherlands, 1981.

[4.6] Kamath,S.M. and Kim,K.S., "Coherent-Light-Shadow Spot of a Crack Under Mode I Loading: Theory and Experiment," Experimental Mechanics, vol. 26, No. 4, December 1986, pp.386-393.

[4.7] Rosakis,A.J., "Experimental Determination of the Fracture Initiation and Dynamic Crack Propagation Resistance of Structural Steels by the Optical Method of Caustics," PhD Thesis, Brown University, June 1982.

[4.8] Ravi-Chander,K. and Knauss,W.G., "An Experimental Investigation into Dynamic Fracture: III On Steady-State Crack Propagation and Crack Branching," International Journal of Fracture, 26, 1984, 141-154.

[4.9] Ravi-Chandar,K., "An Experimental Investigation into the Mechanics of Dynamic Fracture," PhD Thesis, California Institute of Technology, 1982.

[4.10] Kim,K.S., Dickerson,K.L. and Knauss,W.G., "Viscoelastic Behavior of Opto Mechanical Properties and its Application to Viscoelastic Fracture Studies," International Journal of Fracture.

[4.11] Knauss,W.G. and Ravi-Chander,K., "Some Basic Problems in Stress Wave Dominated Fracture," International Journal of Fracture, Vol. 27, 1985, pp. 127-143.

[4.12] Ma,C.C. and Freund,L.B., Brown University Report, September 1984.

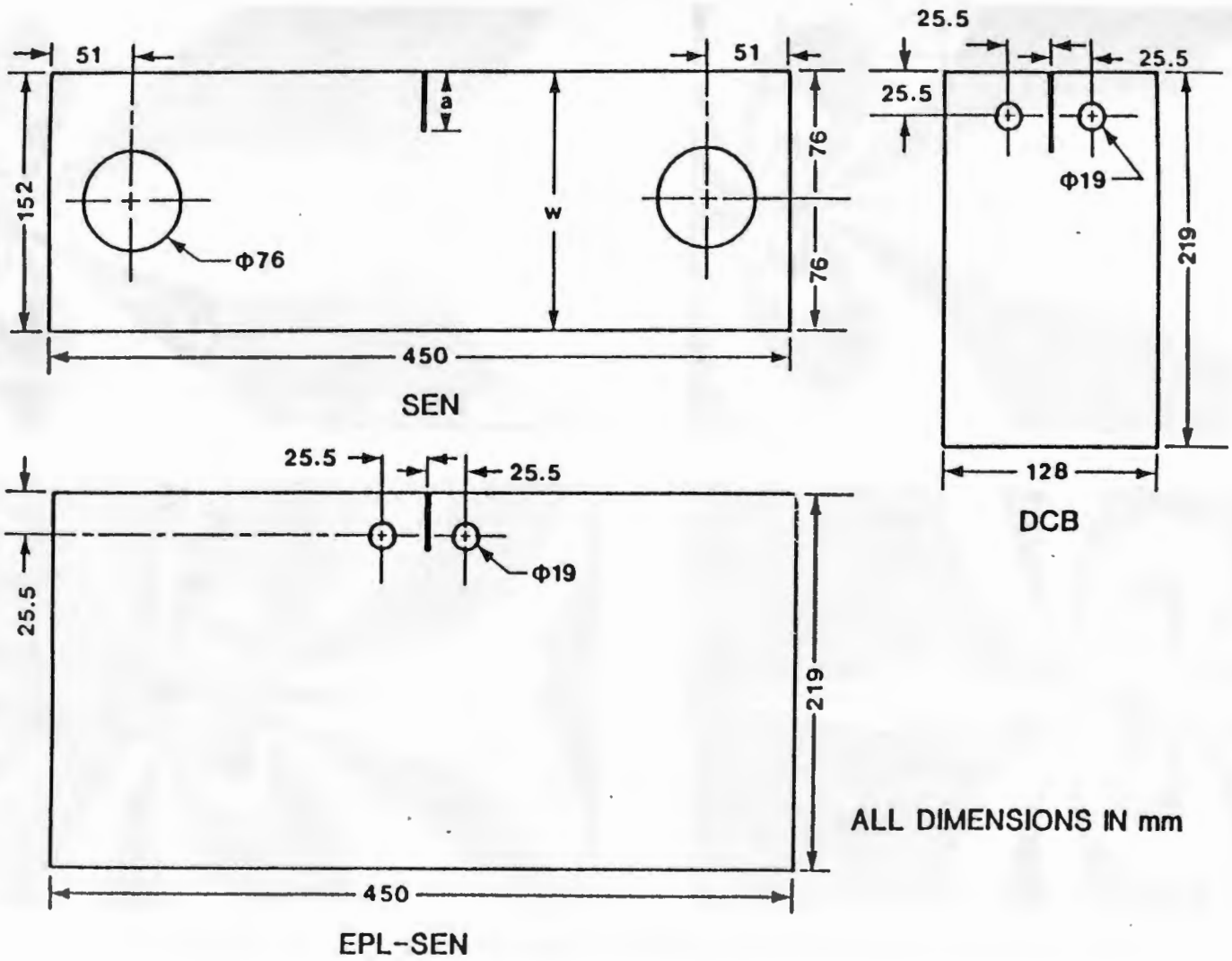

Figure 4.1 Geometry of specimens.

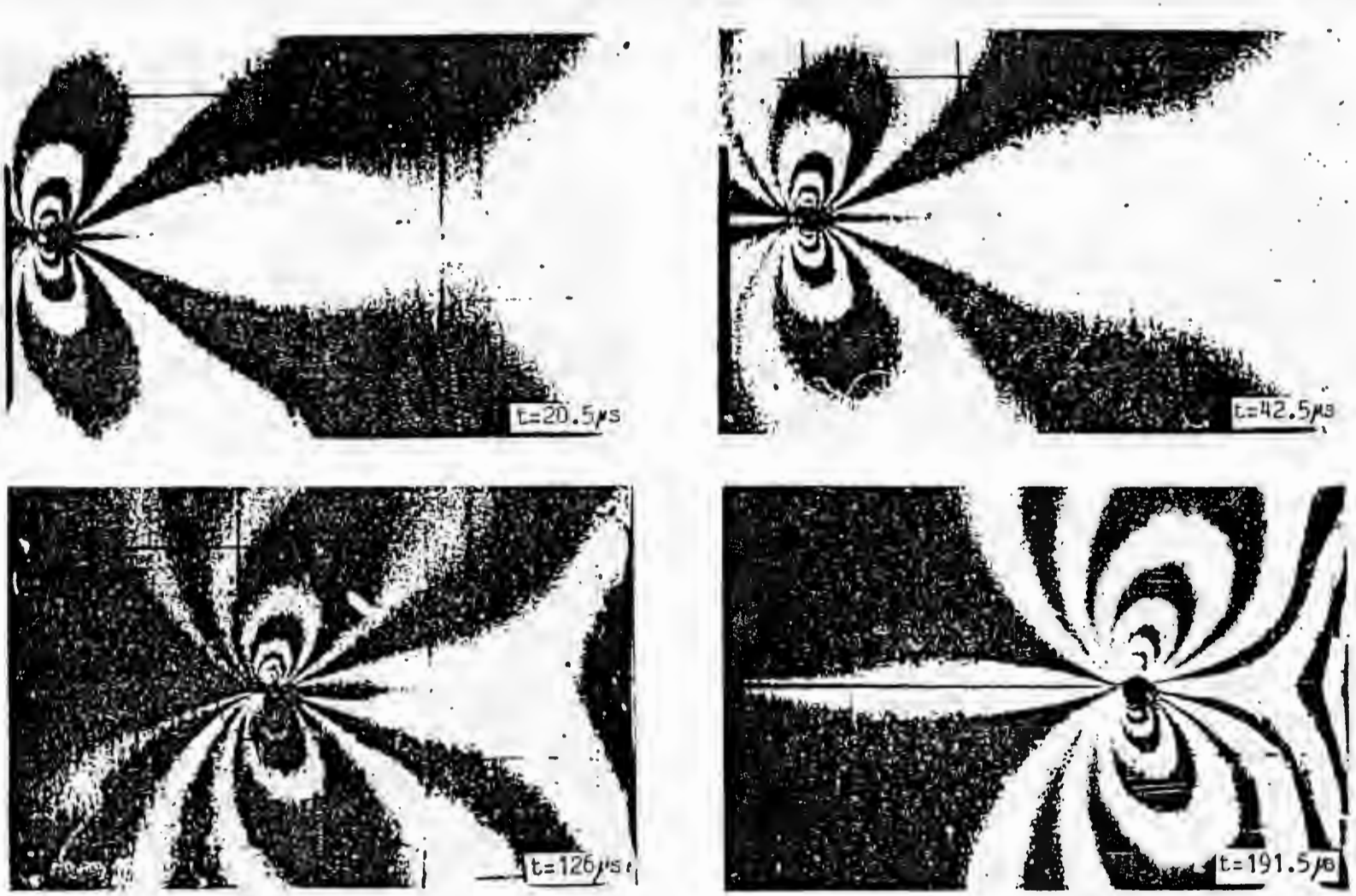

Figure 4.2 Typical isochromatic fringes obtained during a dynamic test of SEN specimens.

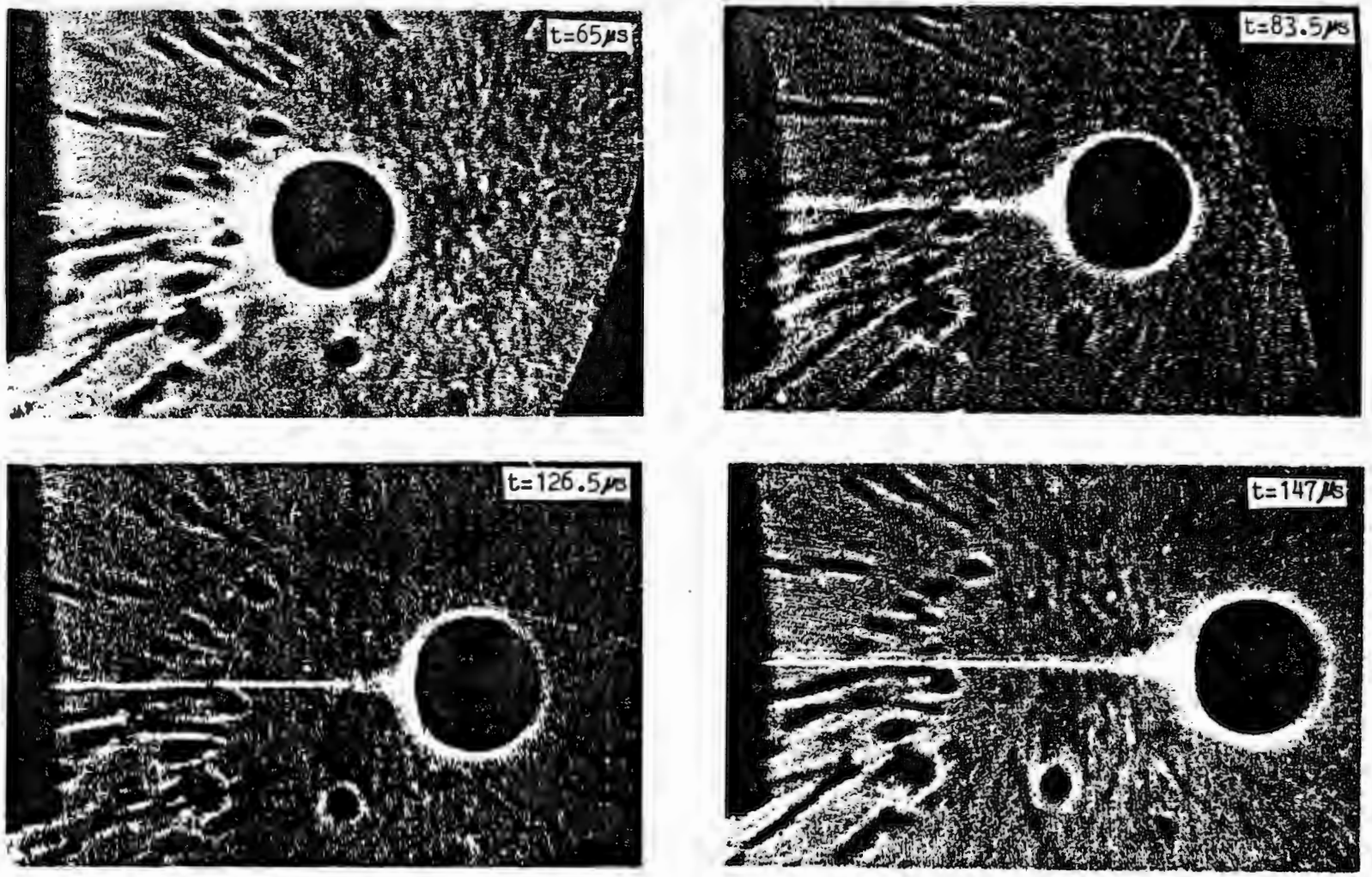

Figure 4.3 Typical caustics obtained during a dynamic test of SEN specimens.

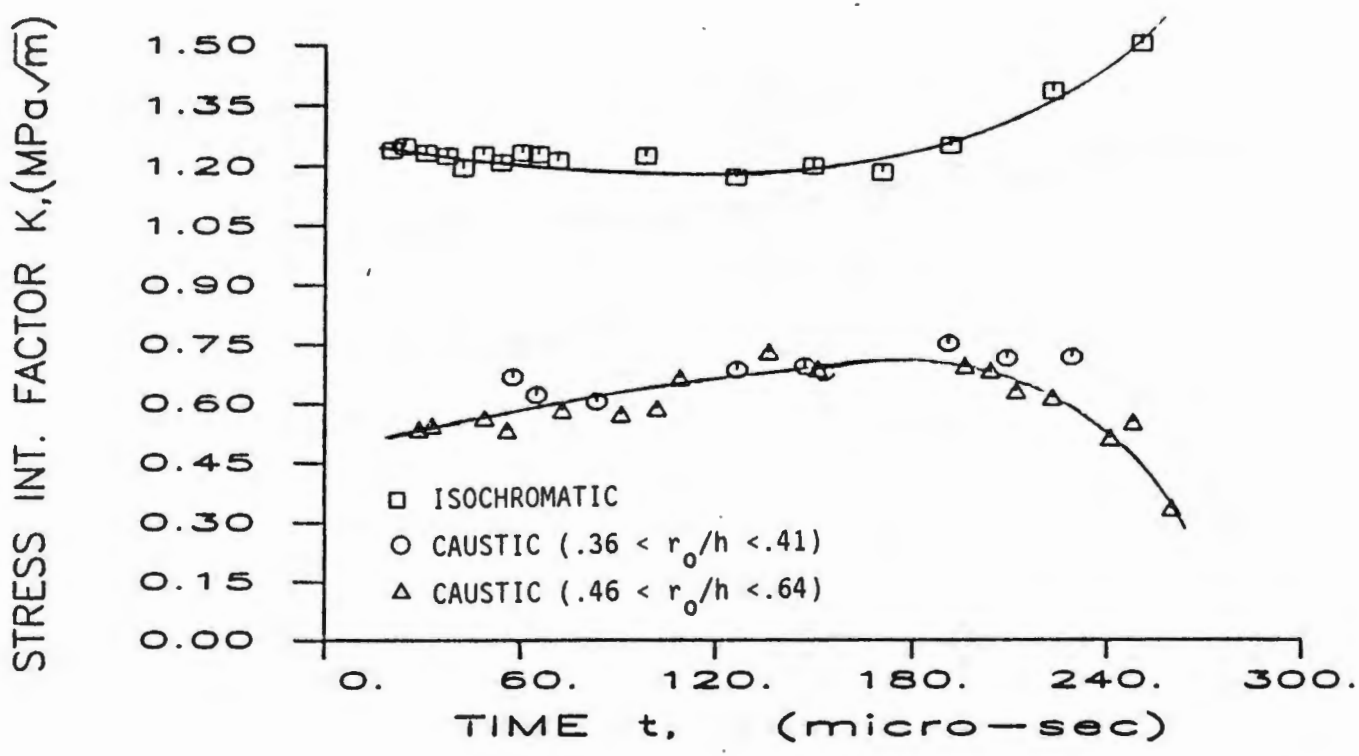

Figure 4.4 Variation of K_I^d with time for the SEN-1 experiment.

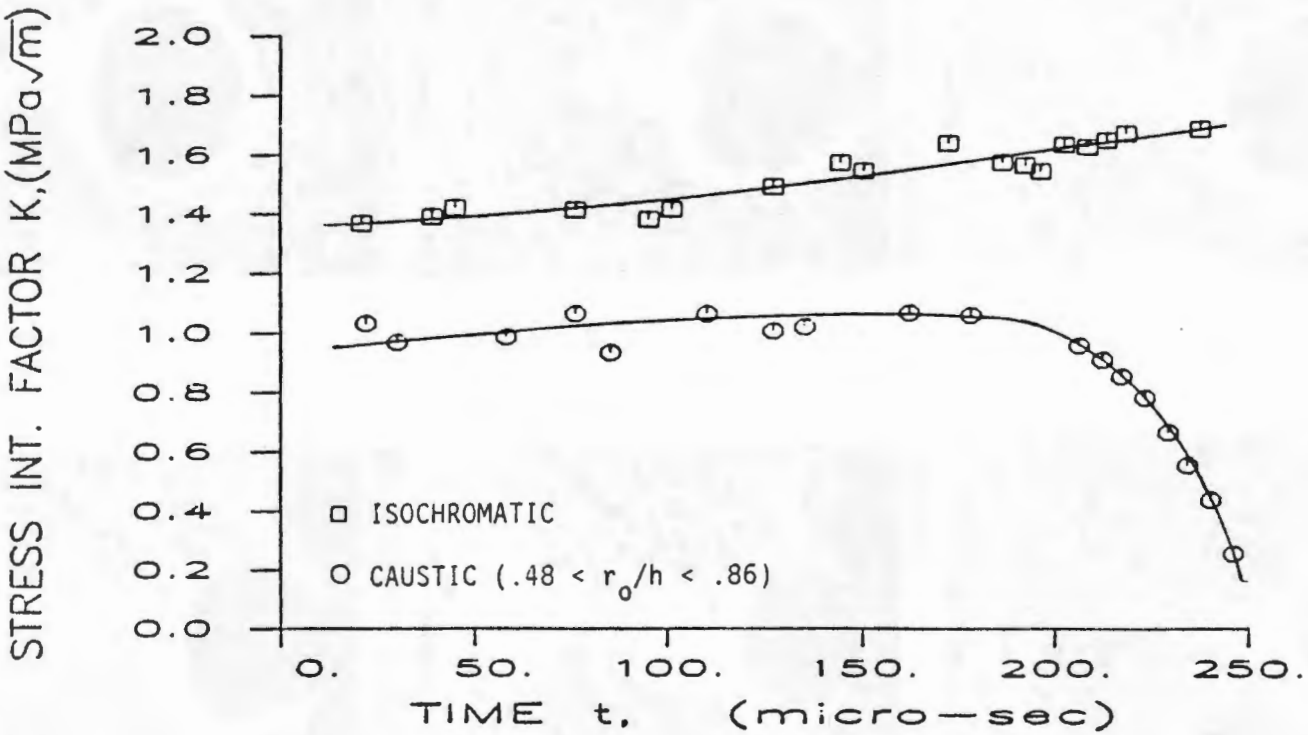

Figure 4.5 Variation of K_I^d with time for the SEN-2 experiment.

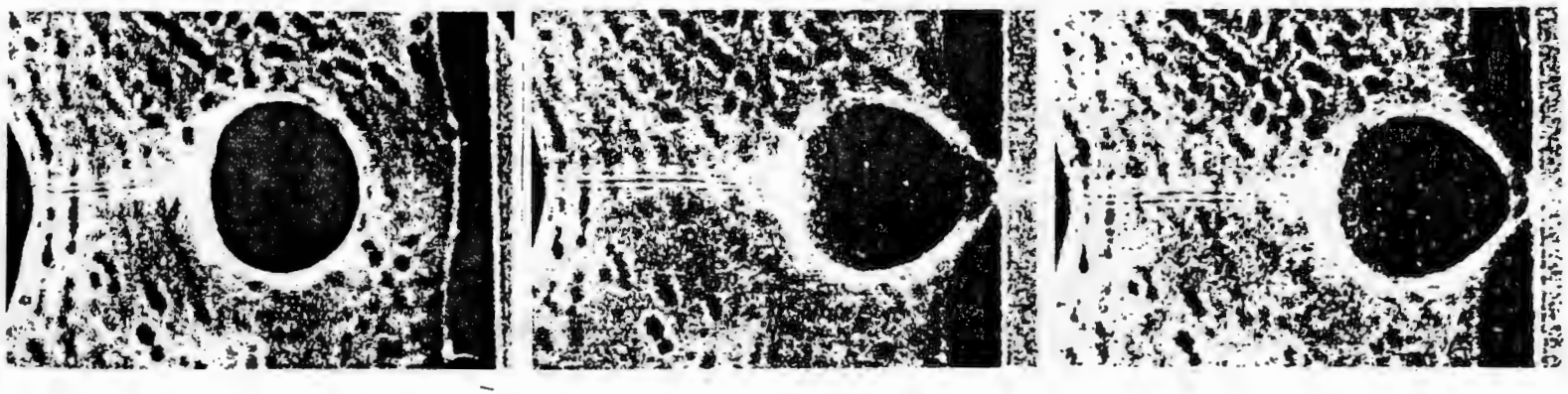

a/w = 0.70 a/w = 0.82 a/w = 0.83

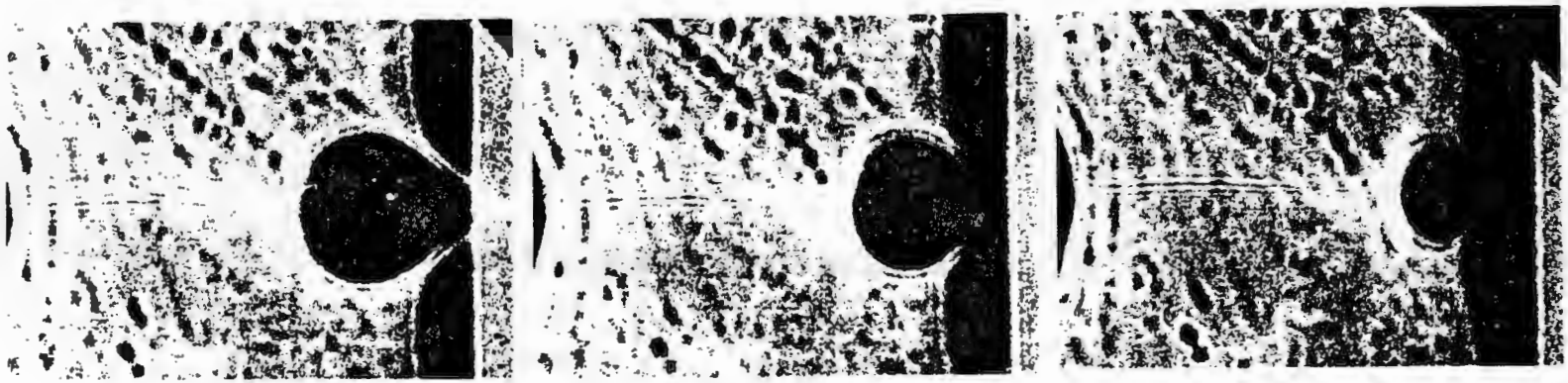

a/w = 0.85 a/w = 0.89 a/w = 0.92

Figure 4.6 Distortion of the caustic shape as the crack approaches the boundary of SEN specimen.

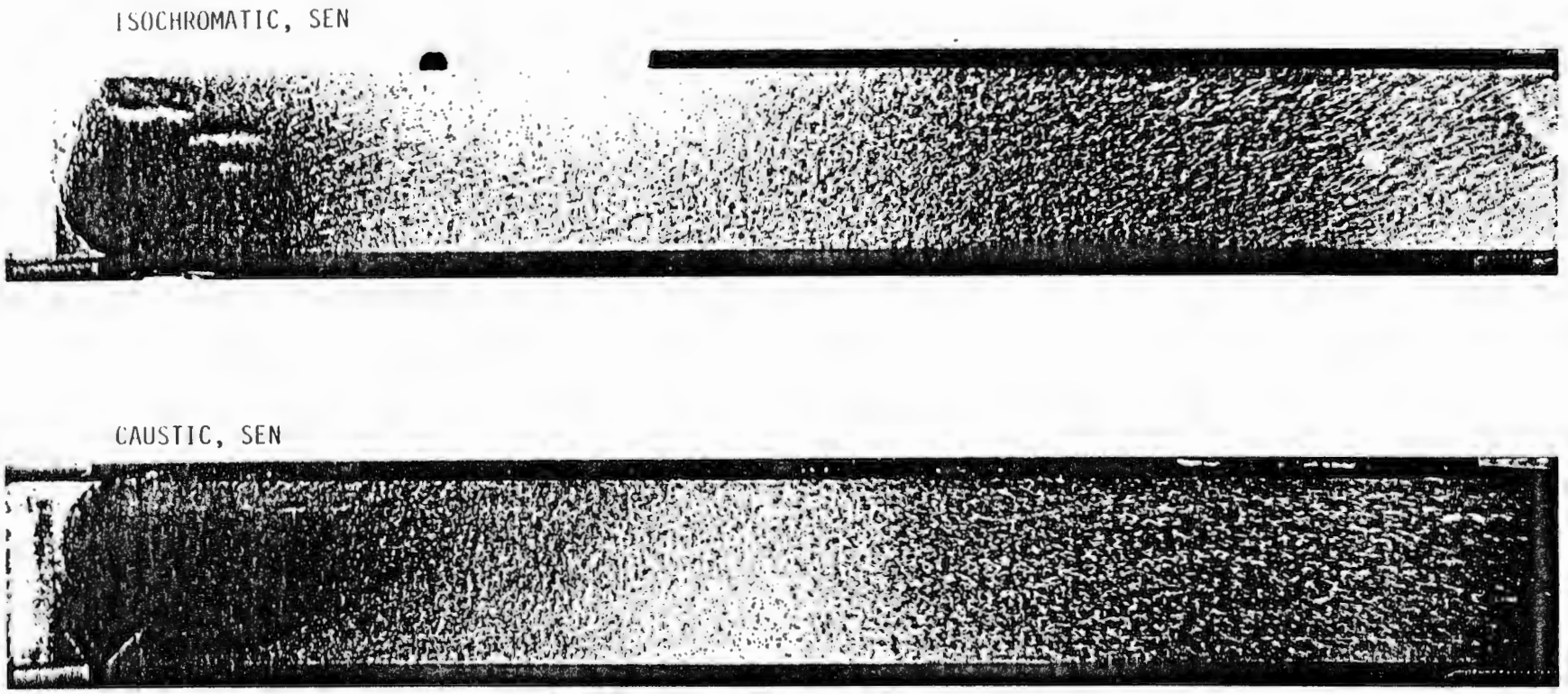

Figure 4.7 Fracture surfaces of specimens used for the caustic and photoelastic SEN specimens.

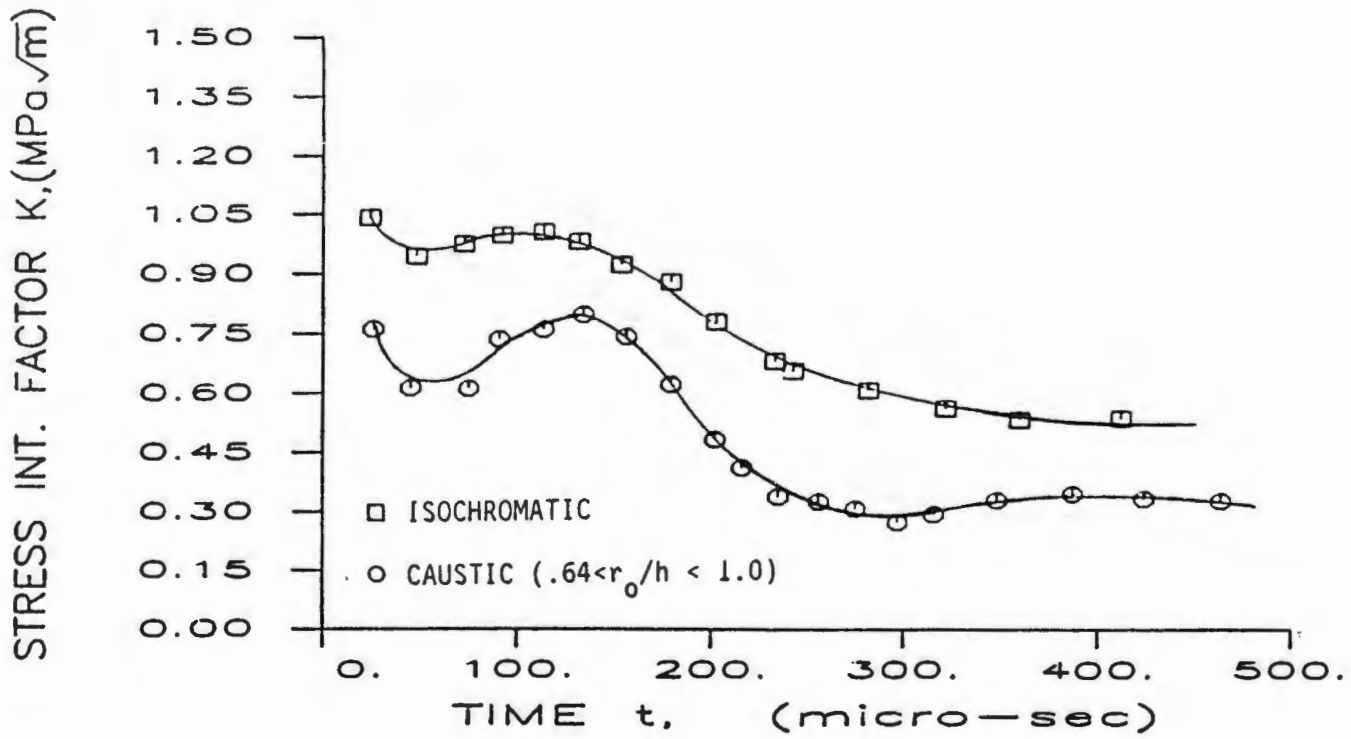

Figure 4.8 Variation of K_I^d with time for the DCB-1 experiment.

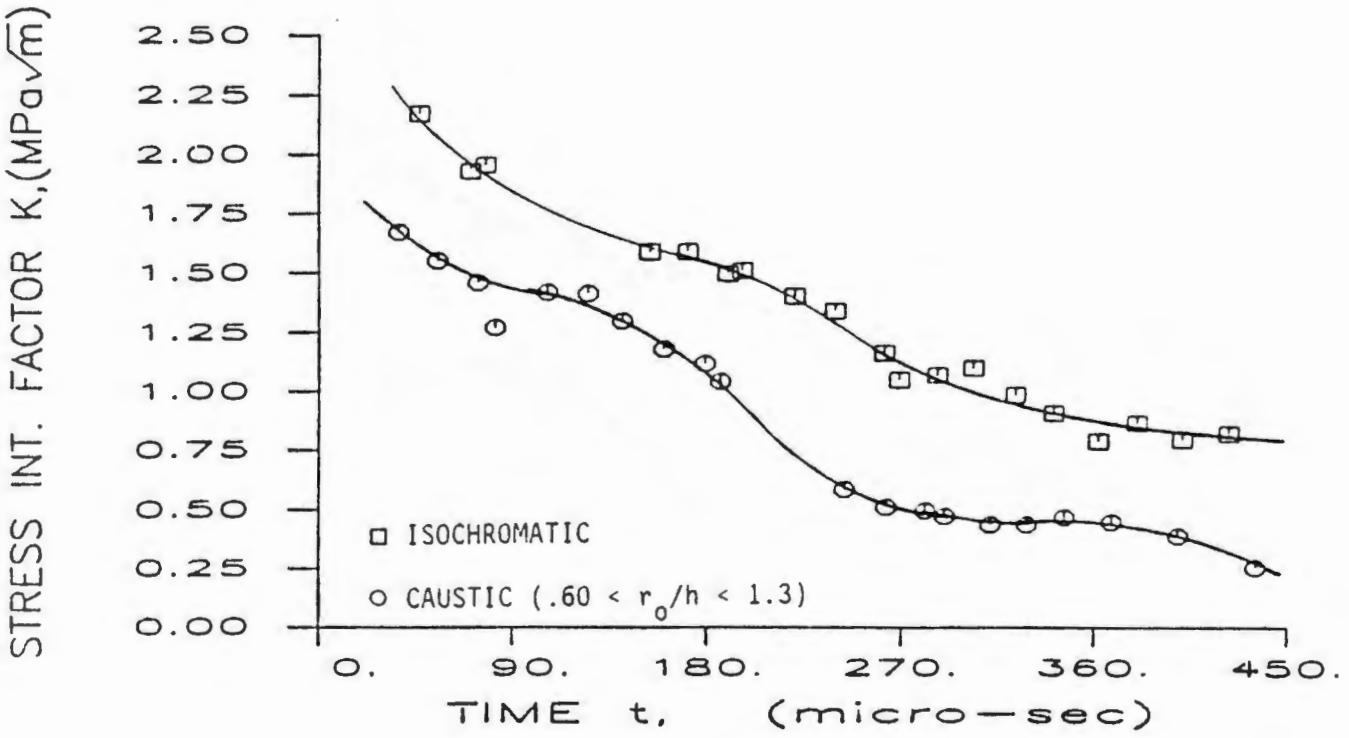

Figure 4.9 Variation of K_I^d with time for the DCB-2 experiment.

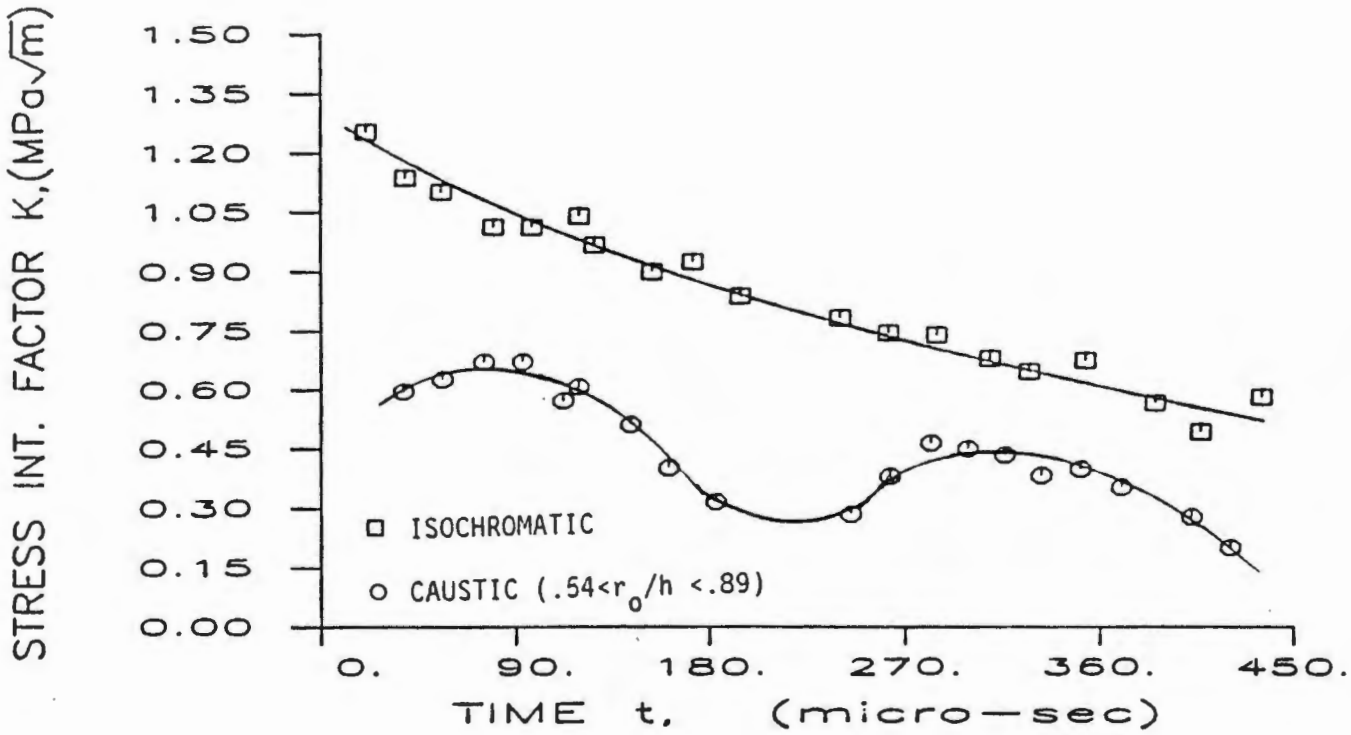

Figure 4.10 Variation of K_I^d with time for the EPL-SEN experiment.

TABLE 4.1

Elastic and Optical Properties of Homalite-100

Modulus of Elasticity	E	3860 MPa, Static 4820 MPa, Dynamic
Poisson's Ratio	ν	0.35, Static 0.35, Dynamic
P wave speed S wave speed	c_1 c_2	2130 m/s 1220 m/s
Index of refraction	n	1.5
Stress optic Coefficient	c	-1.476E-10 m^2/N, Static -1.182E-10 m^2/N, Dynamic
Stress fringe value,(4920 A)	f_σ	18.3 kN/m, Static 21.9 kN/m, Dynamic

CHAPTER 5

EVALUATION OF K_I^d IN METALS

5.1 Introduction:

The fracture behavior of metals is very different from that of linear elastic brittle materials studied in the previous chapter. Because of the ductile nature of metals there is substantial amount of plastic deformation at the crack tip before and during the propagation of the crack.

In the domain of linear elastic fracture mechanics the behavior of a crack is primarily governed by the stress intensity factor defining the stress field near the crack tip[5.1]. Thus it is of practical importance to be able to evaluate the values of stress intensity factor. Analytical solutions can only be obtained for very restricted number of cases and so one has to experimentally determine the stress inensity factors for any engineering application involving finite geometries.

There are many methods which can be used by an experimentalist for evaluating the stress intensity factor for a dynamically moving crack. These methods include various optical and non-optical techniques. Review of the various techniques has already been presented in chapter 2. In this section the method of caustics and strain gages have been used to study dynamic fracture of metals.

The method of caustics[5.2,5.3] gives the first term of the series representing the stress field around the crack tip which is related to the stress intensity factor. The great advantage of the method over other experimental techniques is that it provides a direct measure of the crack tip stress field and the corresponding crack speed without concern of the geometry of the specimen, the boundary conditions, or the complex stress wave pattern in the bulk of the specimen.

Electrical resistance strain gage technique[5.4,5.5] is one of the lesser used methods. The primary hesitation in the use of resistance strain gages for fracture studies was their finite size. Since the crack tip strain field has steep gradients the averaging effects can be large if the strain gages are not small enough. With the use of extremely small strain gages of sizes less than a millimeter square, it is possible to accurately measure strains at any point.

In this chapter the above mentioned techniques have been used to study dynamic fracture of structural metals 4340 steel and 7075-T6 aluminum. Face grooves are made on the aluminum specimens to guide the crack and to ensure failure in tension mode. Instantaneous stress intensity factor values thus obtained are compared with each other and with other available estimates. Results indicate that the two methods compare well.

5.2 Experimental Procedure:

Dynamic experiments have been performed using the techniques of caustics and strain gages. 4340 steel specimens were studied with both the techniques but 7075-T6 aluminum tests were performed only with strain gages because it required face grooves to be made on either side of the specimen for proper guidance of the crack and hence the method of caustics could not be applied. In case of aluminum the strain gage results have been compared with the photoelastic results provided in reference[5.6].

Preparation of the 4340 Steel Specimens:

Steel specimens were machined out of hot-rolled 4340-steel sheet and were given the following heat-treatment: 20 min. at $1550^{\circ}F$, oil quenched to $150^{\circ}F$, air cooled to room temperature, and tempered at $650^{\circ}F$ for 1 hr followed by straightening on a screw press and sand blasting. The hardness thus achieved was close to $Rc49$.

The geometry of the SEN and the DCB specimens used is given in figures (5.1) and (5.2). The specimen for use with caustic technique did not have any face

groove. The SEN specimens were $1/4inch$ in thickness and the DCB specimens were $1/2inch$. The crack is made using a vertical milling cutter. The crack is sharpened using fine angular files.

For caustic application the surface had to be polished to a mirror finish. The surface of the heat treated specimens were ground to attain flatness. This ground flat surface was then polished to achieve mirror finish required for caustic experiments.

For polishing, the ground surface was abraded with 280, 400 and 600 grit emery papers making sure that the abrasion marks of the previous grade paper were completely removed before moving to a finer grade. After this, diamond paste was used with proper extender fluid on fine polishing cloth. 9.0μ, 3.0μ and 1.0μ diamond paste were used and the final finish was given using 0.05μ micro polish alumina. Water is not used any where in the process because the polished surface is very susceptible to corrosion. For cleaning and washing acetone was used.

For strain gage applications the surface was not polished to a mirror finish. It was simply sanded and cleaned in the usual way required for mounting strain gages. Two experiments have been conducted with the SEN geometry, one of them has the face groove and the other does not.

Preparation of the Aluminum Specimens:

Aluminum specimen shown in figure(5.3) was cut out from $1/4inch$ thick 7075-T6 aluminum sheet. The initial crack was a band saw cut with crack length to width ratio of 0.25. In order to control the crack path and to avoid failure in shear, face grooves were made on the specimens with the included angle of 45 degrees. Ratio of the net thickness at the groove center to the specimen thickness, h_n/h, was kept 0.75. The surface was cleaned and sanded to prepare it for mounting the strain gages. The gages were then mounted at an angle of 120° as shown in the specimen geometry.

5.3 Caustics Experiments:

Details of the experimental setup and the analysis technique are discussed in chapter 3. Electrically powered hydraulic pump and hydraulic cylinder were employed to load the model. Since focused light was being used and the optical path was long, slight changes in the angle of the model due to resetting of the model under loading could lead to deflection of the light off the camera. Therefore, the model was loaded in two steps, in the first step it was loaded to 60 percent of the expected fracture load and optical arrangement adjusted to account for any tilt in the model due to loading, in the second step the load was gradually increased until the model fractured.

SEN steel experiment:

The $1/4inch$ thick SEN specimen as shown in fig(5.1) was loaded to a load of $1.713kN$ when the crack started to propagate. The specimen did not have any face grooves. The value of the stress intensity factor calculated from this load and the specimen specifications is $125.6MPa\sqrt{m}$. This value is higher than K_{IC} because the crack tip was fairly blunt. Set of four pictures of the caustics taken from the experiment is shown in figure(5.4). The analysis of the experiment showed that the crack velocity was constant at $1060m/sec$. As the crack moved through the specimen the value of the stress intensity factor increased from about $95MPa\sqrt{m}$ to $135MPa\sqrt{m}$. But when the crack came too close to the boundary $a/w < 0.85$ the value of K_I^d suddenly dropped as had happened in the Homalite SEN experiments discussed in chapter 4. The r_o value for the various pictures was in the range $0.63 < r_o/h < 072$. The plot of stress intensity factor as a function of crack length to width ratio is given in fig(5.5).

DCB steel experiment:

The DCB specimen shown in figure(5.2) is $1/2inch$ in thickness. It was loaded by inserting a wedge in between the two pins placed in the holes of the speci-

men. The analysis of the experiment showed that the crack velocity decreased from $800m/s$ to $200m/s$ as the crack propagated through the specimen. As the crack moved through the specimen the value of the stress intensity factor decreased from about $86MPa\sqrt{m}$ to $49MPa\sqrt{m}$. Since this is a decreasing K_I^d geometry the crack got arrested before passing through the specimen. As can be seen from the plot of stress intensity factor versus crack length to arrested crack length ratio (denoted a/l) the stress intensity factor continues to fall even after the arrest of the crack to low value of $30Mpa\sqrt{m}$ (figure 5.6). The r_o/h value in this experiment is in the range of 0.32 to 0.40. The value is low because the value of the stress intensity factor is low for this kind of specimen geometry.

Strain Gage Experiments:

Details of the strain gage experimental setup and analysis are discussed in chapter 3. Strain gages were mounted on each model as shown in Figures(5.1-5.3). The orientation angle α was 118.7° for steel specimens and 120° for the aluminum specimen. Strain gages were connected to dynamic amplifiers with frequency response of $200kHz$, and the output was recorded on a digital oscilloscope every $500ns$. Oscilloscopes were set to trigger simultaneously at 50 percent of the maximum expected strain value and on the positive slope of the strain profile from the first strain gage with a pretrigger setting of $100\mu sec$. Gages used in this work were EA-13-031DE-120 from Micro- Group. These strain gages have a grid size of $0.79mm \times 0.81mm$. The averaging effect on strain of the strain gage grid is less than 0.5 percent [5.7].

SEN steel experiment 1:

The specimen geometry is the same as that used for the caustic experiment described above. Six gages were mounted in a manner similar to what is shown in the figure. The recording oscilloscopes were triggered from the first strain gage reading. The strain profiles recorded by the six gages is shown in figure(5.7) as a function of time after trigger. The average velocity calculated for this constant

speed propagation experiment is $900m/sec$. From the strain profile the peak strain value of each gage was used to evaluate the stress intensity factor. These values of the stress intensity factor are plotted as a function of crack length to specimen width ratio in figure(5.5) along with the data for the caustic experiment discussed before. The stress intensity factor value varies between $96MPa\sqrt{m}$ and $134MPa\sqrt{m}$. It is seen that the values are close within the experimental error band accepted for such work.

DCB steel experiment:

This experiment was conducted with six gages on the specimen. The specimen was gradually loaded till it broke. The load at which the corresponding caustic specimen broke was slightly lower and hence the crack arrest length for this experiment is $122mm$ which is slightly larger than the arrest length for the caustic experiment ($108mm$). For comparison sake the crack length has been normalized with respect to the crack arrest length. The stress intensity factor calculated from the peak strain is plotted along with the caustic data in figure(5.6). Only two data points could be obtained because the crack arrested before it could pass below the third gage. The two stress intensity factor values are $89.8MPa\sqrt{m}$ and $81.7Mpa\sqrt{m}$. It is seen from the plot that the values obtained from the two techniques are very close and show similar trend. Another experiment conducted with this geometry gave results which are also shown in figure(5.6). The value of K_I^d is seen to vary between $82.5MPa\sqrt{m}$ and $90.3MPa\sqrt{m}$.

SEN steel experiment 2:

The second steel SEN specimen had the face groove on it. This was done to compare the results with the results from experiments performed using photoelastic coatings presented in reference[5.6]. The load at initiation was $126kN$. The crack tip locations corresponding to the peak strains were taken to be right below the strain gage i.e., $\theta = 90°$[5.7]. Instantaneous stress intensity factor were calcu-

lated from the peak strain using equation(3.30). The results obtained are shown in Fig(5.8) together with the results obtained from the method of photoelasticity. The curve shows an increasing trend as expected for from a single edge notch geometry. It can be seen that the K_I^d values obtained using strain gages are in good agreement with the values obtained from the photoelastic coatings. The average crack velocity observed in the experiment was $630m/sec$. Post mortem analysis of the model confirmed that the specimen failed in brittle fracture with the crack faces perpendicular to the model faces and marked with shallow ridges along the model width. No indication of crack front curving in the specimen thickness direction was found.

SEN aluminum experiment:

The aluminum specimen shown in fig(5.3) was loaded to $83.8kN$ at the time of crack initiation. Strain profiles obtained from the test are shown in Fig(5.9). Dynamic fracture toughness, K_I^d, obtained are plotted as a function of crack length to width ratio in Fig(5.10). The curve shows an increasing trend as expected for from a single edge notch geometry. On the same plot are also shown the results obtained from the method of photoelasticity. It can be seen that the K_I^d values obtained using strain gages are in good agreement with the values obtained from the photoelastic coatings. The crack travelled with almost constant crack velocity. The average crack tip velocity obtained for this experiment was $1075m/s$.

5.5 Summary And Conclusions:

This study illustrates the successful use of strain gages and caustics to determine dynamic stress intensity factors in 4340 steel and 7075-T6 aluminum. The results obtained by using the two techniques under similar conditions match well. Also the results match good with the ones obtained using the technique of photoelastic coatings. The problem encountered with caustics was resetting of the model while loading which called for readjustment and checking of the optical path. In

case of using strain gages for dynamic measurements the accurate determination of instantaneous crack velocity is not possible because of limited number of discrete data points. The interpretation of the experimental data obtained in this chapter in the light of $K_I - \dot{a}$ relationship is discussed in detail in the next chapter.

REFERENCES:

[5.1] Chona,R., Irwin,G.R. and Sanford,R.J., "Influence of Specimen Size and Shape on the Singularity-Dominated Zone," Fracture Mechanics: Fourteenth Symposium, vol. 1: Theory and Analysis, ASTM STP 791, J.C.Lewis and G.Sines eds., ASTM, 1983, pp. I-3-I-23.

[5.2] Beinert,J. and Kalthoff,J.F., "Experimental determination of dynamic stress intensity factors by shadow patterns," Mechanics of Fracture, vol. VII, G.C.Sih, ed., Noordhoff Int. Publishing, London, The Netherlands, 1981.

[5.3] Rosakis,A.J., "Analysis of the Optical Method of Caustics for Dynamic Crack Propagation," Report ONR-79-1 Division of Engineering Brown Univ., March 1979, Engineering Fracture Mechanics, vol.13, 1980, pp. 331-347.

[5.4] Dally,J.W. and Sanford,R.J., "Strain Gage Methods for Measuring the Opening Mode Stress Intensity Factor," SEM Spring Conference Proceedings 1985, Las Vegas, pp. 851-860.

[5.5] Dally,J.W. and Berger,J.R., "A Strain Gage Method for Determining KI and KII in a Mixed Mode Stress Field," Proceedings of the 1986 SEM Spring Conference on Experimental Mechanics, New Orleans, June 8-13, 1986, pp. 603-612.

[5.6] Shukla,A., Agarwal,R.K., and Nigam,H., "Dynamic Fracture studies on 7075-T6 Aluminum and 4340 Steel Using Strain Gages And Photoelastic Coatings," To appear in Journal of Engineering Fracture Mrchanics.

[5.7] Shukla,A., Chona,R., and Agarwal,R.K., "Investigation of Dynamic Fracture Using Strain Gages," Society for Experimental Mechanics, Fall meeting, Houston 1987.

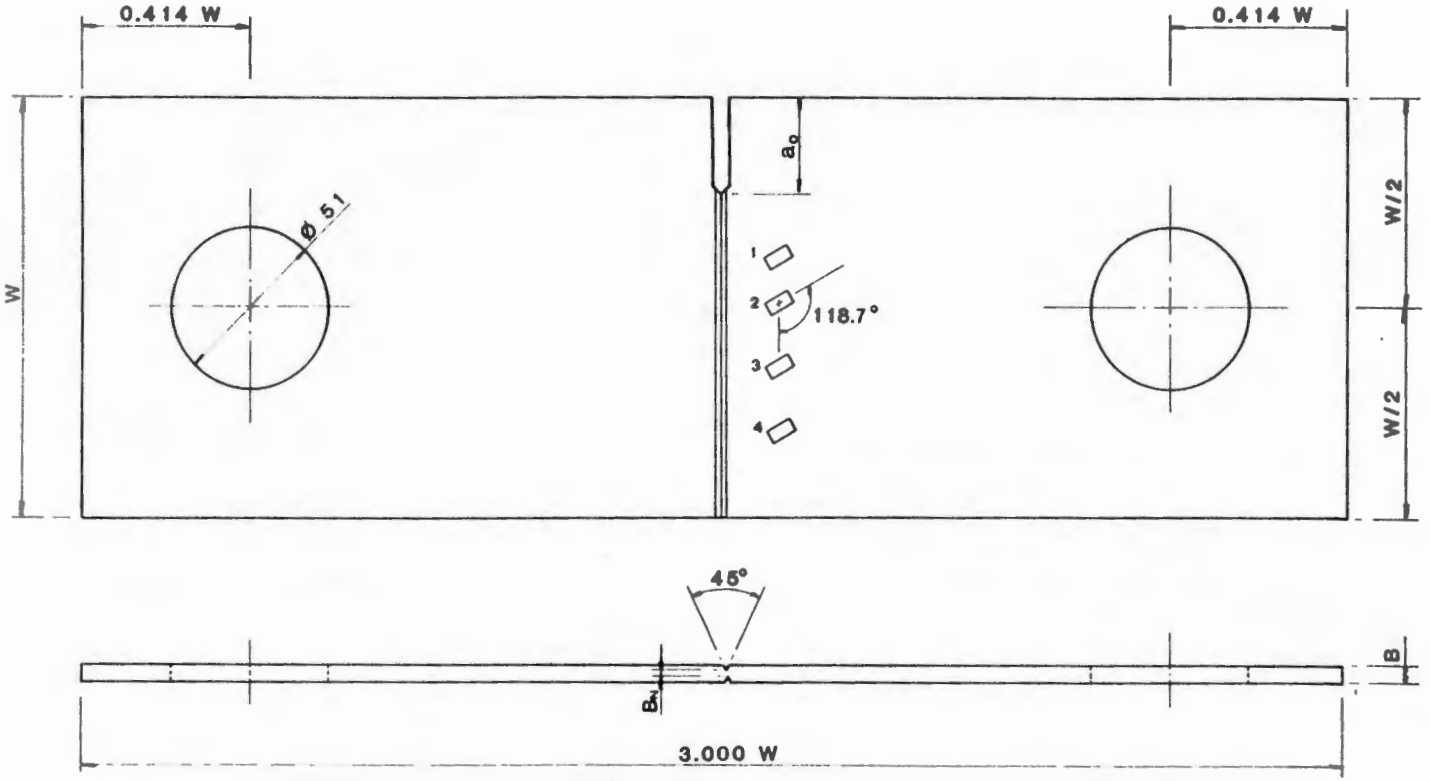

W = 152.0 a_o = 0.25 W B = 6.35 B_N/B = 0.75

Figure 5.1 Geometry of the 4340 steel single edge notch specimen.

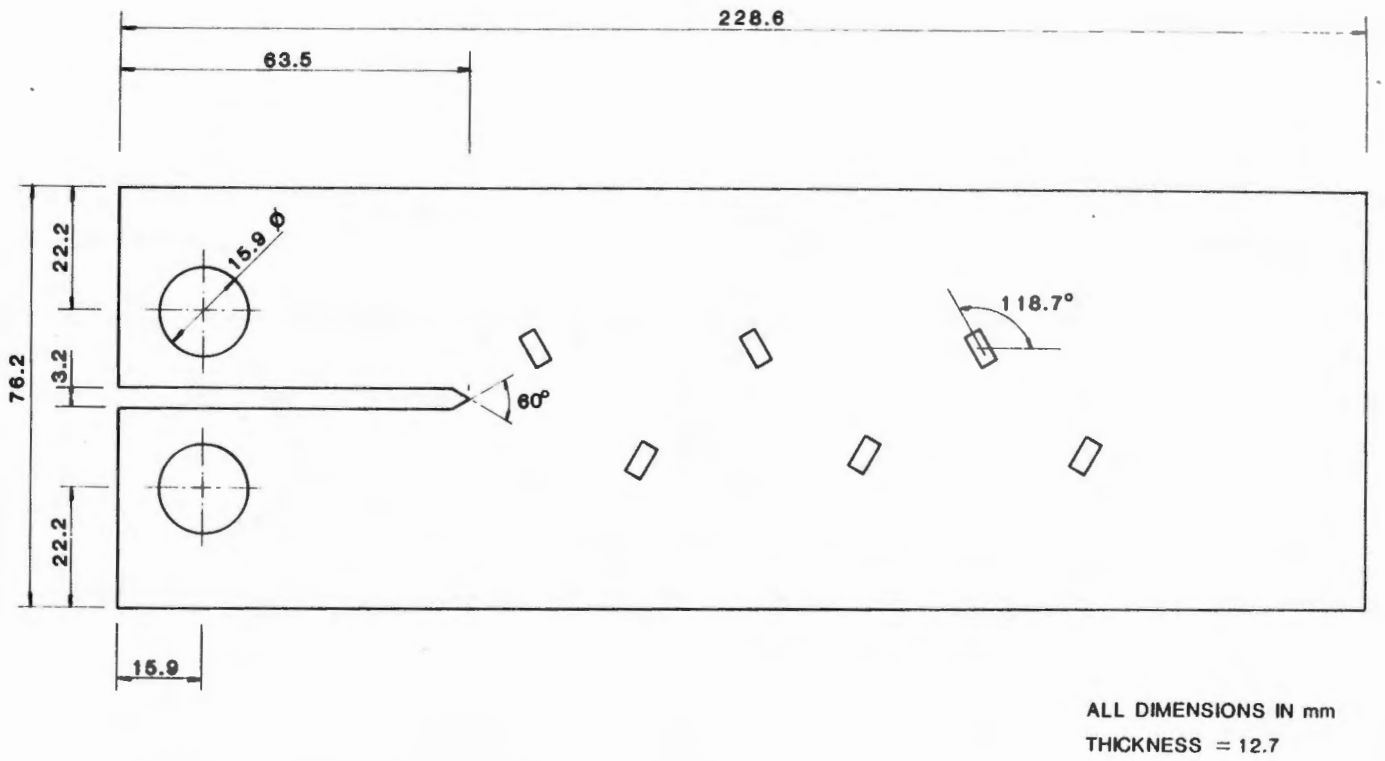

Figure 5.2 Geometry of the 4340 steel double cantilevered beam specimen.

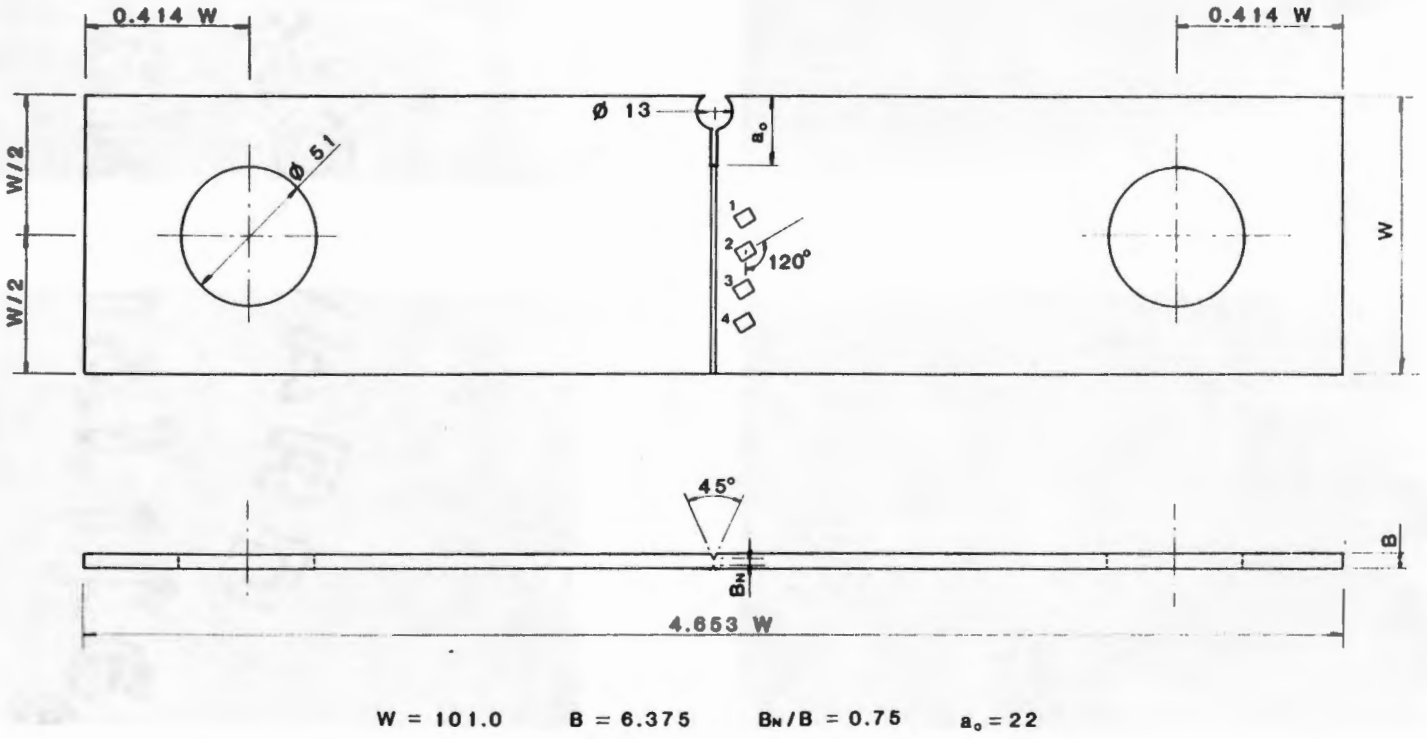

Figure 5.3 Geometry of the 7075-T6 aluminum single edge notch specimen.

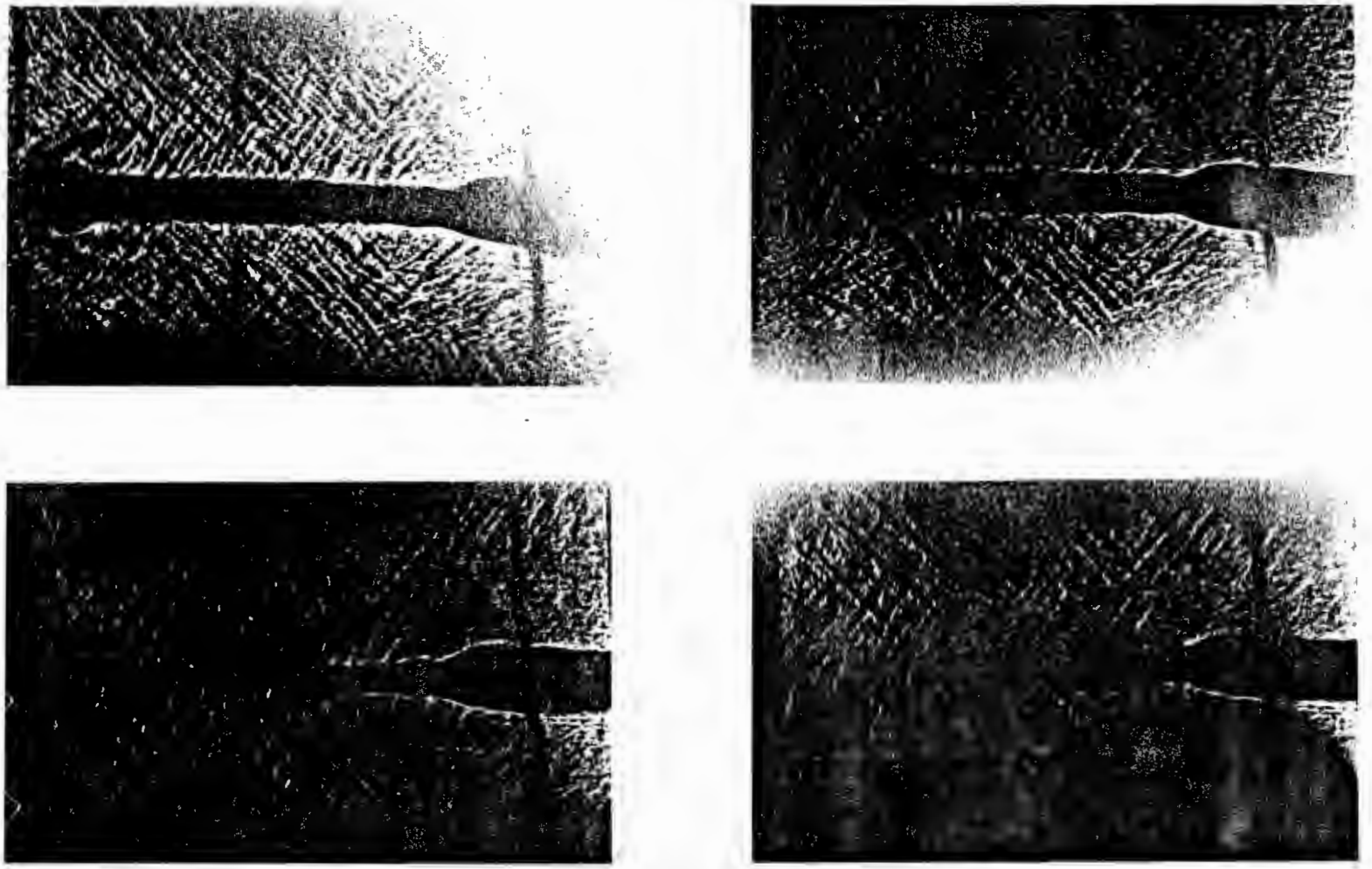

Figure 5.4 Typical caustics obtained from the SEN steel experiment.

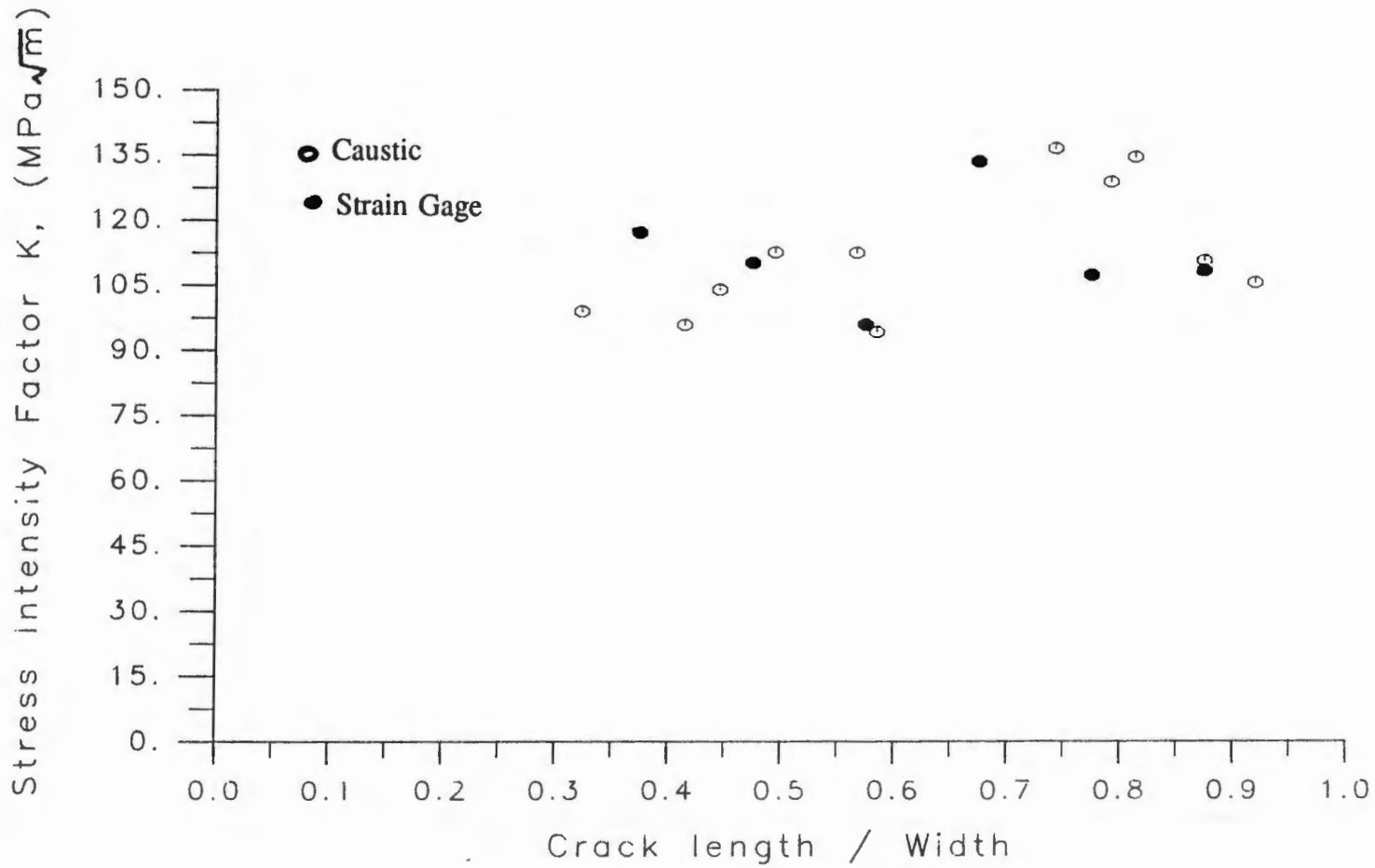

Figure 5.5 K_I^d as a function of crack length for the SEN steel experiment 1.

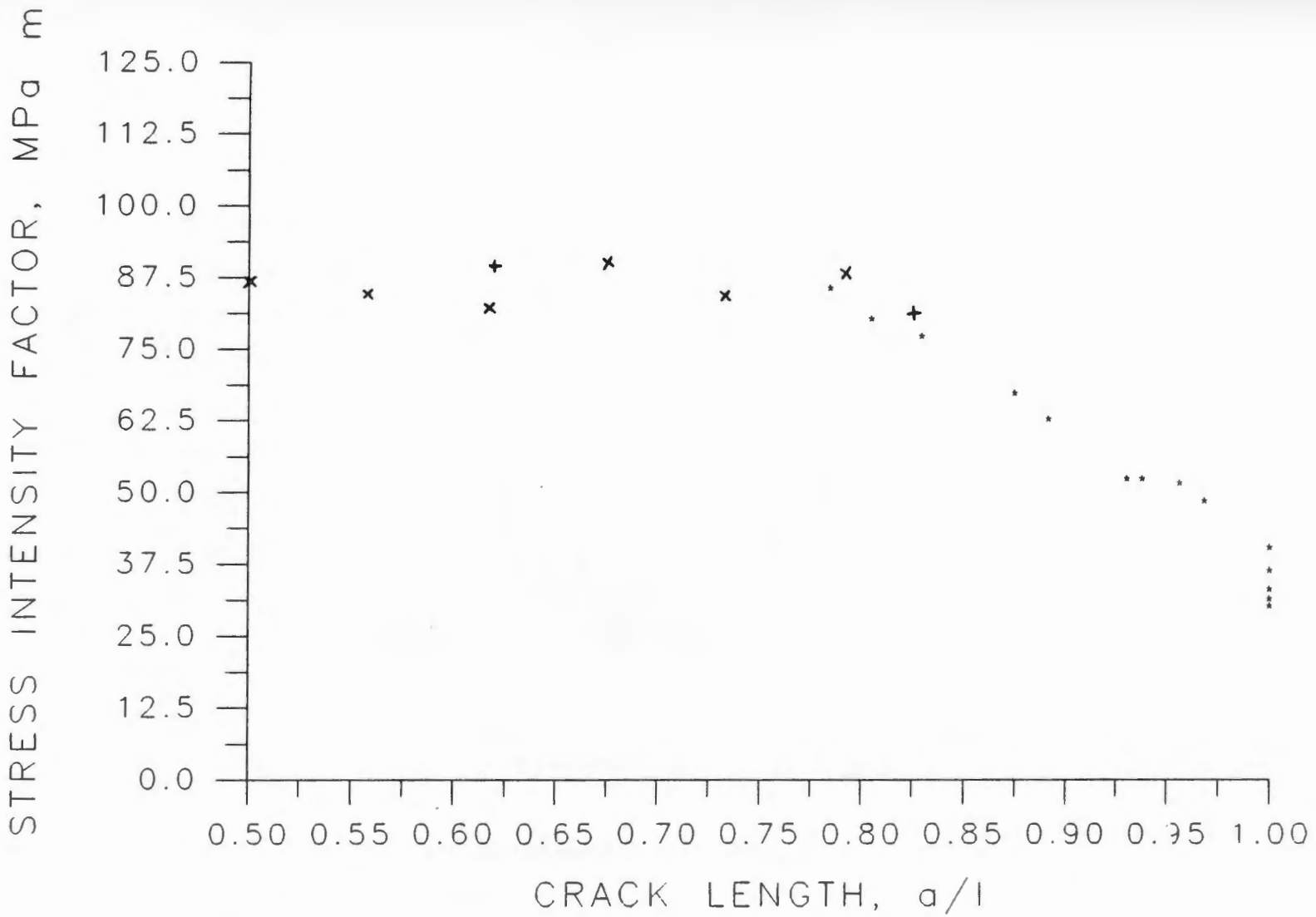

Figure 5.6 K_I^d **as a function of crack length for the DCB steel experiment 1.**

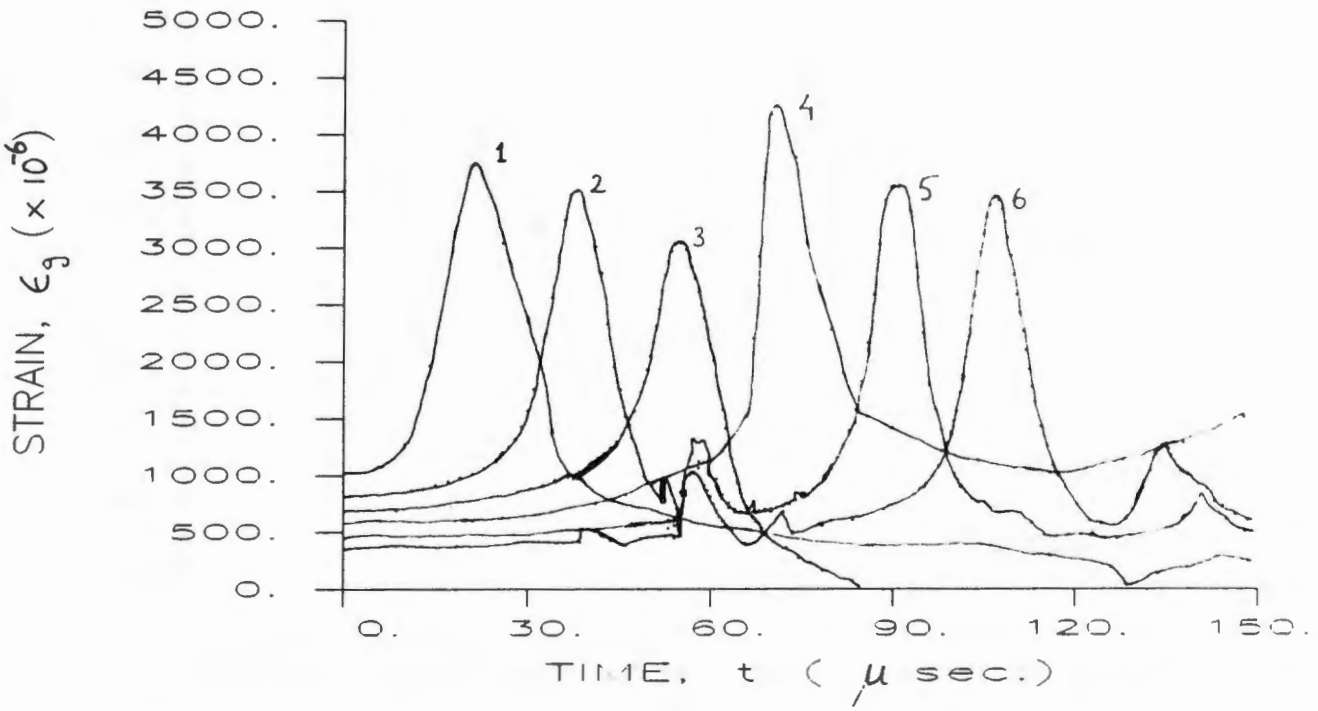

Figure 5.7 Strain profiles obtained from the six gages in the SEN steel experiment 1.

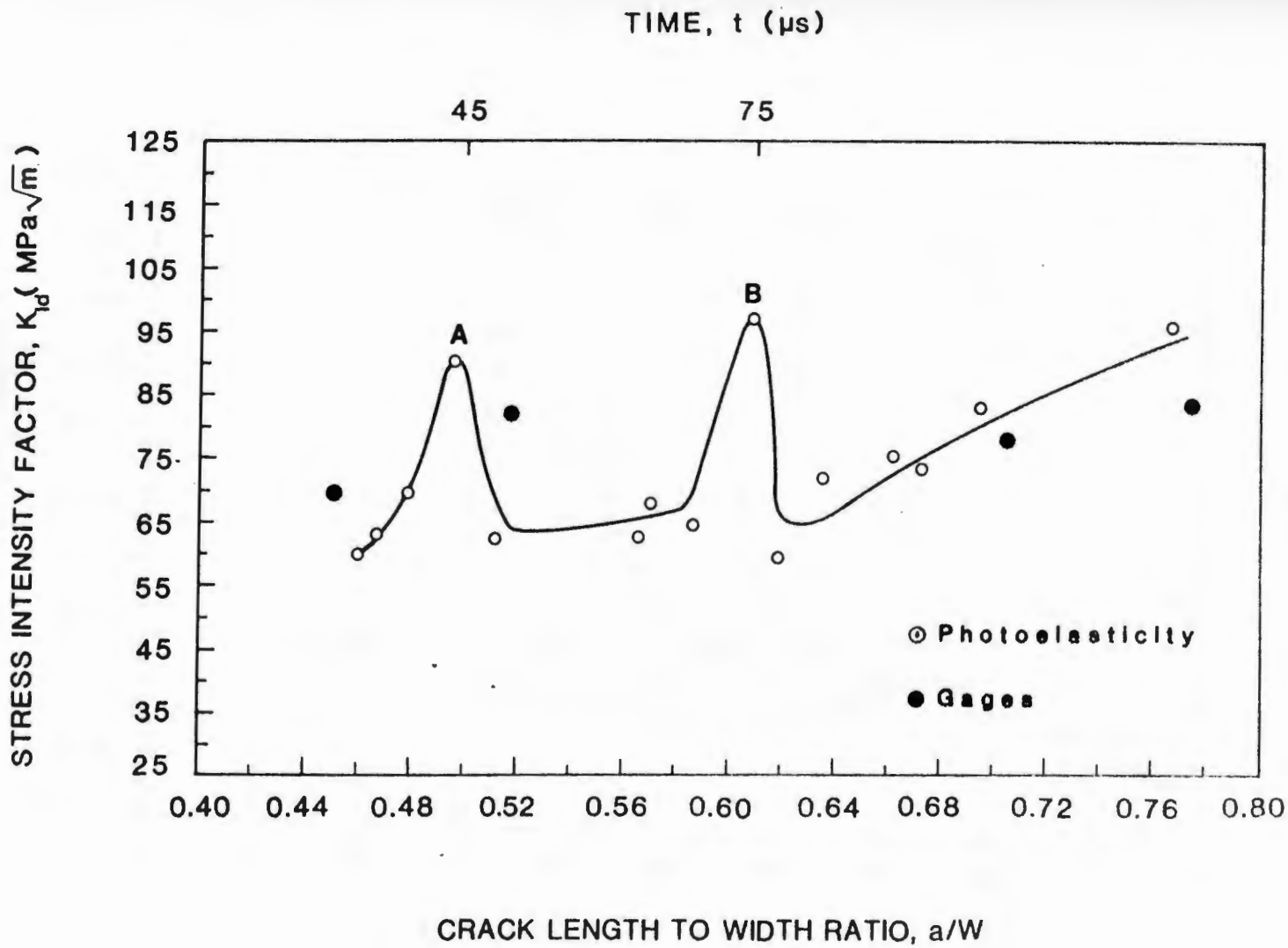

Figure 5.8 K_I^d as a function of crack length for the SEN steel experiment 2.

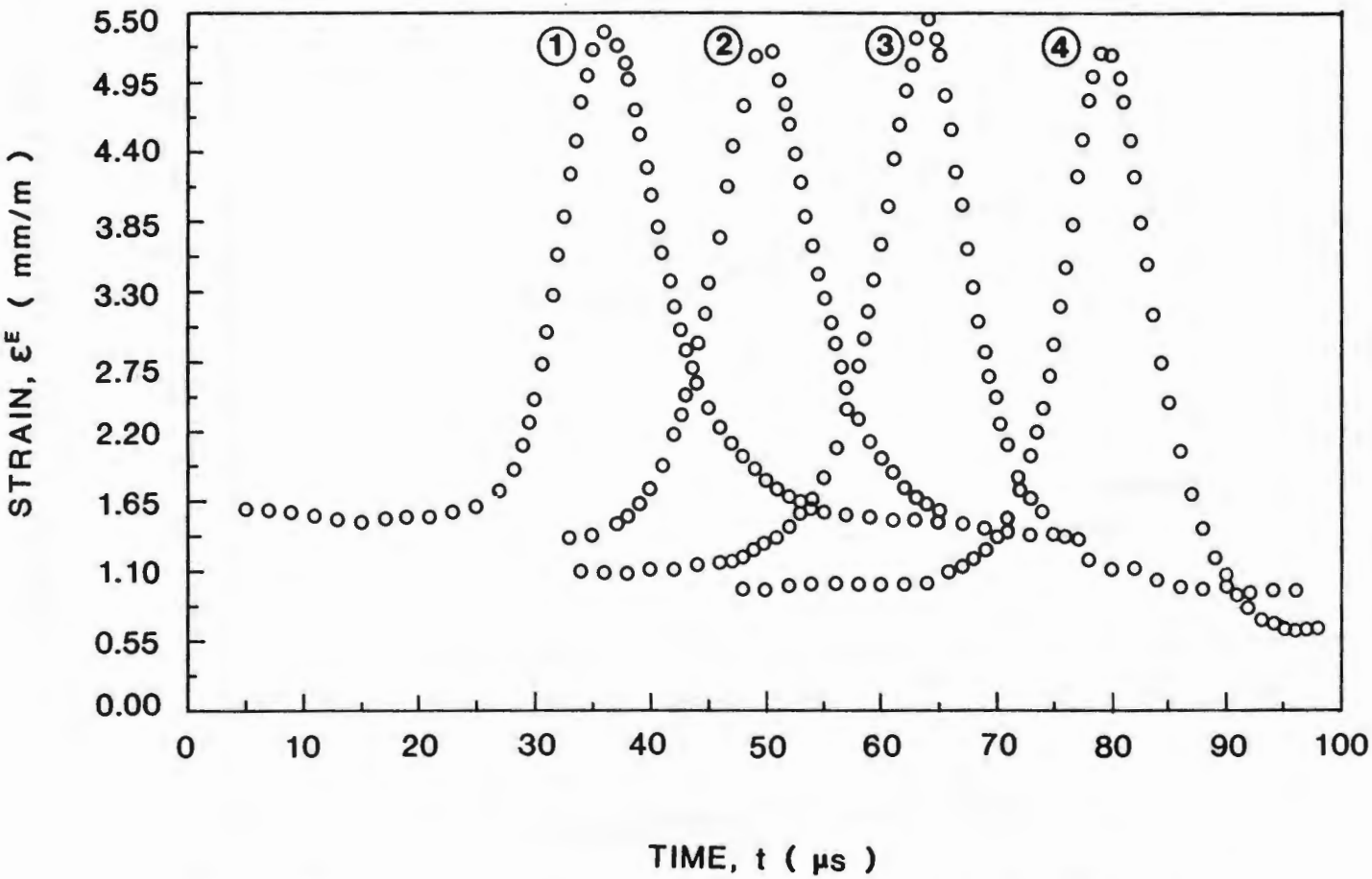

Figure 5.9 Strain profiles obtained from the four gages in the SEN aluminum experiment.

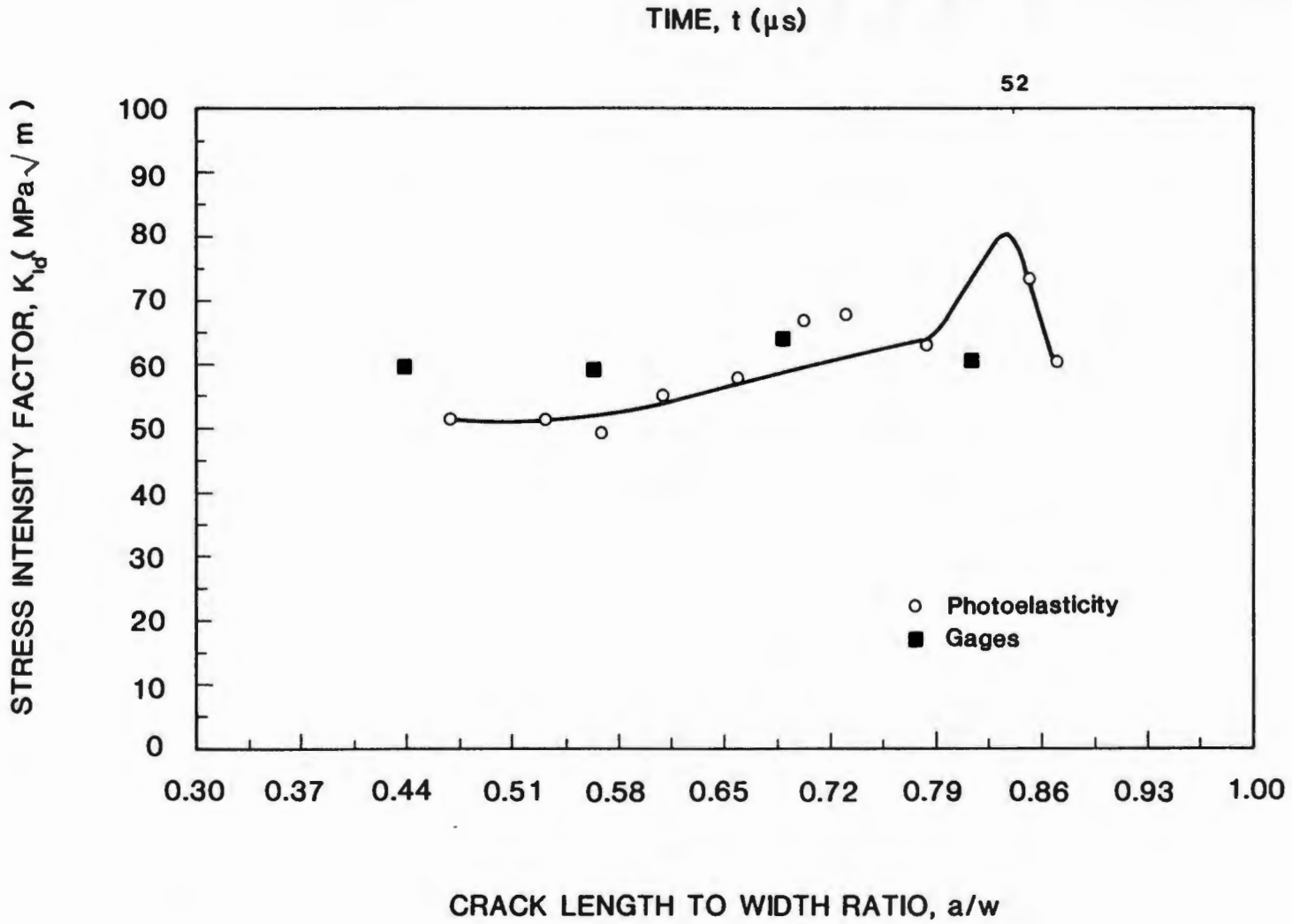

Figure 5.10 K_I^d as a function of crack length for the SEN aluminum experiment.

TABLE 5.1

Mechanical Properties of Steel and Aluminum

PROPERTY	UNITS	4340 STEEL	7075-T6 ALUMINUM
Poisson's ratio	ν	0.30	0.33
Density	ρ (kg/m^3)	7800	2700
Modulus of Elasticity	E (MPa)	210,000	70,000
Wave speed:			
Raleigh wave	c_r (m/s)	3720	3741
Pressure wave	c_1 (m/s)	6201	6236
Shear wave	c_2 (m/s)	3217	2788

CHAPTER 6

RELATIONSHIP BETWEEN K_I^d AND $\dot{a}$

6.1 Introduction:

It is believed that the behavior of a running crack depends on the stress field surrounding it. For linear elastic brittle solids and for elastic- plastic solids under small scale yielding the stress field near the crack tip can usually be described by a single parameter, the stress intensity factor. Thus, intuitively one can expect the crack velocity to depend on the stress intensity factor, i.e., if K_I^d is high the stresses at the crack tip are high and so the crack should advance rapidly. This is only one of the factors which suggests the existence of a relationship between the stress intensity factor, K_I^d, and the crack tip velocity, $\dot{a}$. In actuality, many other factors contribute to determine the dynamic behavior of the crack. Some of the factors are the interaction of crack tip plasticity and inertia, strain rate sensitivity, and local heating at the crack tip.

Studies of this relationship have been performed by many investigators using various experimental techniques on both brittle and ductile materials. A review of the $K_I^d - \dot{a}$ relationship for brittle, linear elastic polymers and metals is given separately in the following section. The data obtained in the dynamic Homalite-100 and 4340 steel experiments is also presented and discussed in the light of the existence and uniqueness of $K_I^d - \dot{a}$ relationship.

6.2 Review of $K_I^d - \dot{a}$ Studies for Non-metals:

The techniques which are primarily being used for the study of dynamic fracture of transparent materials include the methods of caustics and photoelasticity.

In recent years there has been controversy over the data obtained from the two techniques with regard to the dynamic stress intensity factor (K_I^d) versus crack velocity ($\dot{a}$) relationship.

Irwin et.al.[6.1] who used the method of photoelasticity on various types of Homalite 100 specimens obtained the $K_I^d - \dot{a}$ plot shown in Figure(6.1). It is observed that the $K_I^d - \dot{a}$ curve has three distinct regions, the stem, the slope range and the plateau. In the stem region, the crack velocity is independent of K_I^d. Small changes of K_I^d cause considerable changes in the crack velocity up to velocities of about $200m/sec$. The slope range is the transition region covering crack velocities from $200m/sec$ to $381m/sec$. For higher velocities, a large increase in K_I^d is needed even for small increase in $\dot{a}$. This is the plateau region. The highest velocity of crack propagation recorded in these experiments was $432m/sec$. Rossmanith and Irwin[6.2] suggested that the $K_I^d - \dot{a}$ relationship, as obtained from experiments with test specimens, depends in the high velocity region on the type of the test specimen used. Though Dally argued[6.3] that the different results are due to insufficiencies in the current data evaluation procedures and speculated that the $K_I^d - \dot{a}$ curve is unique.

It is noted that the vertical stem of the $K_I^d - \dot{a}$ plot and arrest toughness K_{Ia}^d are independent of the specimen geometry and loading but the horizontal plateau region shows dependence on specimen geometry. Irwin et al[6.1] concluded that K_{Ia}^d can be treated as a material property. Though it has been shown theoretically[6.4] that the maximum crack velocity which can be achieved is $\dot{a} = C_r$, the Raleigh wave speed. This value is not attained for most of the materials in practice because branching occurs at lower velocities and the energy driving the crack is divided.

Kalthoff [6.5] used the method of caustics on Araldite B and obtained a $K_I^d - \dot{a}$ curve shown in Figure(6.2). These curves show strong dependence on specimen geometry. Stress intensity factor values obtained using DCB specimen are up to 20

percent higher than those obtained using SEN specimen.

As opposed to Dally et.al. and Kalthoff who statically loaded the specimens prior to the initiation of the cracks Ravi Chander and Knauss[6.6] applied dynamic loading with an electromagnetic loading device. Their results which are shown in figure(6.3) indicate no relationship between K_I^d and $\dot{a}$. Varying K_I^d values were obtained for any constant velocity. They used the method of caustics with Homalite-100.

Kobayashi[6.7] also concluded that these curves are not unique. To explain the difference in the values for the two types of specimens Kalthoff has differentiated the dynamic stress intensity factor $K_I^d(\dot{a})$, a pure stress field quantity and dynamic fracture toughness $K_{IC}^d(\dot{a})$, a material property and contends that $K_{IC}^d(\dot{a})$ is a lower bound for all the possible $K_I^d(\dot{a})$ curves (from energy considerations). This raises a question whether $K_I^d(\dot{a})$ is unique and completely describes the fracture phenomenon. Experiments have been performed[6.8] to show that $K_I^d(\dot{a})$ has a tendency to be larger than $K_{IC}^d(\dot{a})$.

Noting the confusion which exists presently regarding the uniqueness of $K_I^d - \dot{a}$ relationship it is felt that experiments should be performed under controlled conditions to avoid the scatter in the data arising because of the variation in material properties or because of the use of different techniques of loading or analysis. Keeping this in mind experiments were conducted in an attempt to resolve the confusion. The results of the experiments are discussed below.

6.3 $K_I^d - \dot{a}$ results for Homalite-100:

In this work two series of dynamic experiments were performed on various specimen geometries (fig.4.1) of Homalite-100 specimens cut from the same sheet of material. They were taken out of the same sheet to avoid any variation in material properties which can occur between various castings of the material. One series of experiments was evaluated using the method of photoelasticity and the other by

the method of caustics. Test results were plotted as $K_I^d - t$ plots figures (4.4-4.5 & 4.8-4.10) and the consolidated $K_I^d - \dot{a}$ plot as obtained from the two techniques are presented here. These are compared with each other and with the results obtained by other investigators. The details of the experiments and the results can be found in chapter 4.

Photoelastic Results:

Each photoelastic experiment was systematically analyzed using a two, three, four, five and six parameter stress field representation. A set of 60 data points were randomly selected in the region $0.3 < r/h < 1.0$ where h is the thickness of the material. The region very close to the crack tip was avoided because of the non-linear nature of the stress field as well as the variation of the optical properties in the highly stressed region. The same data set was used for analysis with each higher order model. The values of stress intensity factor obtained from such an analysis are plotted as a function of crack velocity in figure(6.4a-e). Finally, figure(6.4f) shows the best results which were decided after looking at the fringe order error term and the comparison of the fringe replots with the actual experimental data.

It should be noted that the two parameter analysis shows the least scatter but this can be quite misleading as the values themselves are not correct as observed in the fringe pattern replots and the fringe order error terms. At this point it must be mentioned that most of the existing data in the literature[6.9,6.1] has been analyzed with two parameter analysis. It is pointed out that earlier statements[6.10] that the scatter in the data decreases as higher order models are employed is incorrect. Another point to be noted here is that the arrest toughness K_{Ia}^d value does increase in going from a two parameter to any of the higher order models used.

Figure(6.5) which shows the final $K_I^d - \dot{a}$ plot can be compared with the corresponding plot obtained by Kalthoff as shown in figure(6.2). Kalthoff concluded that the $K_I^d - \dot{a}$ plots are geometry dependent and obtained two distinct plots for

DCB and EPL-SEN experiments respectively. His results also showed that the DCB section data of DCB-SEN specimen fell on the DCB curve and the SEN section data fell on the EPL-SEN curve. Such a trend is not observed in this work. In the plateau and transition region each curve is distinct and all these curves show tendency to merge in the stem region. This is consistent with the concept that K_{Ia}^{d} is a unique material property. The value of K_{Ia}^{d} as obtained from this graph is $0.61MPa\sqrt{m}$.

Caustics Results:

The analysis of caustic experiment involved the determination of the diameter of the caustic and the location of the crack tip. The diameter value is used to evaluate the stress intensity factor and also to determine the crack tip location. The plot of stress intensity factor as a function of instantaneous crack tip velocity for various specimen geometries is given in figure 6.6. (details of these experiments are given in chapter 4). It can be noticed that the general behavior of the curve observed by the two techniques is the same. The value of K_{Ia}^{d} obtained is $0.31MPa\sqrt{m}$ which is considerably lower than the value obtained from the photoelastic data.

Since, in the case of caustic the crack tip is not directly visible, its location is estimated by subtracting a fraction of the caustic diameter ($0.518D$) from the beginning of the crack to the end of the caustic. It was found that the crack length data thus obtained had much more scatter than the corresponding photoelastic data where the crack tip location is easier to determine. The scatter leads to difficulty in the determination of velocities. Figure 6.7a and 6.7b shows plots of crack length versus time for two specimen geometries, one with constant velocity (SEN) and one with varying velocity (DCB) for both photoelastic and caustic experiments. It should be noted that in dynamic experiments with finite geometries the scattered waves from the boundaries can drastically effect the crack behavior. As shown in figure 6.8 from[6.11] the stress intensity factor fluctuations are tremendous but variations in velocity are not perceptible. This is because of discrete number of data

points that are available and because generally a 3 point or 5 point curve fitting is used to determine velocity from crack tip locations. Errors of the order of 10 percent are generally expected in velocities.

6.4 Review of $K_I^d - \dot{a}$ Studies for Metals:

Many studies have been performed to determine the $K_I^d - \dot{a}$ relationship. These studies include both experimental and numerical methods. Following is a brief overview of the various relevent studies.

Kobayashi and Dally[6.12] have used birefringent coatings to study dynamic fracture in 4340 steel specimens. The experiments were analyzed to obtain the $K_I^d - \dot{a}$ behavior for the material. Their results are shown in figure 6.9. It can be noticed that the dynamic stress intensity factor increases with velocity as was seen for Homalite-100 but there is no distinct stem or plateau region. The data from specimens 348 and 362 are in agreement and show the same trend of increasing K_I^d with the crack velocity. Apparently the heat treatment for specimen 375 was different which resulted in a material with a lower terminal velocity and lower K_{Ia}^d.

Bilek[6.13] has performed tests on DCB specimens of 4340 steel. He has used both the slow wedging and rapid wedging methods for testing. His results are shown in figure 6.10. It is seen that K_I^d slightly drops as the velocity is increased and for velocities greater than $1000m/sec$ the variation in K_I^d is steep. The general behavior of all the $K_I^d - \dot{a}$ data presented here follows the same trend as observed by Kobayashi and Dally[6.12] and also compares well with the superimposed results of Hahn et al.[6.14] and Angelino[6.15].

Kanazawa et al.[6.16] Performed experiments using DCB and SEN steel specimens. The crack tip position was recorded using gages placed $3cm$ apart. The average velocity thus obtained was used in conjunction with a dynamic finite difference code. They obtained interesting results for SEN specimens with temprature increasing along the crack length. As the crack propagated into the higher temper-

ature region it decelerated to an arrest. The $K_I^d - \dot{a}$ plots for various temperatures shown in figure 6.11 predict such a behavior. The fracture toughness $K_{IC}^d(\dot{a})$ increases with temperature, however the stress intensity factor K_I^d available is nearly constant. Hence, to satisfy the fracture criterion (4.1) the crack must slow down until $K_{IC}^d(\dot{a}) = K_I^d$[6.17]. Cumulative results for $-40°C$ are given in figure 6.12.

Kobayashi et al.[6.18] have also reported similar trend for 4340 steel tests. Rosakis[6.19] has used the method of caustics for dynamic study of fracture in 4340 steel. The $K_I^d - \dot{a}$ curve obtained by him is shown in fig 6.13.

Freund and Douglas[6.20] are the first ones to analytically and numerically study the effect of inertia on a dynamically propagating mode III crack in elastic plastic and elastic viscoplastic materials. From the observed strain distribution they concluded that due to material inertia the level of plastic strain is significantly reduced from its corresponding slow crack growth levels. Combining this conclusion with the requirement of a fixed level of plastic strain at a critical distance in front of the crack tip one expects that for crack growth to occur, K_{III}^d would increase with $\dot{a}$ as shown in figure 6.14.

Lam and Freund[6.21] have analyzed the elastic-plastic, plain strain, mode I problem to develop a theoretical relation between K_{IC}^d and $\dot{a}$. They have related the stress intensity factor to the near tip crack opening displacement through a full field numerical solution. There results are shown in figure 6.15 which shows the variation of normalized stress intensity factor with normalized crack speed for different values of δ_c/r_m. δ_c is the critical value of the crack opening displacement at a characteristic distance r_m. Here also an increase in the stress intensity factor is observed with crack tip velocity.

Freund and Hutchinson[6.22] have studied high strain rate crack growth in rate dependent plastic solids. For the material model used it was shown that the elastic strain rates dominate near the crack tip. Thus the near crack tip field has

the same $r^{-1/2}$ singularity as an elastic material, but with a different amplitude factor. At higher crack tip velocities the fracture toughness increases sharply with the increasing crack velocities. This is similar to the case of rate independent materials.

Most of the analytical work done is with the constant crack speed assumption. Brickstad[6.23] performed a set of experiments to investigate the effect of crack tip acceleration, $\ddot{a}$. Using a streaching screw on the side of the specimen away from the machined precrack, an initially increasing and then decreasing K_I^d field was obtained. This provided a crack growth with both acceleration and deceleration. The results from this study are shown in figure 6.16 where K_I^d and $\dot{a}$ have been plotted as functions of crack length, a for an experiment. It can be seen that both the quantities show same trend through out the crack propagation. Figure 6.17 shows data from many specimens. It indicates dependence of K_I^d on $\dot{a}$ but not on $\ddot{a}$.

6.5 $K_I^d - \dot{a}$ results for 4340 steel:

Dynamic tests were performed on heat treated 4340 steel. The details of the heat treatment and the experimental conditions are discussed in chapter 5. The heat treatment used is the same as that by Rosakis[6.21] and hence the results are compared with the ones obtained by him. Four experiments were performed using the techniques of caustics and strain gages. The specimen geometries studied included the single edge notch and the double cantilevered beam.

The single edge notch specimes were constant velocity tests. The results obtained are given in figure 6.18 along with Rosakis's results. The data from these appear as vertical points in the high velocity region. The highest value of K_I^d recorded in these experiments was $137MPa\sqrt{m}$. The experiments performed with the DCB geometry gave decreasing velocity for the crack. It can be seen that the

results follow the same trend as has been predicted by many investigators. At lower velocities the K_I^d increases slowly but as the velocity increases to around $800m/sec$ the rate of increase of the stress intensity factor increases. In brittle materials like Homalite 100 when the crack is moving with high velocities and the stress intensity factor is high the crack branching occurs. Though there has been various attempts to attain high dynamic stress intensity factors in metals, branching in metals has not yet been reported.

6.6 Conclusions:

The results from a series of dynamic experiments performed with four different geometries of Homalite 100 show that the $K_I^d - \dot{a}$ curve is distinct for each geometry in the plateau and the transition region indicating that a single parameter characterization of dynamic fracture in terms of K_I^d may not be justified in the high velocity region. However, these curves tend to merge in the vertical stem region indicating that the arrest toughness K_{Ia}^d is unique in brittle materials. The results differ from those of Kalthoff's[6.5] who used similar specimen geometries with the method of caustics. Their conclusion that each geometry produces distinct $K_I^d - \dot{a}$ curve is not seen here.

In case of 4340 steel it is observed that the $K_I^d - \dot{a}$ curve shows a behavior where the dynamic stress intensity factor increases with velocity. The increase in K_I^d is small for lower velocities but for velocities greater than $1000m/sec$ the rate of increase is very high. One major problem encountered in all dynamic experiments is the determination of velocity. Better methods of determining velocity are required to be able to assess the uniqueness of the $K_I^d - \dot{a}$ behavior.

References:

[6.1] Irwin,G.R., Dally,J.W, Kobayashi,T., Fourney,W.L., Etheridge,M.J. and Rossmanith,H.P., "On he Determination of the $\dot{a}$ -K Relationship for Birefringent

Polymers," Experimental Mechanics, vol. 19, No. 4, April 1979, pp. 121-128.

[6.2] Rossmanith,H.P. and Irwin,G.R., "Analysis of Dynamic Isochromatic Crack Tip Stress Patterns," University of Maryland Report.

[6.3] Dally,J.W., Kobayashi,T. and Fourney,W.L., "Influences of Specimen Geometry on Crack Propagation and Arrest Behavior," VIth International Conference of Experimental Stress Analysis, Society for Experimental Stress Analysis, Munich, West Germany, September 1978, pp. 18-22.

[6.4] Yoffe,E.H., "The Moving Griffith Crack," Philosophical Magazine, Series 7, 42, 739(1951).

[6.5] Kalthoff,J.F., "On some Current problems in Experimental Fracture Dynamics," Workshop on Dynamic Fracture, California Institute of Technology, February 11-25, 1983.

[6.6] Ravi-Chander,K. and Knauss,W.G., "Process Controlling the Dynamic Fracture of Brittle Solids," Workshop on Dynamic Fracture, Calif. Inst. of Tech., February 1983, pp. 119-128.

[6.7] Kobayashi,A.S. and Mall,S., "Dynamic Fracture Toughness of Homalite-100," Experimental Mechanics, 18(1978), pp. 11-18.

[6.8] Shockey,D.A., Kalthoff,J.F., Klemm,W. and Winkler,S., "Simultaneous Measurements of Stress Intensity and Toughness for Fast Running Cracks in Steel," Experimental Mechanics, Vol. 23, No. 2, June 1983.

[6.9] Dally,J.W., "Dynamic Photoelastic Studies of Fracture," Experimental Mechanics, vol. 19, No. 10, October 1979. pp. 349-361.

[6.10] Chona,R., Fourney,W.L., Sanford,R.J. and Shukla,A., "Determining Stress Intensity Factor for Running Cracks," Proceedings of CFC10, "Modeling Problems in Crack Tip Mechanics," at Univ. of Waterloo, August 24-26, 1983.

[6.11] Kalthoff,J.F. et al, "Experimental Analysis of Dynamic Effects in Different Crack Arrest Test Specimens," ASTM STP 711 - Crack Arrest Methodology

and Applications, American Society for Testing and Materials, Philadelphia, USA, 1980, 109-127.

[6.12] Kobayashi,T., and Dally,J.W., "Dynamic Photoelastic Determination of the $\dot{a}-K$ Relation for 4340 Alloy Steel," Crack Arrest Methodology and Applications, ASTM STP 711, G.T.Hahn and M.F.Kanninen, Eds., American Society for Testing Materials, 1980, pp. 189-210.

[6.13] Bilek,Z., "Some Comments on Dynamic Crack Propagation in a High Strength Steel," Crack Arrest Methodology and Applications, ASTM STP 711, G.T. Hahn and M.F.Kanninen, Eds., American Society for Testing Materials, 1980, pp. 240-247.

[6.14] Hahn, G.T., et al., Reports to the U.S. Nuclear Regulatory Comission, Batelle Columbus Laboratories, 1974-1976.

[6.15] Angelino, G.C., "Influence of the Geometry on Unstable Crack Extension and Determination of Dynamic Fracture Mechanics Parameters," Fast Fracture and Crack Arrest, ASTM STP 627, American Society for Testing and Materials, 1978, pp. 392-407.

[6.16] Kanazawa,T., Machida,S., and Teramoto,T., "Study on Fast Fracture and Crack Arrest," Experimental Mechanics, vol. 38, 1981, pp. 78-88.

[6.17] Zehnder,A.T., "Dynamic Fracture Initiation and Propagation in Metals: Experimental Results and Techniques," Ph.D. Thesis, California Institute of Technology, 1987,

[6.18] Kobayashi,A.S., et al., "Dynamic Fracture Toughness," International Journal of Fracture, vol. 30, 1986, pp. 275-286.

[6.19] Rosakis, A.J., "Experimental Determination of the Fracture Initiation and Dynamic Crack Propagation Resistance of Structural Steels by the Optical Method of Caustics," Ph.D. Thesis, Brown University, June 1982.

[6.20] Freund,L.B., and Douglas,A., "The Influence of Inertia on Elastic Plastic An-

tiplane Shear Crack Growth," Journal of Mechanics and Physics of Solids, vol. 30, 1982, pp. 169-191.

[6.21] Lam,P.S., and Freund,L.B., "Analysis of Dynamic Crack Growth of a Tensile Crack in an Elastic Plastic Material," Journal of Mechanics and Physics of Solids, vol. 33, 1985, pp. 153-167.

[6.22] Freund,L.B., and Hutchinson,J.W., "High Strain-Rate Crack Growth in Rate Dependent Plastic Solids," Journal of Mechanics and Physics of Solids, vol. 33, 1985, pp. 169-191.

[6.23] Brickstad,B., "A FEM Analysis of Crack Arrest Experiments," International Journal of Fracture, vol. 21, 1983, pp. 177-194.

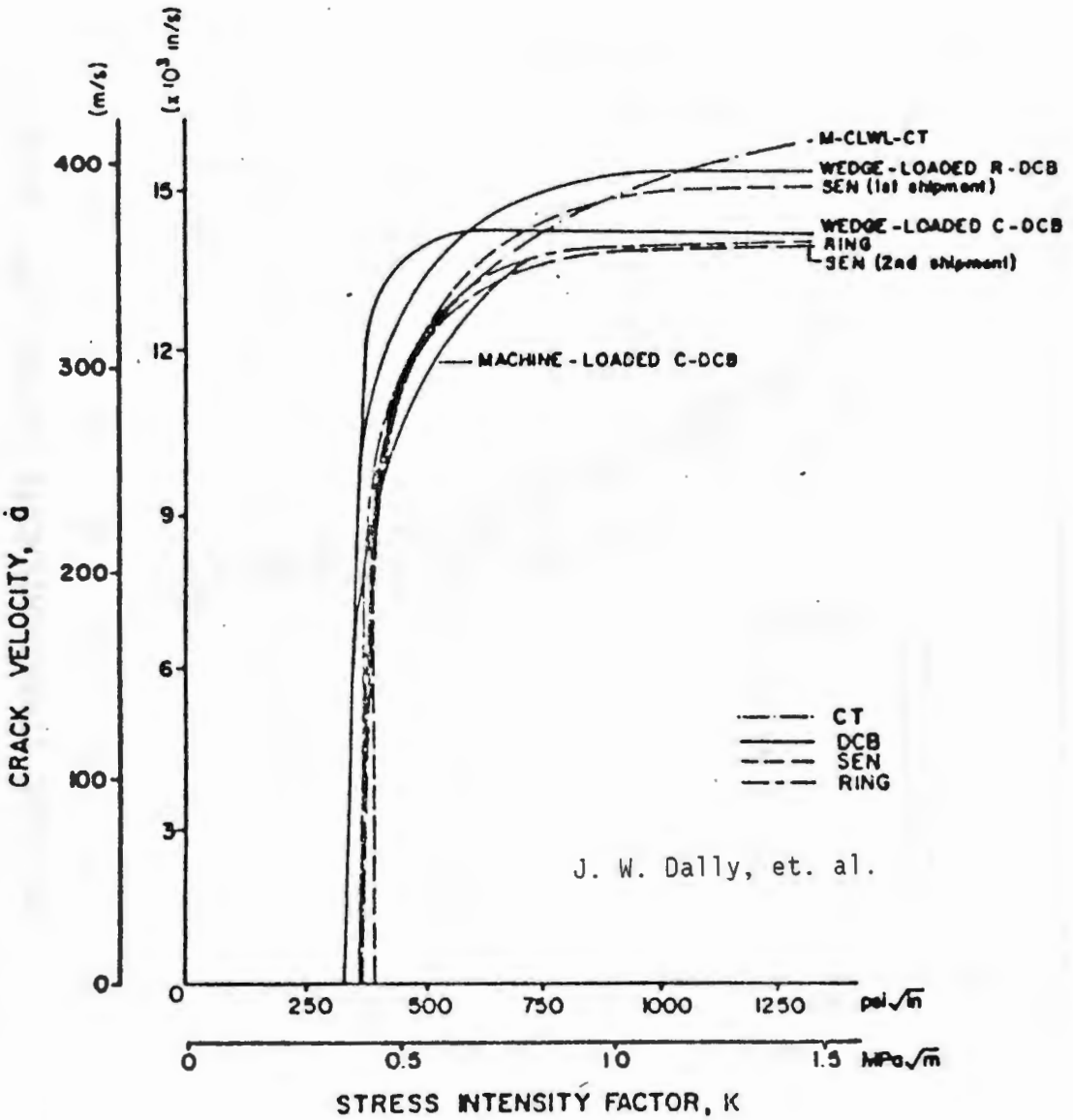

Figure 6.1 The relationship between crack velocity and the instantaneous stress intensity factor for Homalite 100.[6.1]

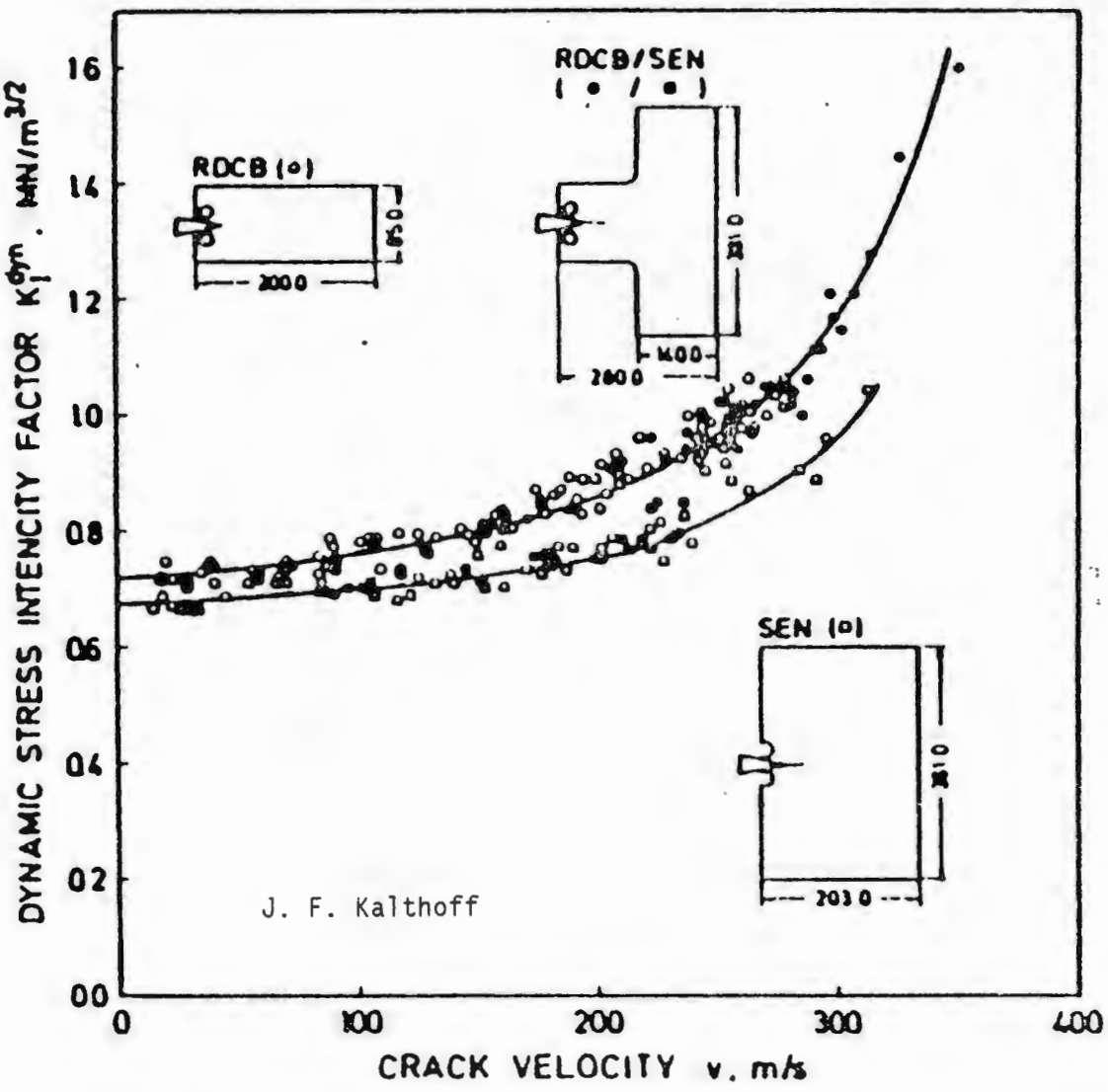

Figure 6.2 The relationship between crack velocity and the instantaneous stress intensity factor for Araldite B.[6.5]

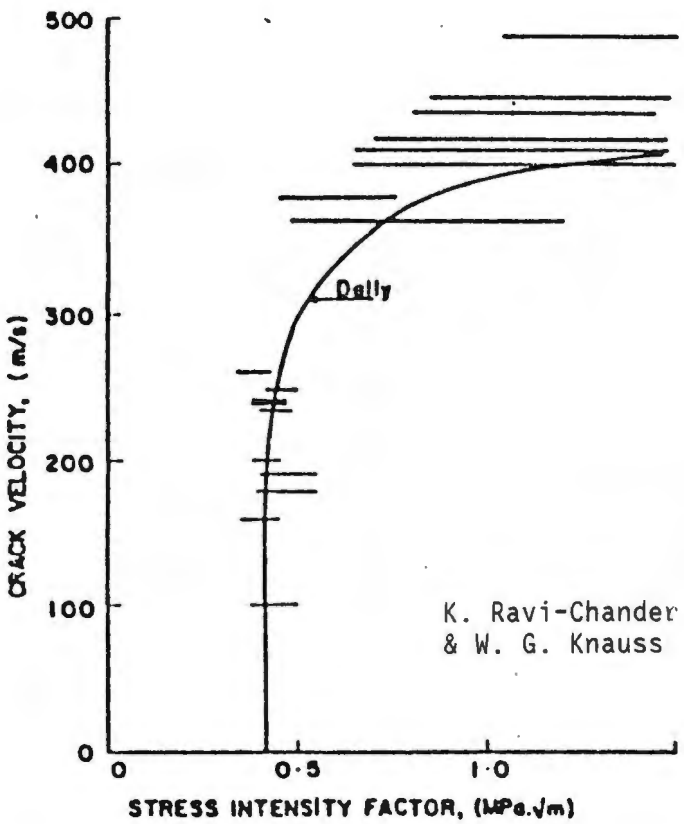

Figure 6.3 The relationship between crack velocity and the instantaneous stress intensity factor for Homalite 100.[6.6]

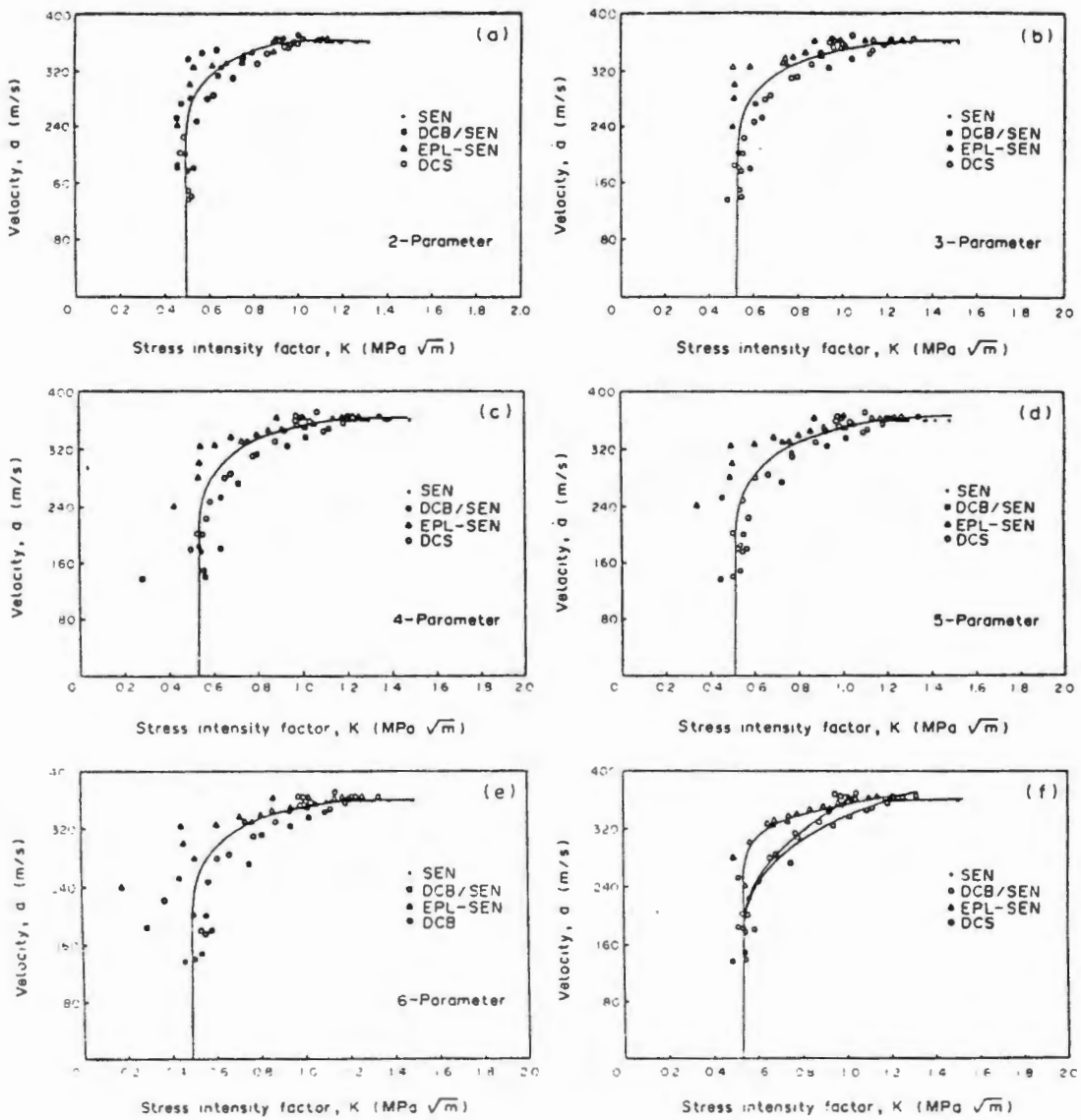

Figure 6.4 $K_I^d - \dot{a}$ relationship for Homalite 100. (a) Two parameter, (b) three parameter, (c) four parameter, (d) five parameter and (f) closest obtained values.

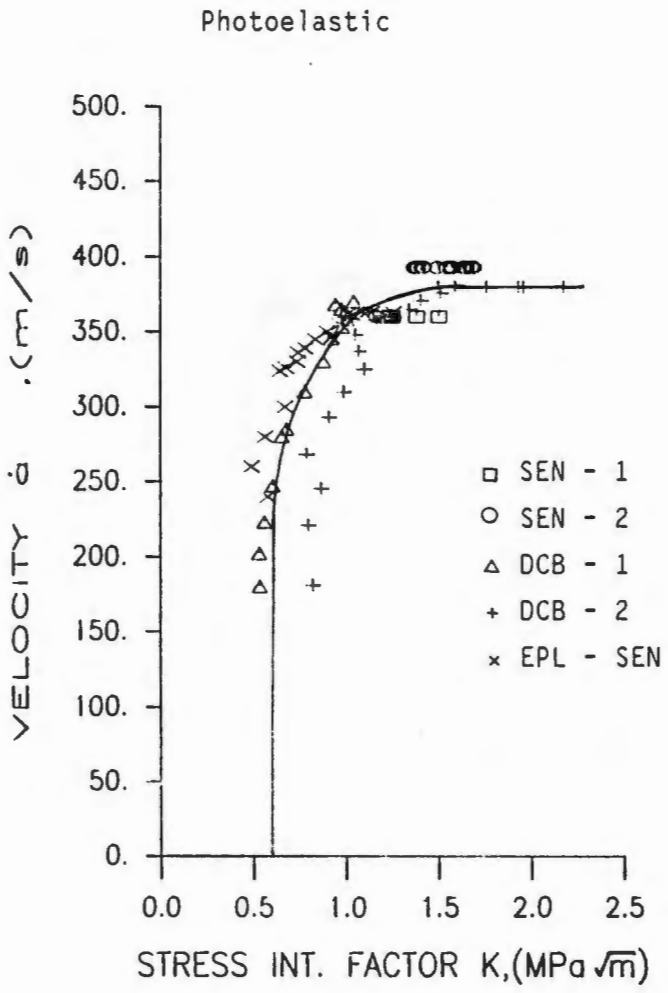

Figure 6.5 $K_I^d - \dot{a}$ relationship for Homalite 100 using photoelasticity.

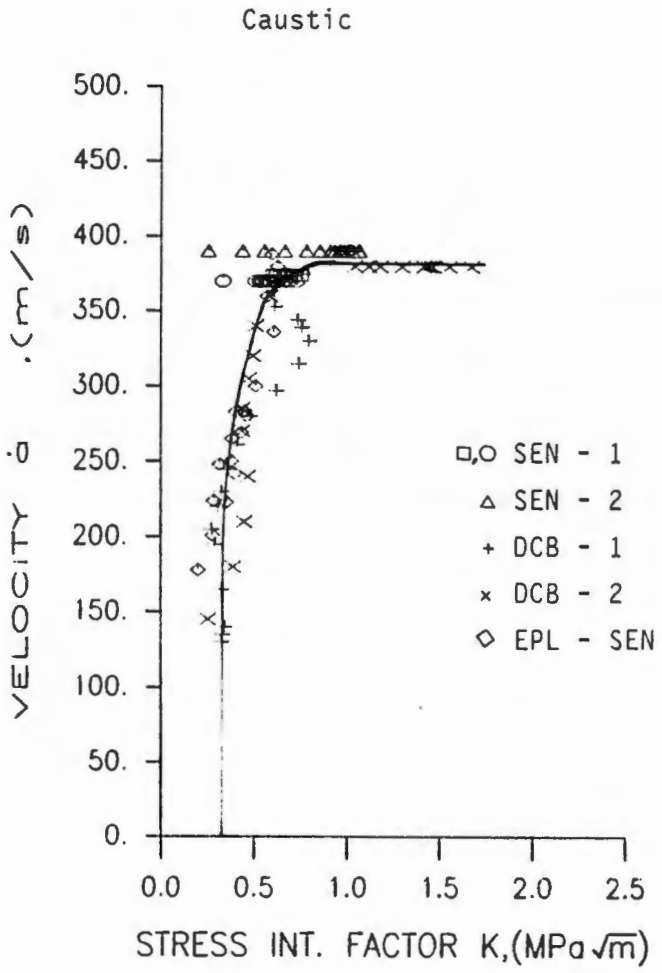

Figure 6.6 $K_I^d - \dot{a}$ relationship for Homalite 100 using caustics.

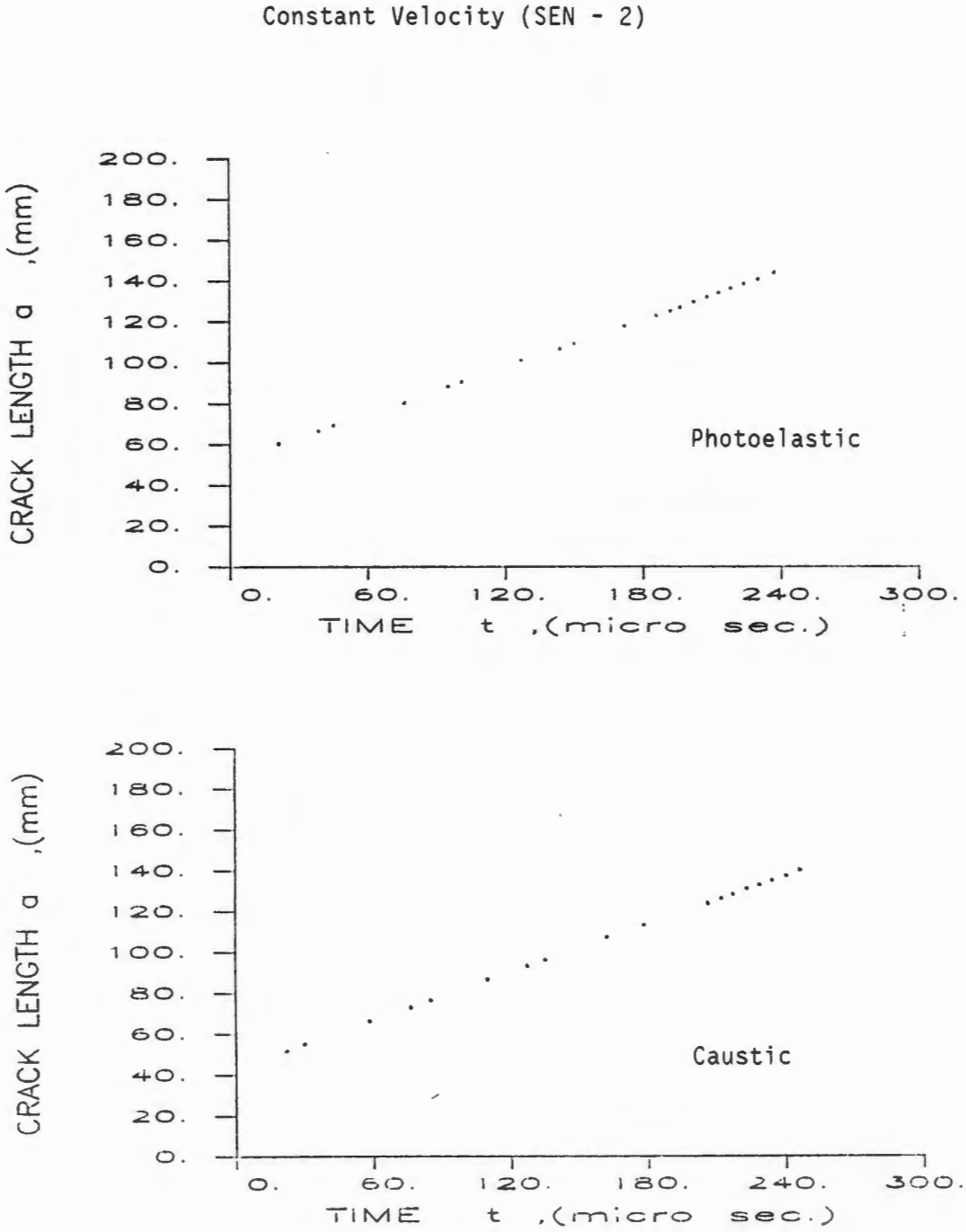

Figure 6.7a Crack length versus time plot for caustic and photoelastic experiment with constant velocity.

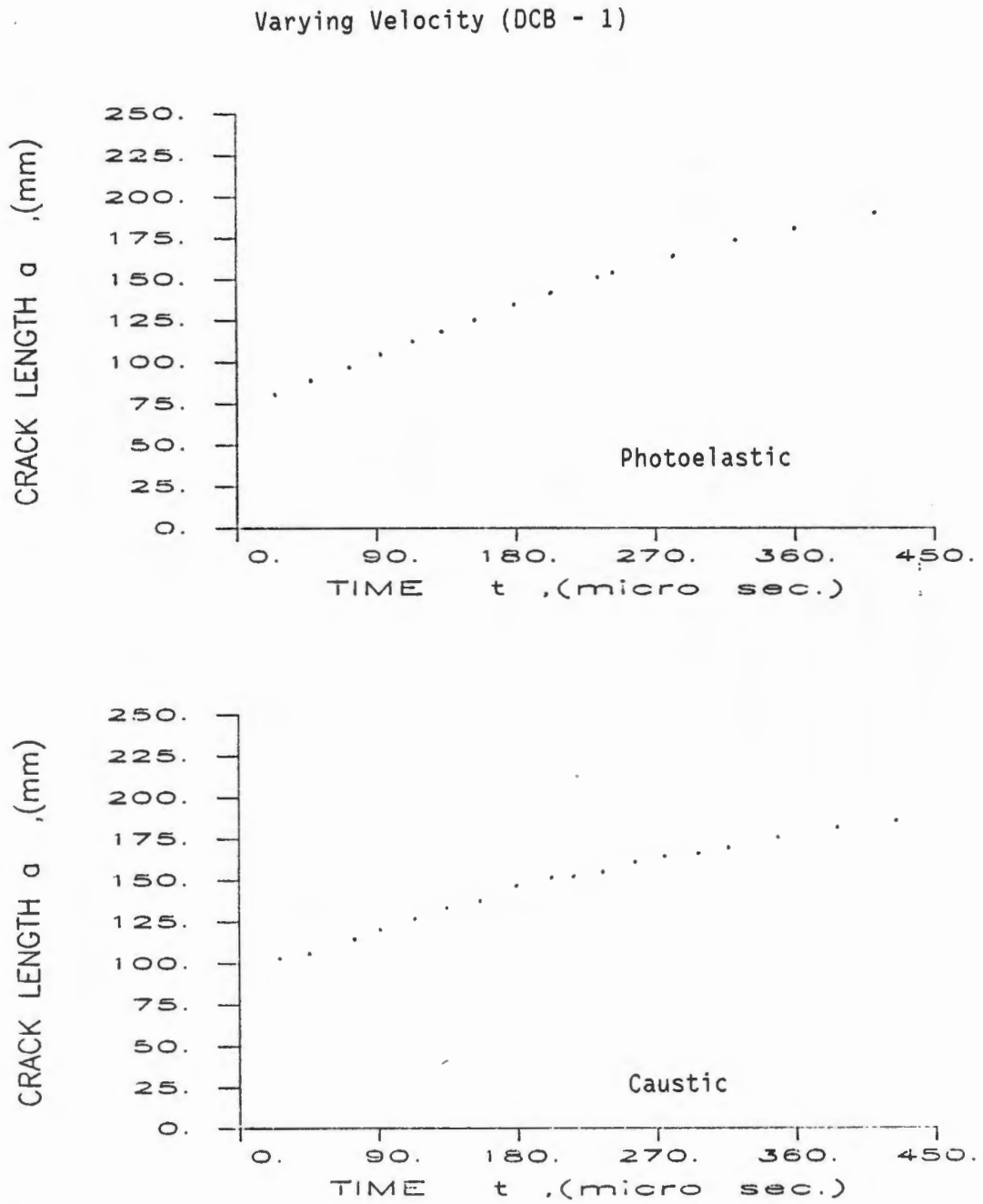

Figure 6.7b Crack length versus time plot for caustic and photoelastic experiment with varying velocity.

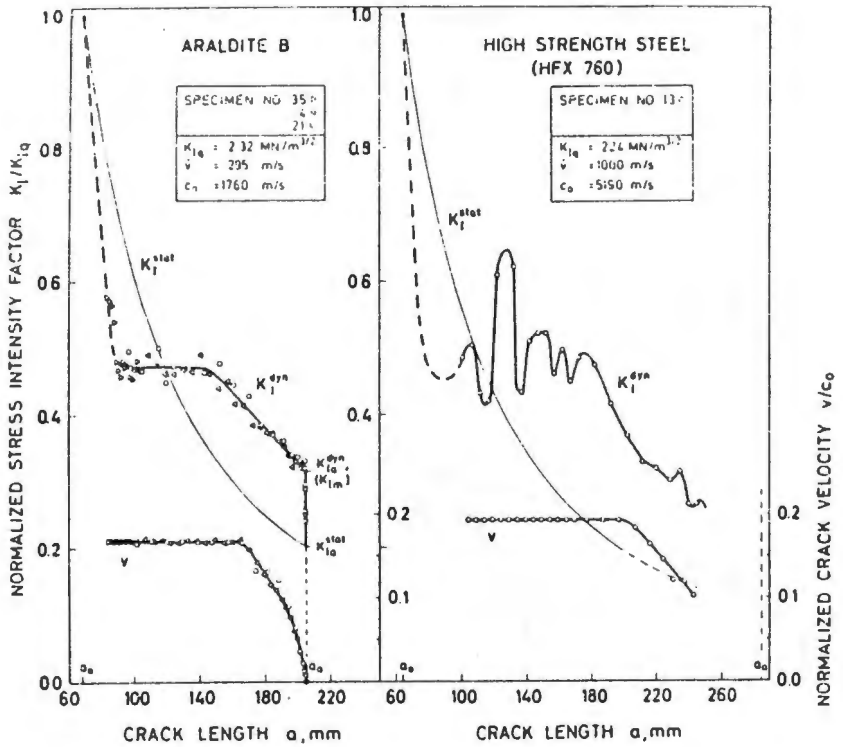

* Kalthoff, et.al.

Figure 6.8 Variation of K_I^d and velocity with crack length in a dynamic experiment.[6.11]

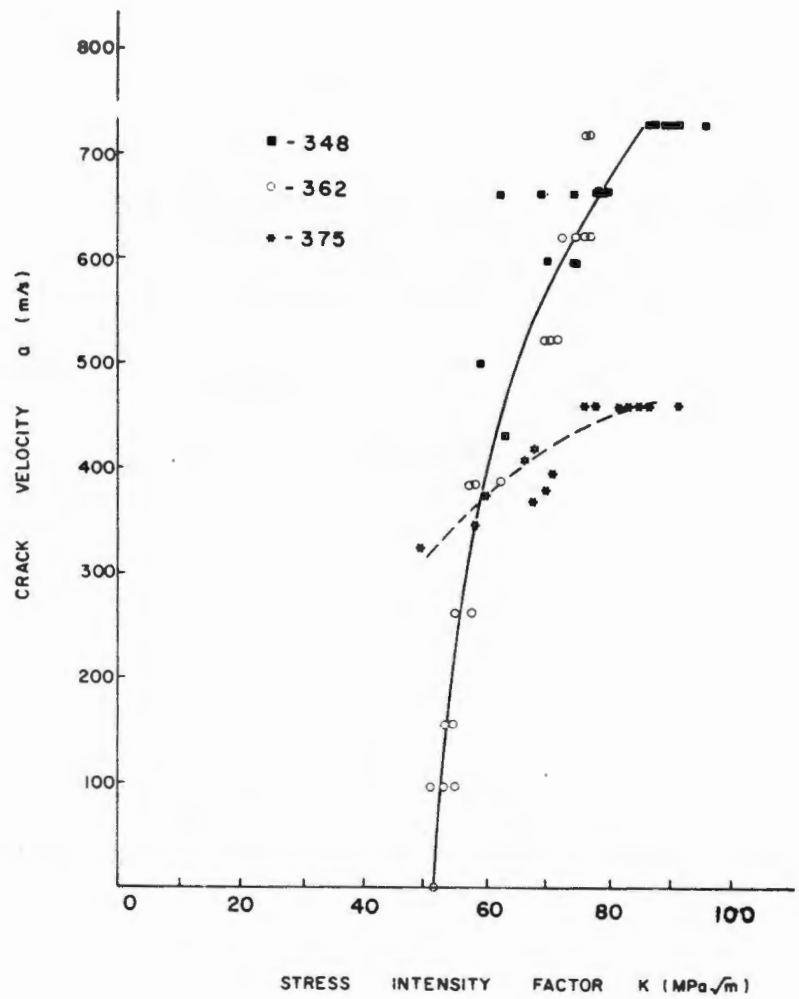

Figure 6.9 Crack velocity as a function of K_I^d for 4340 steel.[6.12]

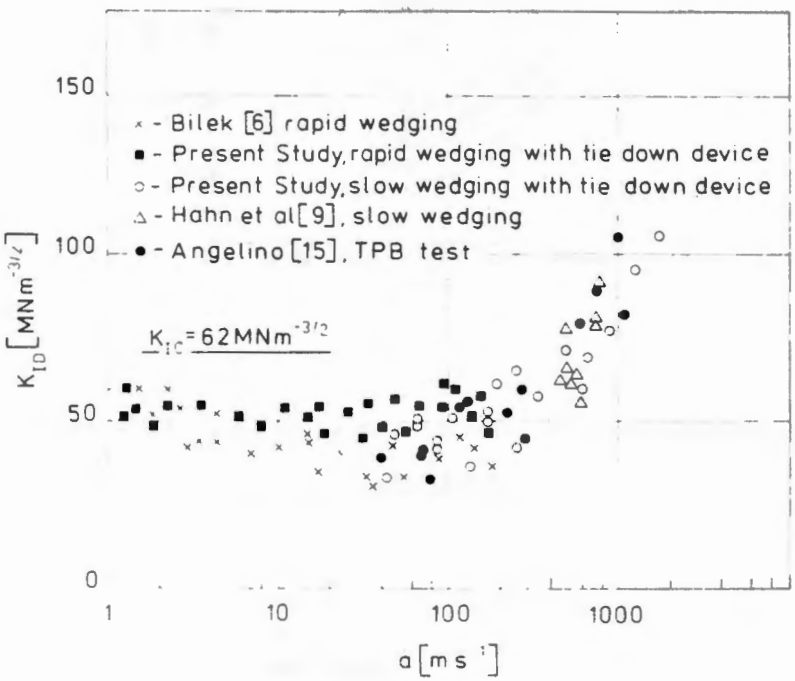

Figure 6.10 Crack velocity as a function of K_I^d for SAE4340 steel.[6.13]

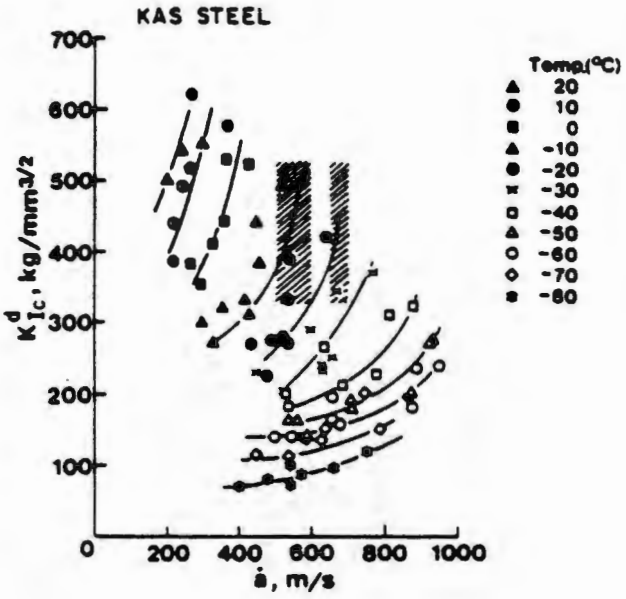

Figure 6.11 $K^d_{IC} - \dot{a}$ as a function of crack tip velocity for different temperatures.[6.16]

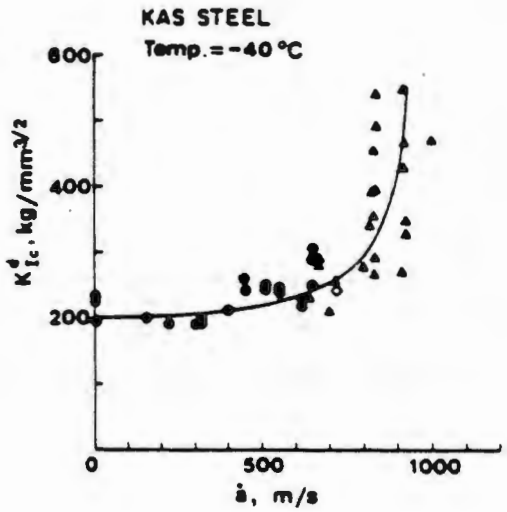

Figure 6.12 $K^d_{IC} - \dot{a}$ as a function of crack tip velocity for $-40°C$ temperature.[6.16]

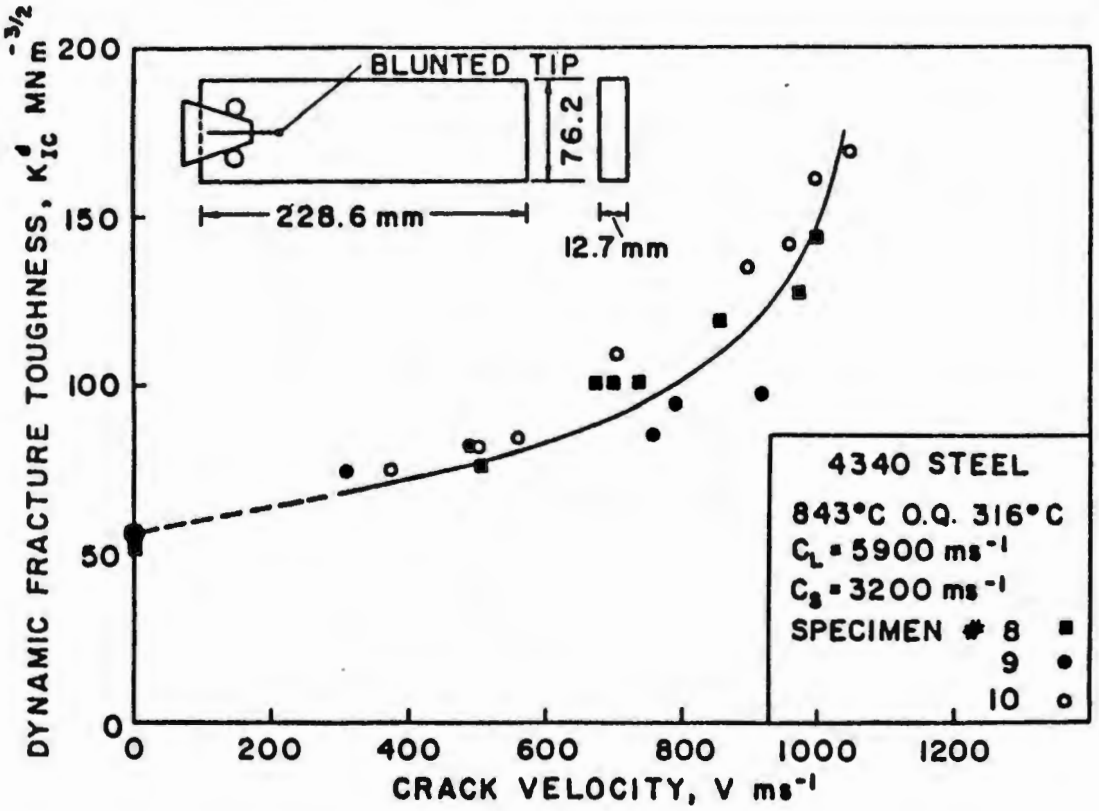

Figure 6.13 Crack velocity as a function of K_I^d for 4340 steel.[6.17]

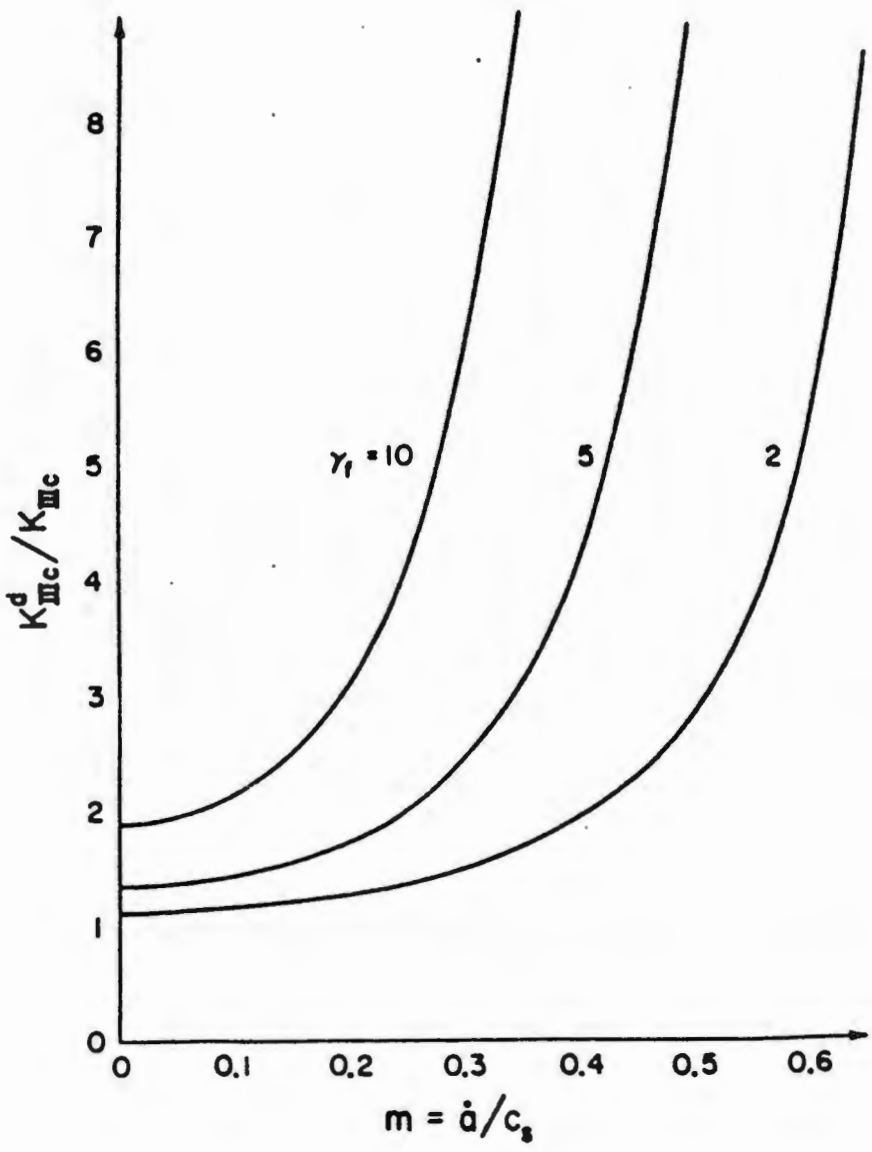

Figure 6.14 K^d_{III} as a function of crack speed in an elastic-ideally plastic, rate insensitive material according to critical plastic strain criterion.[6.18]

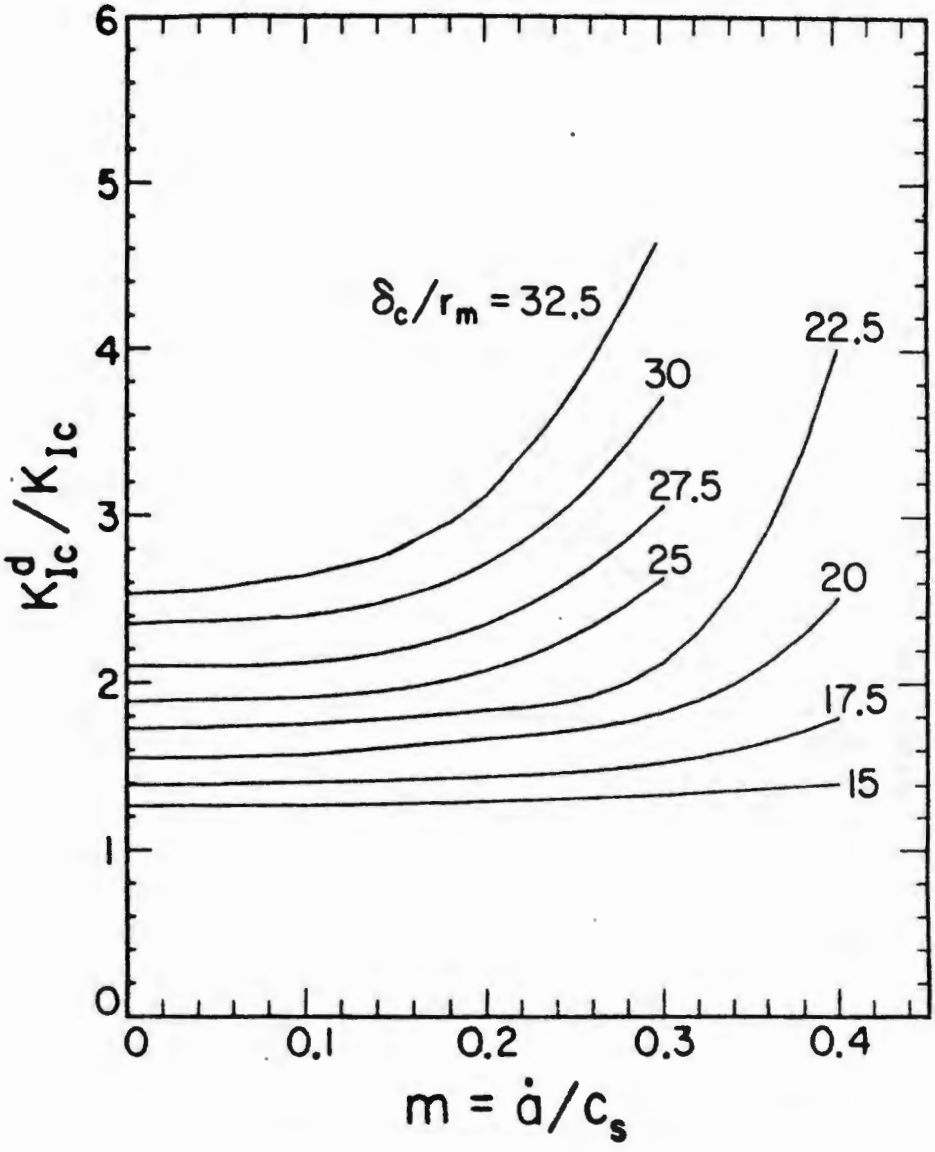

Figure 6.15 K_I^d as a function of crack speed according to the critical crack tip opening angle fracture criterion.[6.19]

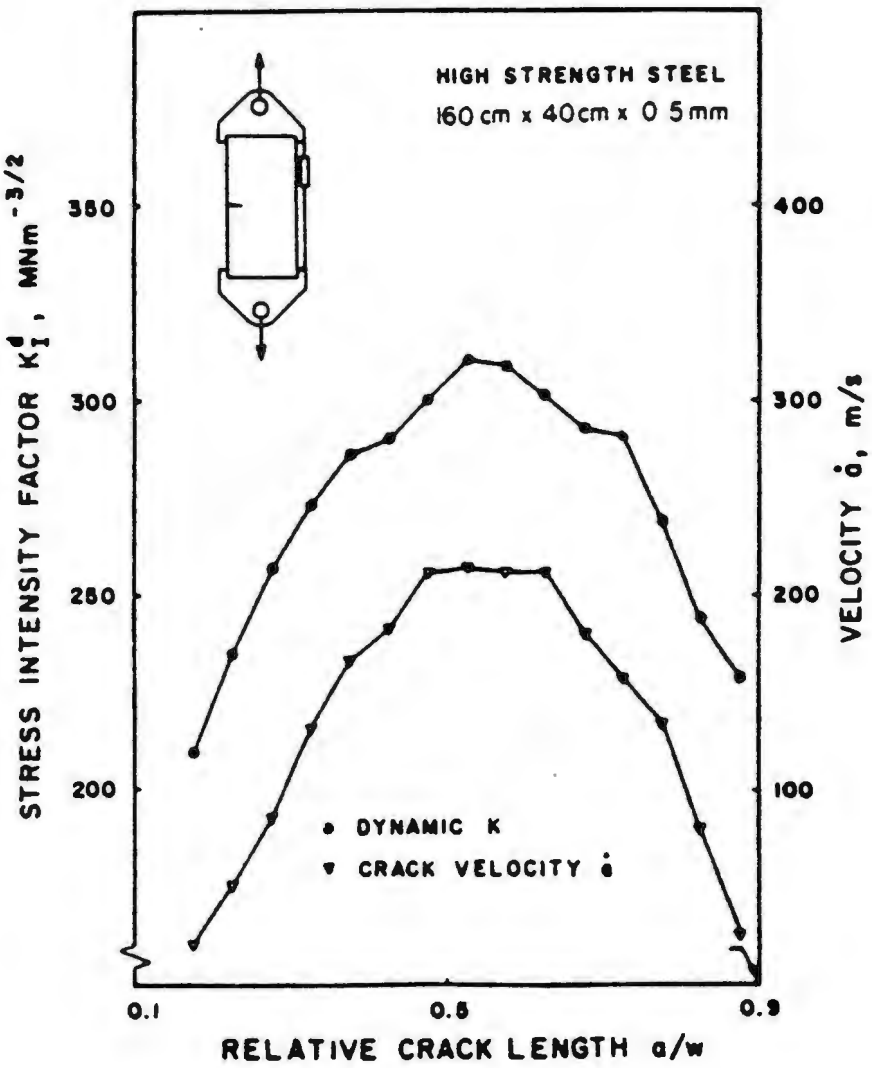

Figure 6.16 Stress intensity factor and crack velocity as functions of crack length.[6.21]

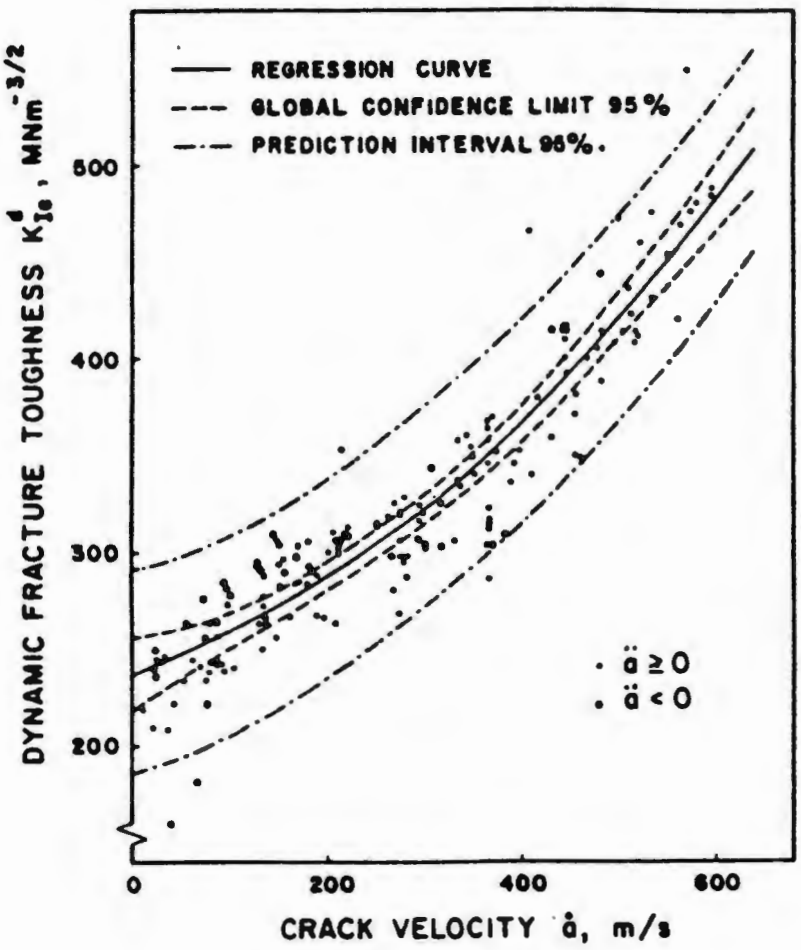

Figure 6.17 Dynamic fracture toughness as a function of crack velocity for a high strength steel.[6.21]

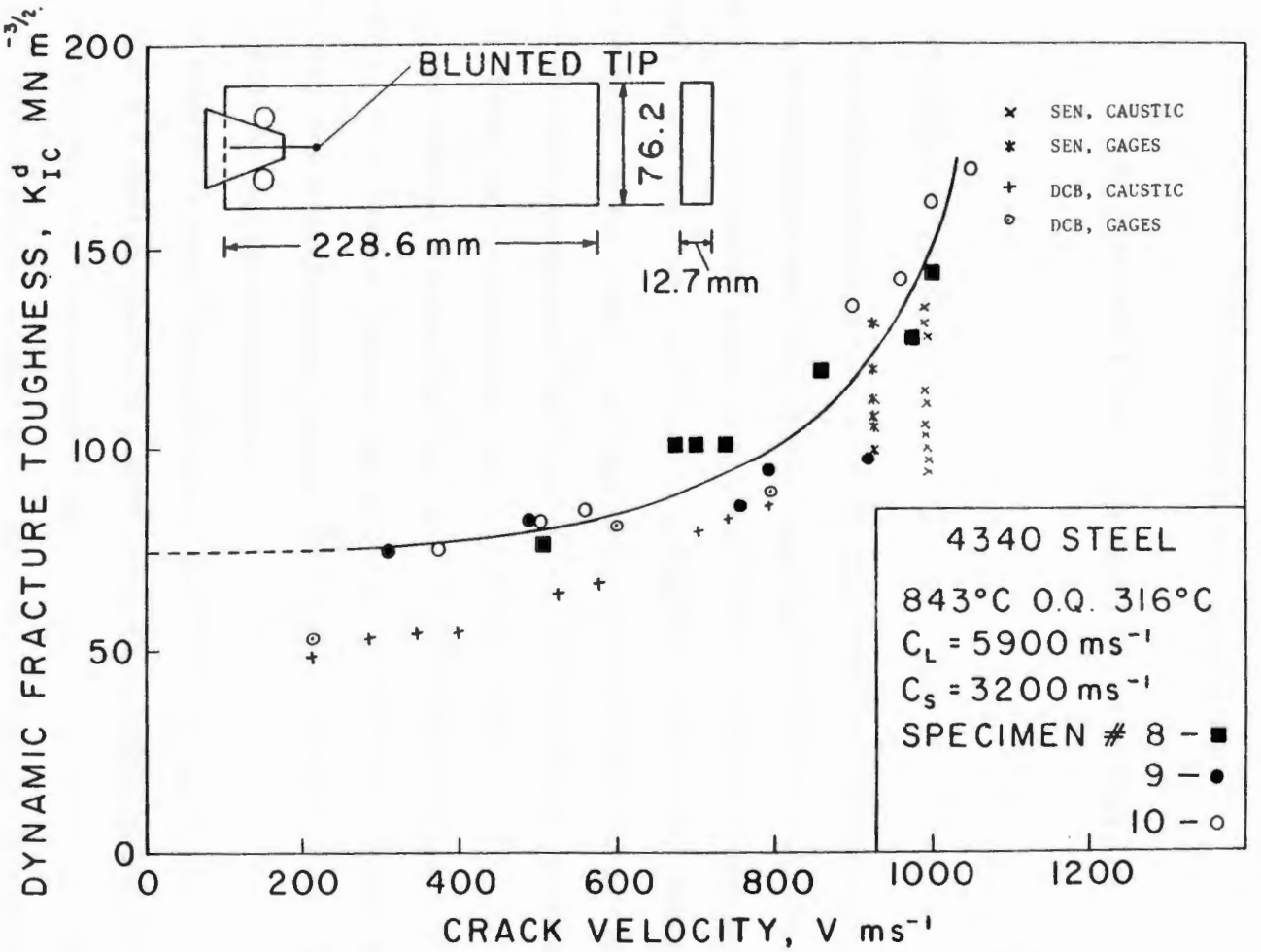

Figure 6.18 K^d_I $\dot{a}$ results for 4340 steel superimposed on the results taken from[6.17].

CHAPTER 7

J INTEGRAL EVALUATION

IN POWER LAW HARDENING MATERIALS

7.1 INTRODUCTION:

The use of strain gages to measure the stress and strain field around a crack tip has many advantages over the commonly used optical techniques like the method of caustics and the method of photoelasticity. With the use of extremely small strain gages of sizes less than a millimeter it is possible to accurately measure strains at any point. In this chapter the relationship between J-integral and measurable strains has been derived and the details of using strain gages for direct evaluation of J in power law hardening materials has been discussed.

Kawahara and Brandon[7.1] were the first to use strain gages to evaluate J integral. Their approach was an indirect one. It involved the measurement of strains at various points along a contour for the evaluation of J. Such a method is not feasible for practical applications.

Rosakis and Freund[7.2] and Marchand et al[7.3] have experimentally evaluated the value of J using the method of caustic in the HRR singularity dominated region around the crack tip. The method of caustic can only be used on transparent or highly polished opaque materials and it requires an elaborate optical setup. This hinders the use of the technique for routine testing.

In a recent paper Kang and Kobayashi[7.4] have used moire interferometry to evaluate J for aluminum specimens from the displacements in the direction normal to the crack. Their technique gave good results for both far field and near field

J-integral values.

Another technique which has been used to study the details of HRR field is by Chao, Lee, Sutton and Peters[7.5]. Their technique is based on the existence of a relationship between fourth order contrast and plastic strain in any material. They use computer vision techniques to measure surface optical parameters of the polished surface of the specimen.

Chiang and Hareesh[7.6] have used combined laser projected grating method and the inplane moire method to obtain three dimensional displacement fields. These are then used to evaluate the value of J-integral.

All the existing techniques mentioned above are promising but they cannot be used easily outside the laboratory environment because they require precise control of the setup and surface conditions. Strain gages, in contrast, are not very sensitive to surface conditions and are much more easier to use on location.

Before investigating the deformation field for power law hardening materials it is useful to note some features of linear elastic material response. When a large plate containing a long through crack is applied a mode-I loading, the near tip stress and strain fields assume a known spatial distribution the magnitude of which can be satisfactorily described by a single scalar parameter customarily known as the stress intensity factor. Hence, in the domain of plane stress analysis the near tip strain field is completely defined if the stress intensity factor is known and vice versa. Using the fact that deformation field distribution is known and only the magnitude is to be determined, Dally and Sanford[7.7] have derived a relationship between the strain measured by a gage and the stress intensity factor. They have successfully used it to evaluate stress intensity factor in linear elastic materials[7.8].

Using the asymptotic elastic plastic analysis suggested by Hutchinson, Rice and Rosengren it has been shown that for near crack-tip field in power law hardening material there exists a scalar parameter which gives the magnitude of the stress and

strain fields. For plane stress analysis with small strains and proportional stress histories for stationary cracks, the value of Rice's J- integral has been suggested as the parameter describing the magnitude of the fields and thus can be treated as a plastic intensity factor. Rosakis, Ma and Freund[7.9] have related J to the out of plane deformation of the material which they evaluate using the method of caustic. In this work a method of evaluating J from the in-plane surface displacements as measured by strain gages is proposed.

A brief description of the HRR field and the conditions under which it is valid is given in the following section. Using these field equations a relationship between J and linear strain is derived. Details of the variation of linear strain with location and orientation of the gage and material properties are investigated. Experiments have been conducted to evaluate J using the HRR field equation in the elastic-plastic region.

7.2 THE HRR SINGULARITY FIELDS:

Hutchinson[7.10,7.11] and Rice and Rosengren[7.12,7.13] have presented the strain hardening and non-hardening plasticity solutions which describe the behavior of stress and strain fields at the tip of a stationary crack under plane strain and plane stress conditions. The asymptotic solutions are obtained from governing equations which neglect the deformation-induced finite geometry changes associated with blunting at the crack tip. The amplitude of the singularity fields is given by the value of Rice's[7.14] path independent J integral. These HRR singularity fields and the J integral provide the theoretical basis for non linear fracture mechanics.

In the asymptotic analysis of near crack tip field only the plastic part of the stress-strain relationship is important because close to the crack tip the elastic strains are negligible compared to the plastic strains. Hutchinson, Rice and Rosengren considered a power law material where the uniaxial plastic strain is related to the uniaxial stress by

$$\frac{\epsilon}{\epsilon_o} = \alpha[\frac{\sigma}{\sigma_o}]^n \tag{7.1}$$

where σ_o is the yield stress, $\epsilon_o = \sigma_o/E$, α is a material constant and n is the strain hardening exponent. Details of the definitions of σ_o, ϵ_o, and n are discussed later in the section on experimental work. Generalization of the uniaxial stress-strain relation (7.1) by J2 deformation plasticity to multi-axial state yields

$$\frac{\epsilon_{ij}}{\epsilon_o} = \frac{3}{2}\alpha[\frac{\sigma_e}{\sigma_o}]^{n-1}\frac{s_{ij}}{\sigma_o} \tag{7.2}$$

where,

$$\sigma_e^2 = \frac{3}{2}s_{ij}s_{ij} \tag{7.3}$$

$$s_{ij} = \sigma_{ij} - \frac{1}{3}\delta_{ij}\sigma_{kk} \tag{7.4}$$

Within small strain formulation, the asymptotic stress and strain distribution in the crack tip region is given with reference to polar coordinates, r and θ, by the following equations[7.10-7.12]

$$\sigma_{ij} = \sigma_o[\frac{J}{\alpha\sigma_o\epsilon_o I_n r}]^{\frac{1}{n+1}} S_{ij}(n,\theta) \tag{7.5}$$

$$\epsilon_{ij} = \alpha\epsilon_o[\frac{J}{\alpha\sigma_o\epsilon_o I_n r}]^{\frac{n}{n+1}} E_{ij}(n,\theta) \tag{7.6}$$

Here the dimensionless constant I_n and the θ -variations of the dimensionless functions E_{ij} and S_{ij} depend on n, on the symmetry of the fields with respect to the crack plane and on whether plane strain and plane stress conditions prevail at the vicinity of the crack tip. For plane stress case I_n decreases from 5 to 2.57 for n varying from 1 to infinity. The values of I_n, E_{ij} and S_{ij} have been tabulated in [7.15,7.16] for various values of n.

7.3 J AND THE STRAIN MEASURED BY THE GAGE:

Structural materials containing cracks undergo substantial amount of plastic deformation before any crack growth takes place. In such materials when plastic deformation has taken place, the near tip stress field is no longer the inverse square root singularity type. It is no more governed by the stress intensity factor and the linear elastic fracture mechanics approach is not applicable. In the elastic-plastic region near the crack tip the stress and strain fields are controlled by J and hence there is a need to measure its value. There are some methods available to measure J for ductile fracture specimens but most of them are indirect and are based on the load and displacement data.

Since, the HRR strain field which exists near the crack tip is controlled by the value of J, one can expect to evaluate its value from the strain and deformation measurements taken from this region. Marchand et. al.[7.3] have used the method of caustic on ductile steels to make measurements from this region by keeping the initial curve sufficiently small. In this section the HRR strain field equations are used to infer J values from the strain data taken from close to the crack tip where HRR field exists.

Consider a large plate of uniform thickness of elastic-plastic material that exhibits power law hardening behavior. Let there be a long through-crack in it as shown in figure 7.1. Suppose a strain gage is placed at a location (r, θ) with an orientation making an angle θ with the direction of the crack. The strain field is given by the equation (7.6) which can be expanded as

$$\begin{aligned}
\epsilon_{rr} &= \alpha\epsilon_o[\frac{J}{\alpha\sigma_o\epsilon_o I_n r}]^{\frac{n}{n+1}} E_{rr}(n,\theta) \\
\epsilon_{\theta\theta} &= \alpha\epsilon_o[\frac{J}{\alpha\sigma_o\epsilon_o I_n r}]^{\frac{n}{n+1}} E_{\theta\theta}(n,\theta) \\
\epsilon_{r\theta} &= \alpha\epsilon_o[\frac{J}{\alpha\sigma_o\epsilon_o I_n r}]^{\frac{n}{n+1}} E_{r\theta}(n,\theta)
\end{aligned} \tag{7.7}$$

Since the gage measures only linear strains, the strain ϵ_g in the direction of the

gage can be evaluated by the following strain transformation equation

$$\epsilon_g = \frac{(\epsilon_{rr} + \epsilon_{\theta\theta})}{2} + \frac{(\epsilon_{rr} + \epsilon_{\theta\theta})}{2}\cos(2\alpha) + \epsilon_{r\theta}\sin(2\alpha) \tag{7.8}$$

where $\alpha = \beta - \theta$. Substituting (7.7) in (7.8) yields

$$\epsilon_g = \frac{A}{2} J^{\frac{n}{n+1}} [E_{rr} + E_{\theta\theta} + (E_{rr} - E_{theta\theta})\cos(2\alpha) + 2E_{r\theta}\sin(2\alpha)] \tag{7.9}$$

where,

$$A = \alpha\epsilon_o [\frac{1}{\alpha\sigma_o\epsilon_o I_n r}]^{\frac{n}{n+1}} \tag{7.10}$$

Rearranging equation (7.9) gives the value of J in terms of ϵ_g, strain gage location parameters (r, θ, β) and material dependent parameters $(\alpha, n, \sigma_o, \epsilon_o, I_n, E_{ij})$. Hence we get

$$J = \alpha\sigma_o\epsilon_o I_n r [\frac{2\epsilon_g}{\alpha\epsilon_o\{E_{rr}(1+\cos(2\alpha)) + E_{\theta\theta}(1-\cos(2\alpha)) + 2E_{r\theta}\sin(2\alpha)\}}]^{\frac{n+1}{n}} \tag{7.11}$$

The above relation can be used to evaluate J from the strain gage reading if the location and orientation are known. But from a practical point of view it is not possible to mount the gage anywhere. The gage has to be mounted so that maximum sensitivity is obtained. With this in mind it becomes necessary to investigate the influence of various parameters on the measurable strain value.

Figure 7.2 shows how the strain varies as the gage is placed at a particular location r and θ and rotated to obtain varying β. The plot has been generated for r being $4mm$ and theta being 42°. The value of β corresponding to maximum strain as shown in the figure will henceforth be referred to as β_{max}.

Figure 7.3a and 7.3b show that as the strain gage location direction is changed the β_{max} value changes. The values of β_{max} and the corresponding values of strain

shown have been plotted for a gage placed at 4mm from the crack tip and with a J of 10kNm.

As the gage is moved away from the crack tip, ie, as r is increased the strain value drops as $n/(n+1)$ power as can be seen from equation(7.9) and from figure 7.4. The sign of strain remains the same for a particular strain hardening exponent value but the magnitude depends strongly on it.

7.4 EXPERIMENTS AND OBSERVATION:

Two experiments have been conducted on 1/4" thick plate of 4340 steel with different heat treatments to evaluate the value of J at various locations around the crack tip. The specimen geometry used in the first experiment is the single edge notch type and its dimensions are shown in figure(7.5). The second experiment specimen geometry is also SEN with the specimen width of 6 inches and crack length to width ratio of 0.6.

Before performing the experiment it was necessary to perform a material tension test to obtain accurate values of $\sigma_o, \epsilon_o, \alpha$ and n. Figure (7.6) shows a typical stress-strain curve and indicates the values of σ_o, ϵ_o and E. Once σ_o and ϵ_o are determined equation (7.1) is used to get the values of α and n which give a close approximation to the experimental curve.

Figure (7.7) shows the experimental stress-strain curve with the theoretical curve for the material used in the first experiment. It is noticed that no one value of α and n can be chosen to fit the curve in the whole strain range. Since most of the experimental data fell in the range less than $3000\mu\epsilon$ the values of n and α are n=2.0 and α=1.4. Figure (7.8) shows the experimental stress-strain curve with the theoretical curve for the material used in the second experiment. The values of n and α are n=5.69 and α=3.0.

The specimens have two strips of ten strain gages each mounted on it. One set of gages is mounted in the direction along the crack ($\theta = 0°$) and the other set

perpendicular to it ($\theta = 90°$). The specimens were loaded gradually in steps and the strain readings from all the gages were recorded. The strain profiles recorded are shown in figures (7.9) and (7.10) for gages along the crack and perpendicular to the crack for the two experiments.

7.5 RESULTS AND DISCUSSION:

Experiment 1:

The strain data observed in the previous section can be analyzed to obtain the values of the J integral. Figure (7.11a,b) show the J values obtained by using the strain values in equation (7.11) for ($\theta = 0°$) and ($\theta = 90°$) directions respectively. The values of n and α used are $n = 2.0$ and $\alpha = 1.4$.

The theoretical value of J used in this case has been calculated using the expression taken from reference [7.17].

$$J_{th} = \frac{\pi a_e F^2}{w^2}\frac{P^2}{E} + \alpha\sigma_o\epsilon_o c\frac{a}{w}h_1(\frac{a}{w}, n)[\frac{P}{P_o}]^n + 1 \qquad (7.12)$$

with,

$$P_o = 1.072\delta c\sigma_o$$

$$c = w - a$$

$$a_e = a + \phi r_p$$

$$\delta = [1 + (\frac{a}{c})^2]^{1/2} - \frac{a}{c}$$

$$r_p = \frac{1}{2\pi}[\frac{n-1}{n+1}](K/\sigma_o)^2$$

$$\phi = \frac{1}{1 + (P/P_o)^2}$$

where P is the load per unit thickness,P_o is the load per unit thickness for perfectly plastic case, w is the specimen width and a is the crack length. Values of h_1 and F are taken from references [7.17] and [7.18].

Figure (7.12) shows the normalized J value (ratio of the experimental J value to the theoretical J value) variation with the plastic zone size. As the load is increased the plastic zone size grows (r_p is proportional to $load^2$). It is seen that for very low loads the error is high but as the load increases there is a range of r_p ($2mm < r_p < 10mm$ for $\theta = 0°$ and $r_p > 9mm$ for $\theta = 90°$) for which all the gages give results within 25 percent. When the load is increased further the error in all the gages increases.

Intuitively, one expects that the zone of validity of HRR field should be dependent on some relationship to the plastic zone size. Keeping this in mind figures(7.13) were obtained. It is noticed from the plot of J/Jth against r_p/r_g (r_g is the location of the gage) that when r_p/r_g is about 0.9 the values of J obtained are accurate to 10 percent for $\theta = 0°$ direction. For $\theta = 90°$ direction the data shows the development of a similar trend for a higher ratio value but r_p is not able to grow to that size before the crack becomes unstable.

In an attempt to investigate the size of J evaluation range and its variation with load figure (7.14a,b) has been plotted. The figure shows the variation of J/Jth with the location of the gages from the crack tip for gages placed along and perpendicular to the crack respectively for different loads.

From figure(7.14a) we note that as the load is increased the accuracy with which the gage measures the J value changes. For instance, for lower loads the gages close to the crack tip give less errors but when the load increases to 58.6 kN the errors are high as shown in the figure.

Figure (7.14b) shows the same data for gages placed perpendicular to the crack. Here it is seen that as the load is increased the experimental values get closer and closer to the theoretical value for the load range considered.

The percentage error information extracted from figure(7.14a,b) has been consolidated in figure (7.15a,b) where the accuracy of the J evaluation using strain gages is plotted with respect to load and gage location. The figure shows the regions for placement of gages as the load is varied to obtain results to a desired accuracy.

Experiment 2:

The strain profiles obtained for this experiment were shown in figure (7.10). The strains obtained in this experiment are much higher than the ones obtained in the previous experiment. These strain values have been used with equation (7.11) to obtain the experimental J values plotted in figure (7.16). The figure shows both the theoretical and the experimental values of J from the gages placed along and perpendicular to the crack tip. It is seen that for this material and specimen geometry the experimental values for gages along the crack direction are consistently low. For $\theta = 90°$ direction values both lower and higher than the theoretical values are obtained.

In figure (7.17) the J/J_{th} values have been plotted against the plastic zone size. In the range studied it is seen that for $\theta = 0°$ direction the values from the various gages tend to stabilize at different levels of J/J_{th}. For $\theta = 90°$ direction the trend observed is that the values from various gages tend to converge towards $J/J_{th} = 1.0$ for higher r_p values. Figure (7.18) is the plot of J/J_{TH} as a function of r_p/r_g. With the data available a clear intersection of values from various gages is not observed as in the first experiment.

The variation of J/J_{th} as a function of gage location is given in figures(7.19a,b) for four different loads. It is once again seen that the accuracy of the gages changes

with the applied load. The percentage error information extracted from figures such as (7.19) hass been used to obtain figures(7.20a,b) where the regions for various accuracies have been outlined. It is noticed that for this experiment much smaller regions are available for accurate results.

From the above results it is evident that strain gages can be used to determine the value of J integral for stress field surrounding a mode I crack tip. The location and orientation of placing the gage are important for getting accurate results. Also, it is noticed that the zone in which a gage can be placed varies with the size of the plastic zone. The difference in the trend of the results of the two experiments indicates strong dependence on material properties and requires detailed study of this behavior.

In this work studies were done only in two directions, i.e., $\theta = 0°$ and $\theta = 90°$. Further studies should be conducted for other directions to obtain the complete shape of the J evaluation zone. Also, more work needs to be done to investigate the variation of the accuracy of the technique with material properties.

REFERENCES:

[7.1] Kawahara,W.A. and Brandon,S.L., 'J-Integral Evaluation by Resistance Strain Gauges," Engineering Fracture Mechanics, vol. 18, No 2, pp. 427-434, 1983.

[7.2] Rosakis,A.J. and Freund,L.B., "Optical Measurement of the Plastic Strain Concentration at a Crack Tip in a Ductile Steel Plate," Journal of Engineering Materials and Technology, vol. 104, April 1982, pp. 115-120.

[7.3] Marchand,A., Freund,L.B., Ma,C.C. and Duffy,J., "Use of the Shadow Spot Method in Evaluating J for Ductile Steels," Brown University Technical Report ONR 0597/1 MRL E-160, February, 1986.

[7.4] Kang,B.S.-J. and Kobayashi,A.S., "J-Resistance Curves in Aluminum SEN Specimens," Proceedings of the 1987 SEM Spring Conference on Experimental

Mechanics, Houston, Texas, June 14-19, 1987, pp. 243-249.

[7.5] Chao,Y.J., Lee,C., Sutton,M.A. and Peters,W.H., "Spread of Plastic Deformation in Cracked Plate," Proceedings of the 1987 SEM Spring Conference on Experimental Mechanics, Houston, Texas, June 14-19, 1987, pp. 438-445.

[7.6] Chiang,F.P. and Hareesh,T.V., "Experimental Studies of Crack-Tip Deformation and the HRR Singularity Field," Proceedings of the 1987 SEM Spring Conference on Experimental Mechanics, Houston, Texas, June 14-19, 1987, pp. 782-783.

[7.7] Dally,J.W. and Sanford,R.J., "Strain Gage Methods for Measuring the Opening Mode Stress Intensity Factor," SEM Spring Conference Proceedings 1985, Las Vegas, pp. 851-860.

[7.8] Dally,J.W. and Berger,J.R., "A Strain Gage Method for Determining KI and KII in a Mixed Mode Stress Field," Proceedings of the 1986 SEM Spring Conference on Experimental Mechanics, New Orleans, June 8-13, 1986, pp. 603-612.

[7.9] Rosakis,A.J., Ma,C.C. and Freund,L.B., "Analysis of the Optical Shadow Spot Method for a Tensile Crack in a Power- Law Hardening Material," Journal of Applied Mechanics, vol. 105, December 1983, pp. 777-782.

[7.10] Hutchinson,J.W., "Singular Behavior at the End of a Tensile Crack in a Hardening Material," Journal of the Mechanics and Physics of Solids, vol. 16, 1968, pp. 13-31.

[7.11] Hutchinson,J.W., "Plastic Stress and Strain Fields at a Crack Tip," Journal of the Mechanics and Physics of Solids, vol. 16, 1968, pp. 337-347.

[7.12] Rice,J.R. and Rosengren,G.F., "Plane Strain Deformation Near a Crack Tip in a Power Law Hardening Material," Journal of the Mechanics and Physics of Solids, vol. 16, 1968, pp. 1-12.

[7.13] Rice,J.R., "Mathematical Analysis in the Mechanics of Fracture," in Fracture: An Advanced Treatise (ed. H. Liebowitz), vol. 2, Academic Press, 1968, pp.

191-311.

[7.14] Rice,J.R., "A Path Independent Integral and the Approximate Analysis of Strain Concentration by Notches and Cracks," Journal of Applied Mechanics, vol. 35, 1968, pp. 379-386.

[7.15] Shih,C.F., "Tables of Hutchinson-Rice-Rosengren Singular Field Quantities," Brown University Report MRL E-147, Materials Research Laboratory, Brown University, June 1983.

[7.16] Shih,C.F., "Elastic - Plastic Analysis of Combined Mode Crack Problems," Ph.D. Thesis, Harvard University, Cambridge, Massachusetts, 1973.

[7.17] Kumar,V., German,M.D. and Shih,C.F., "An Engineering Approach for Elastic-Plastic Fracture Analysis," EPRI Report NP-1931, July 1981.

[7.18] Tada,H., Paris,P.C. and Irwin,G.R., "The Stress Analysis of Cracks Handbook," Del Research Corporation, Hellertown, Pennsylvania, 1973.

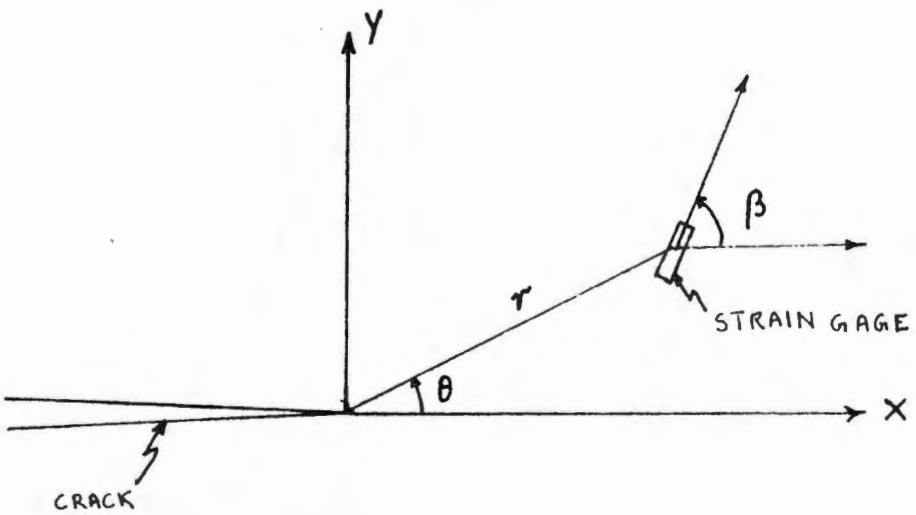

Figure 7.1 The coordinate system for strain gage analysis.

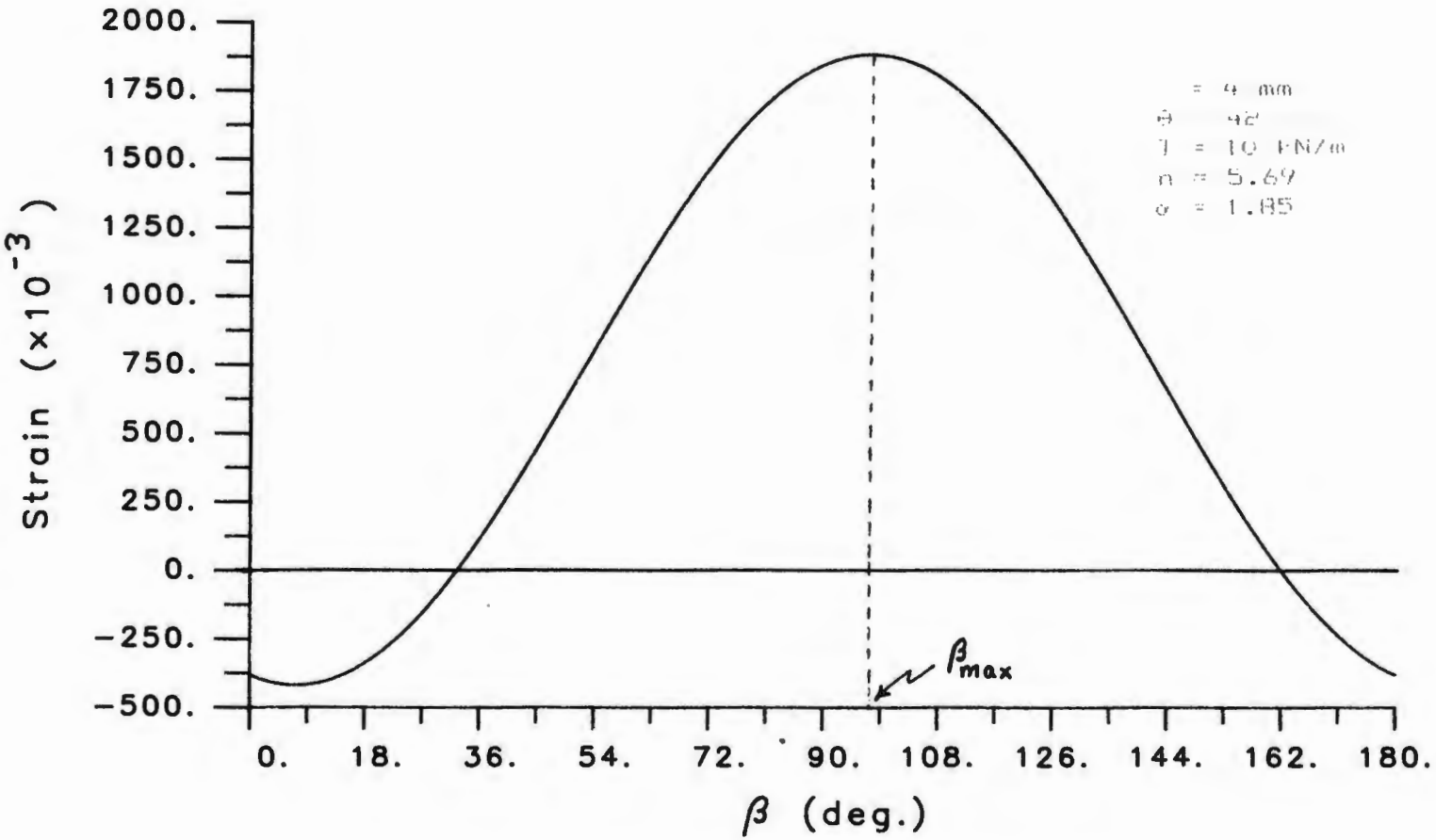

Figure 7.2 Variation of measured strain as the strain gage is rotated at any location.

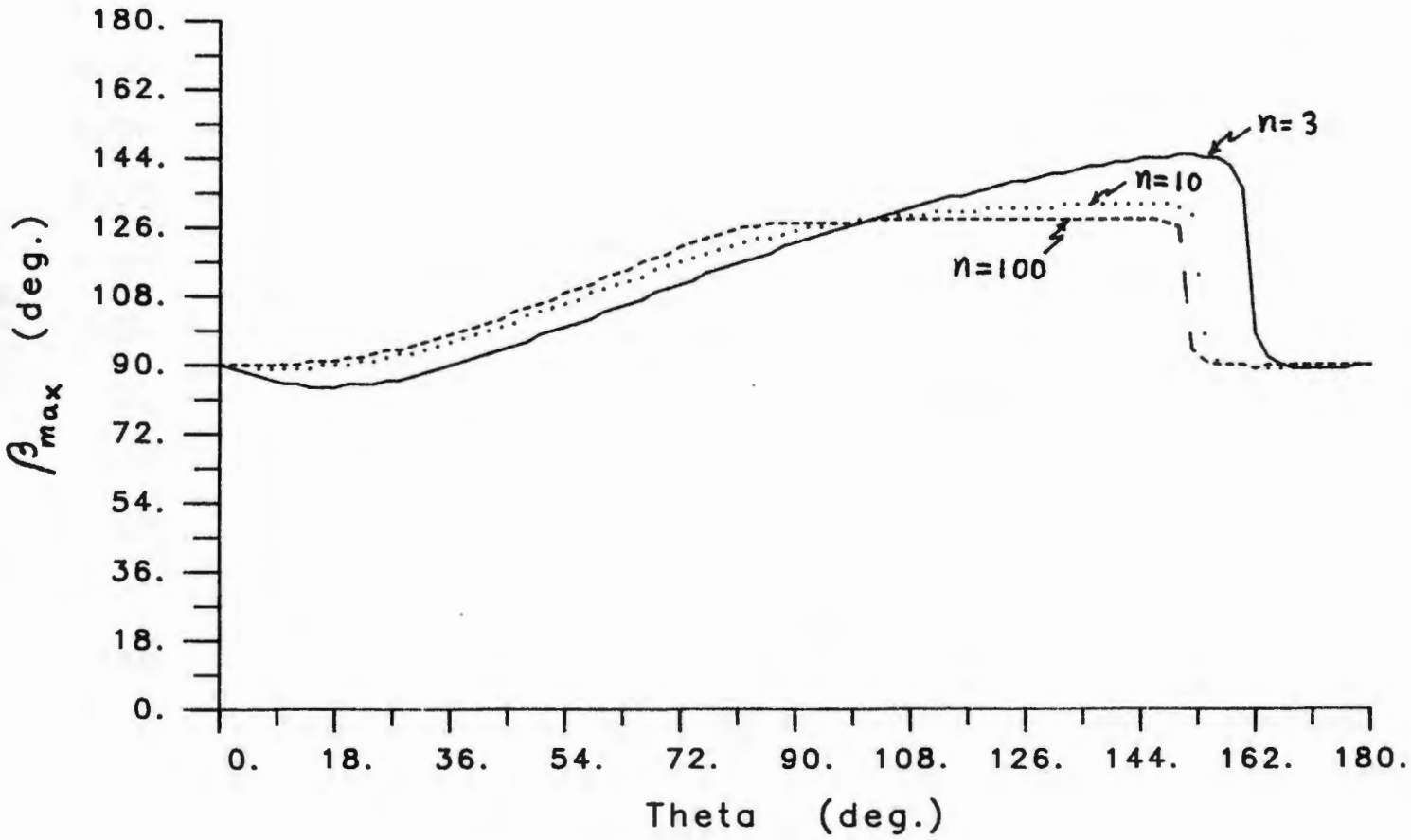

Figure 7.3a Variation of β_{max} as θ is changed.

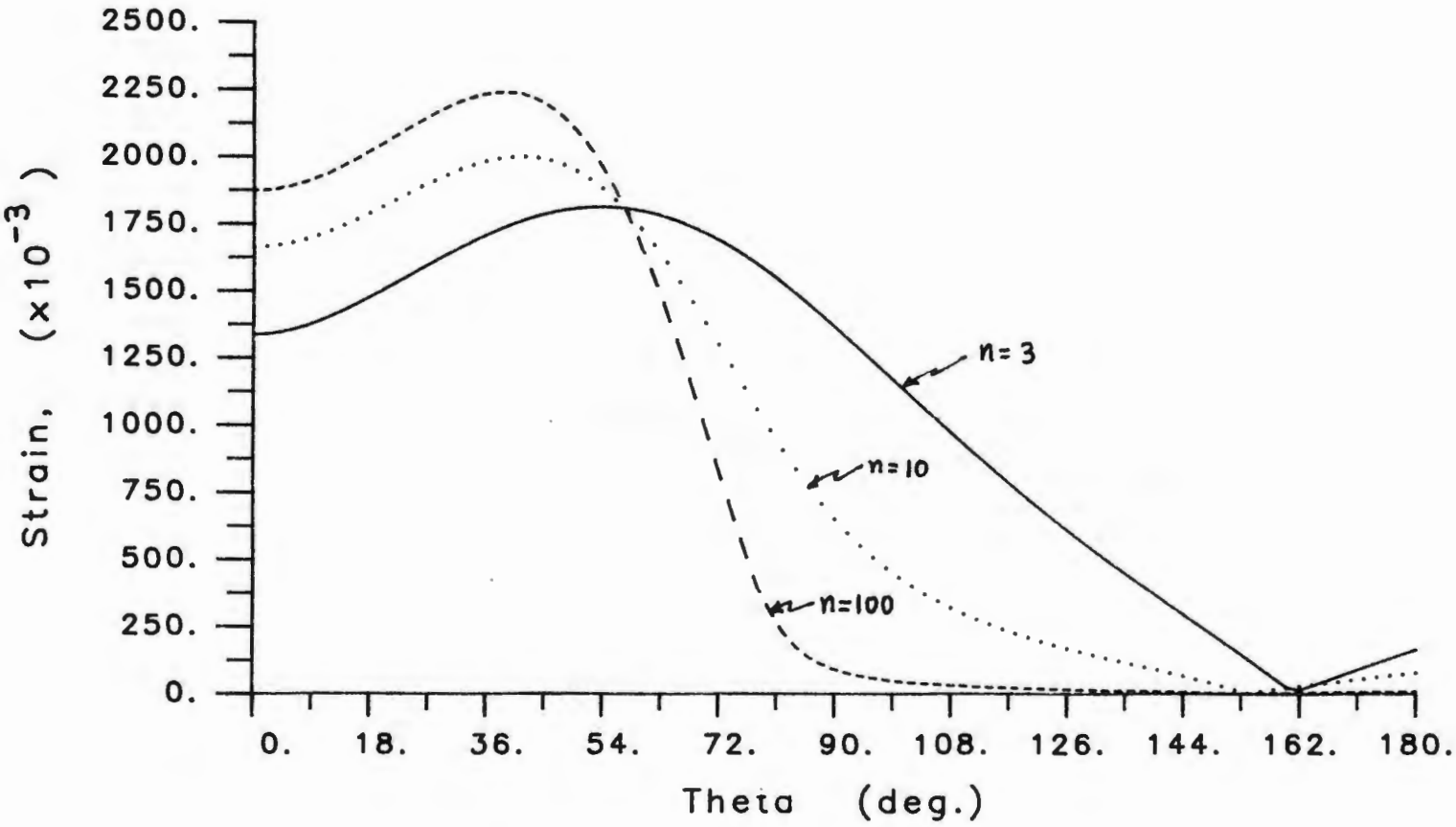

Figure 7.3b Maximum strain obtainable at any location θ.

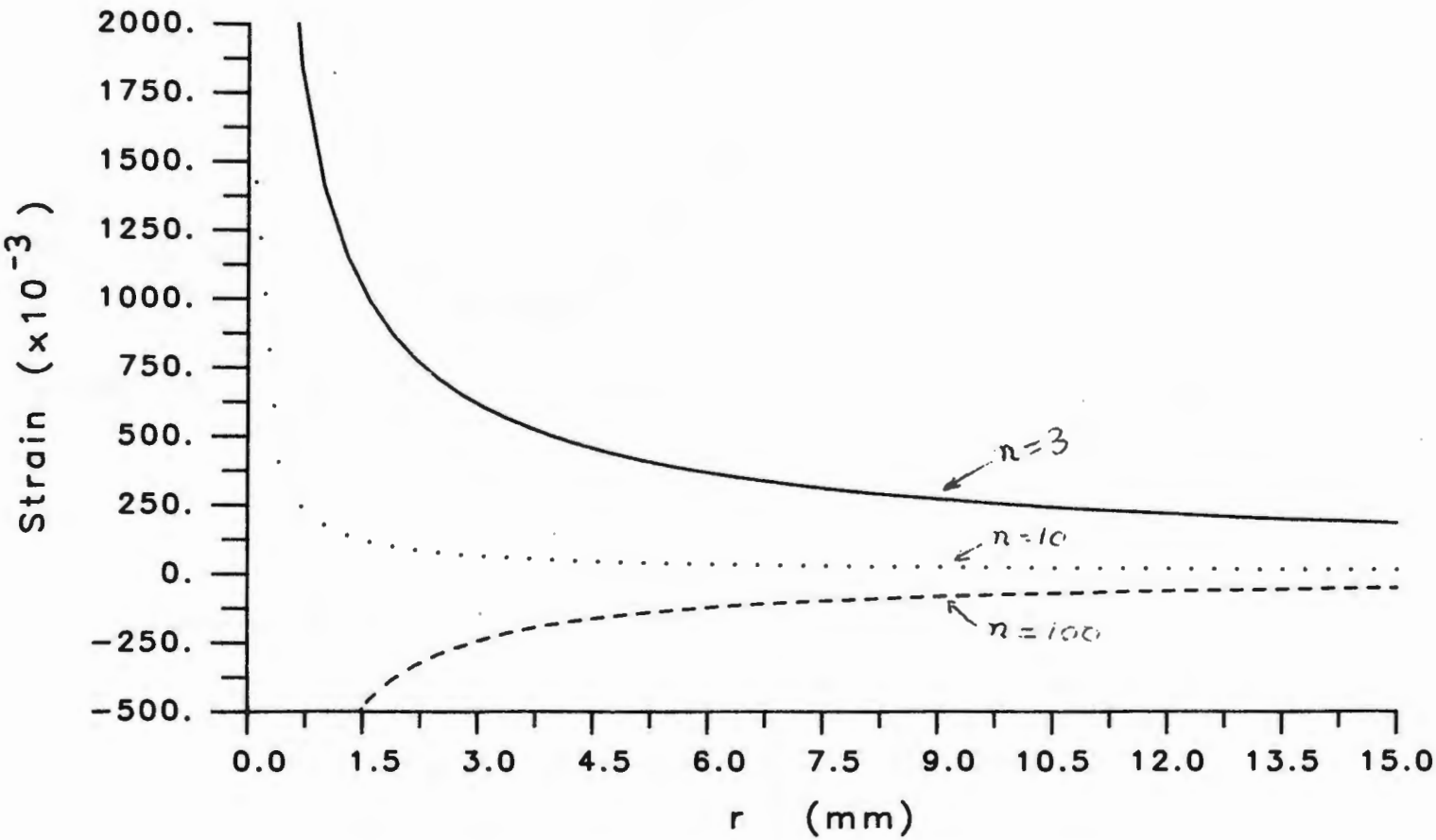

Figure 7.4 Strain drops as the $n/n+1$ power as r increases.

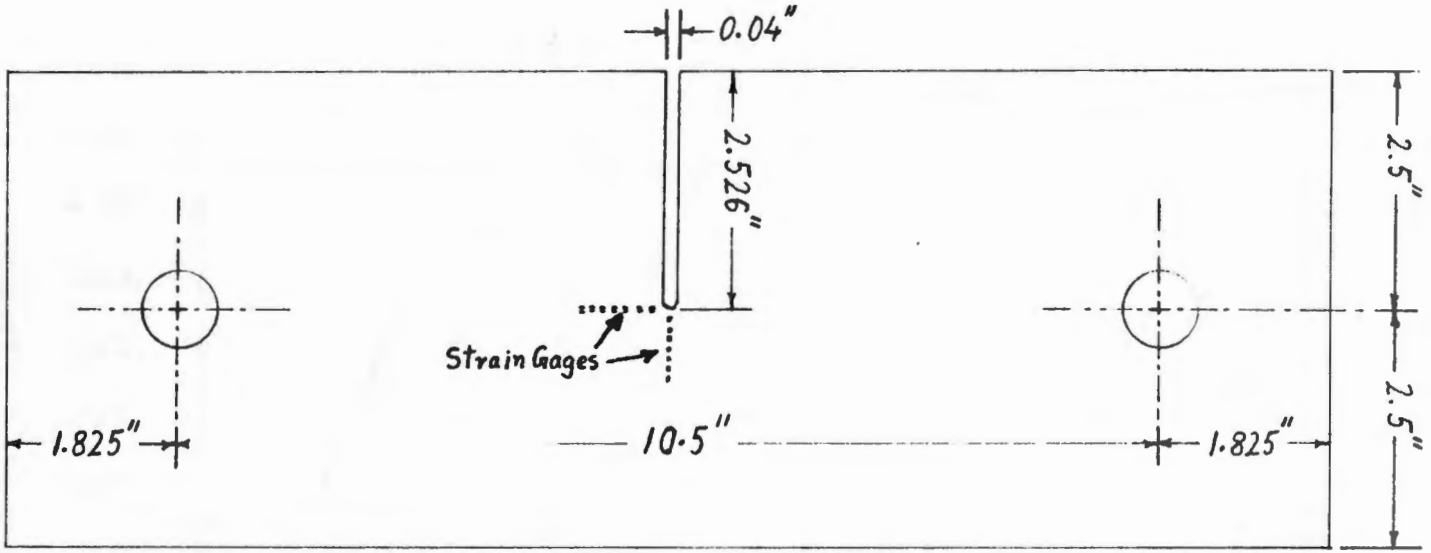

Thickness 0.245" Hole diameter 0.75"

Figure 7.5 Specimen geometry used for J integral testing.

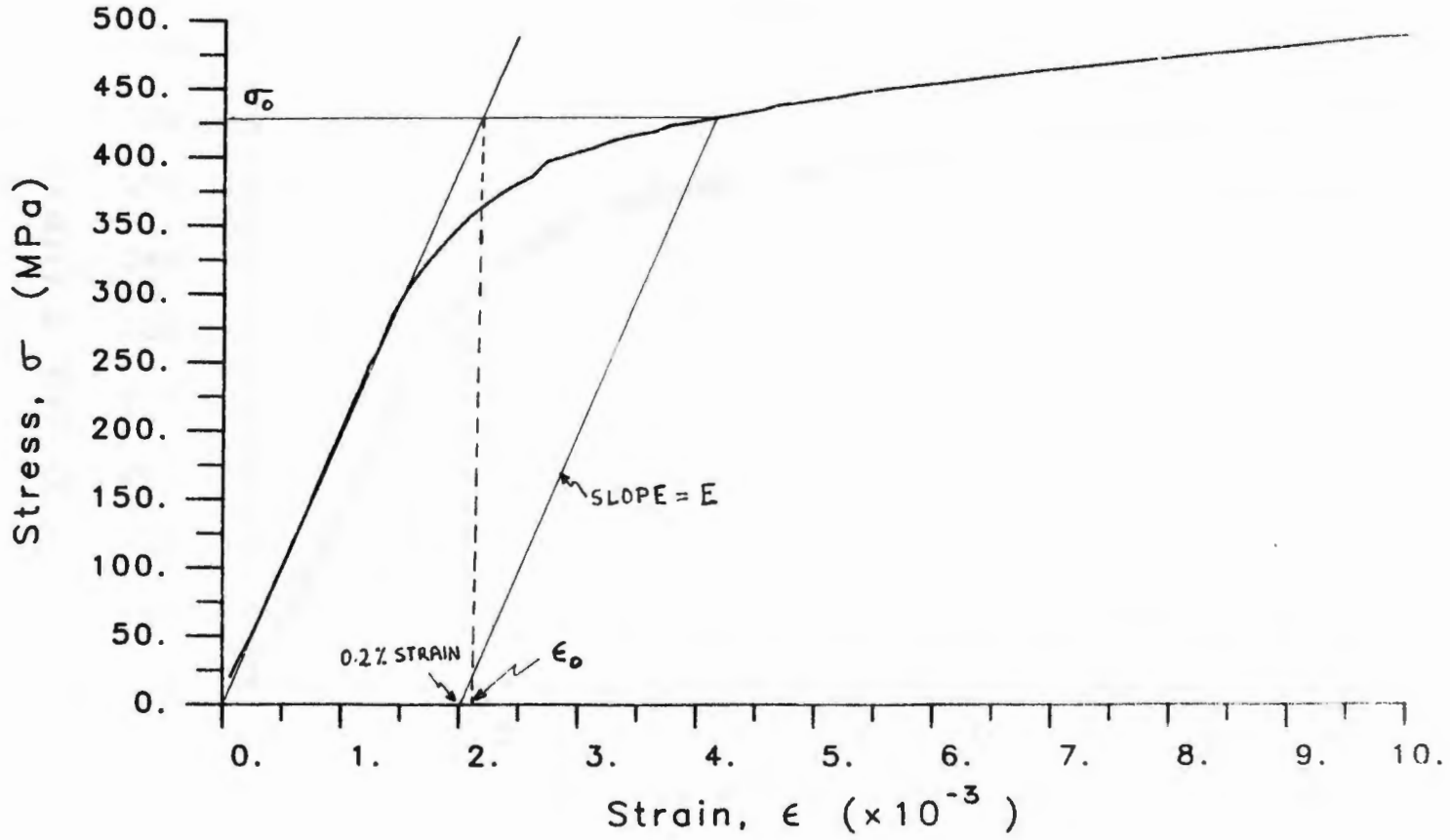

Figure 7.6 Definitions of σ_o, ϵ_o and E.

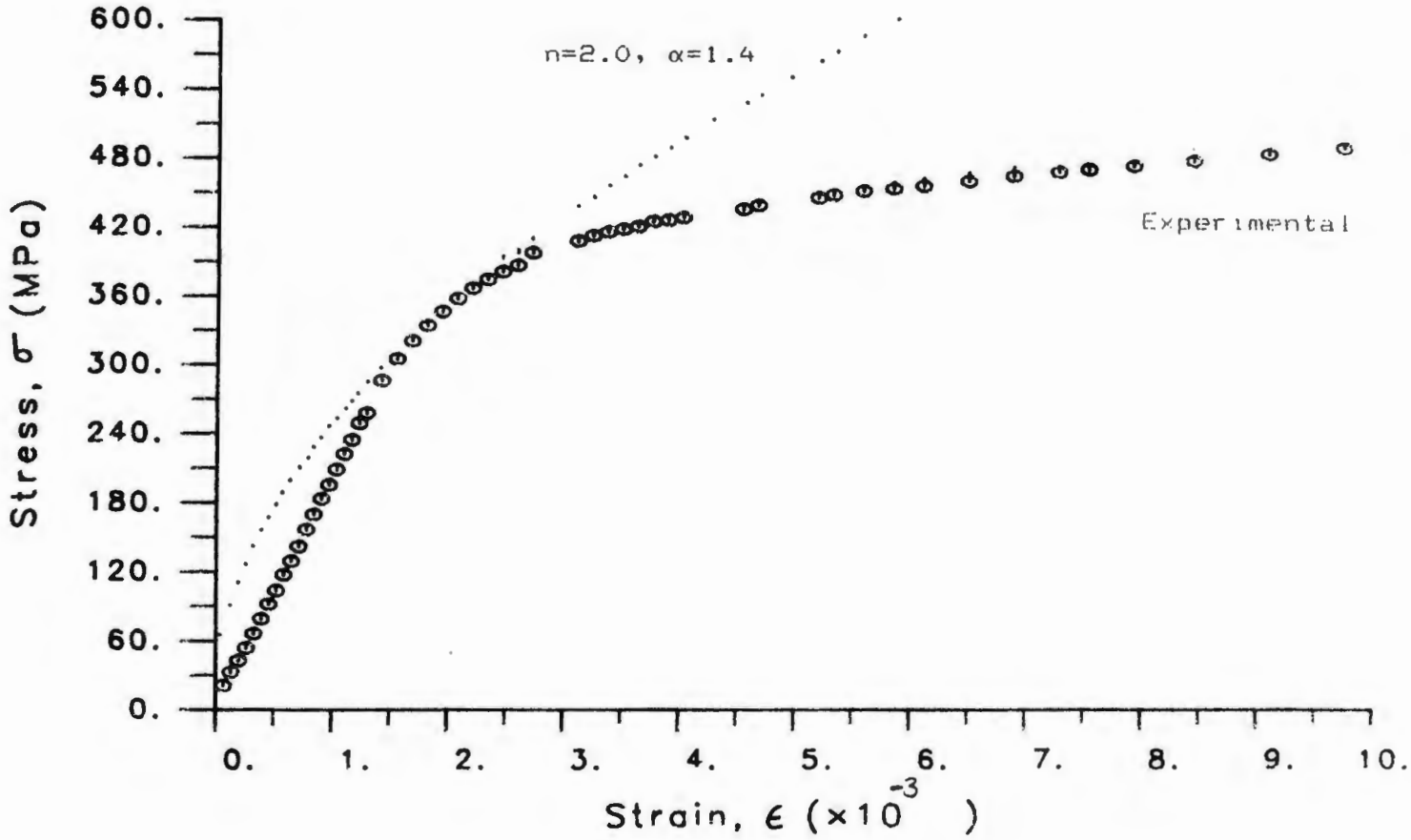

Figure 7.7 Theoretical and experimental stress-strain curve for 4340 steel used in experiment 1.

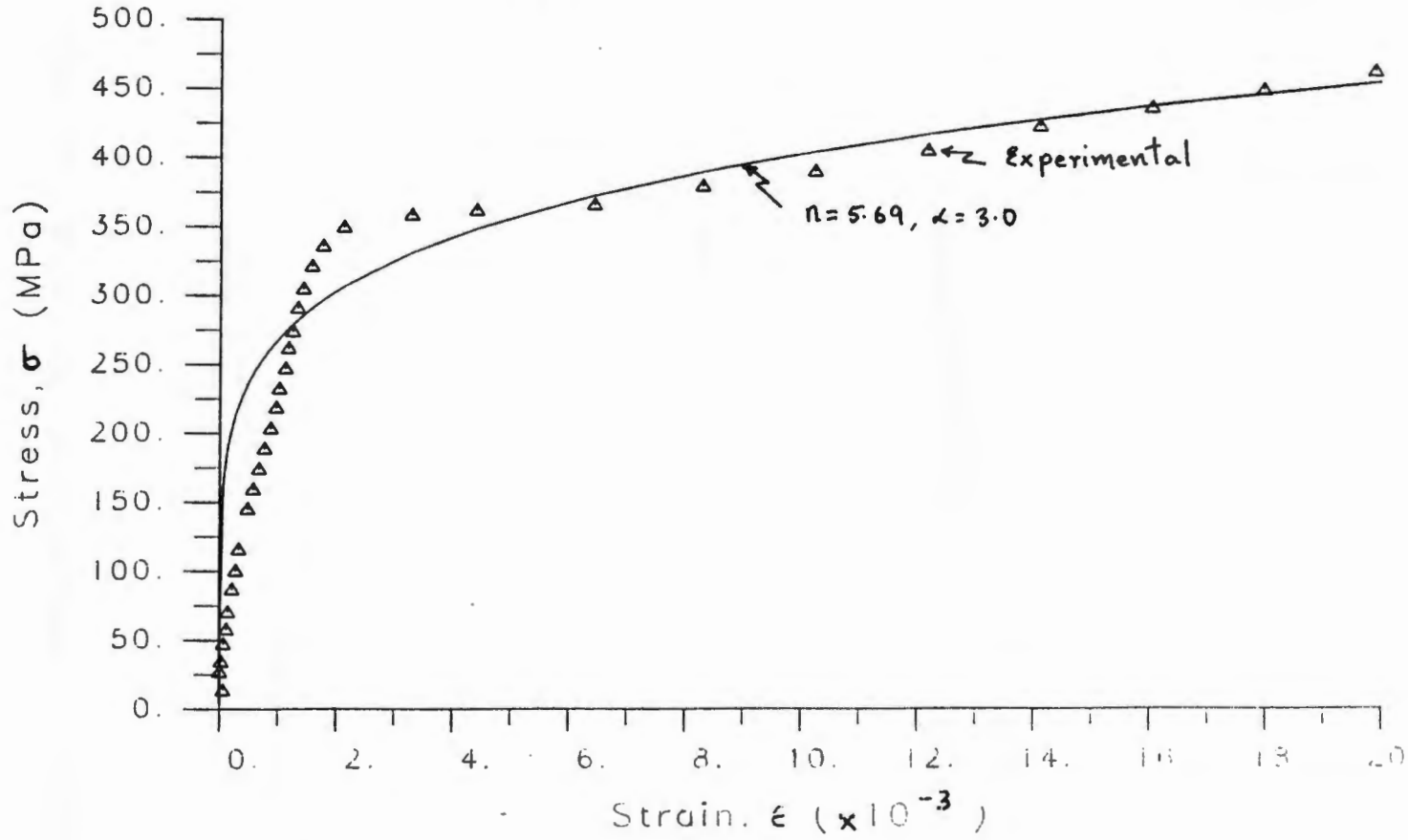

Figure 7.8 Theoretical and experimental stress-strain curve for 4340 steel used in experiment 2.

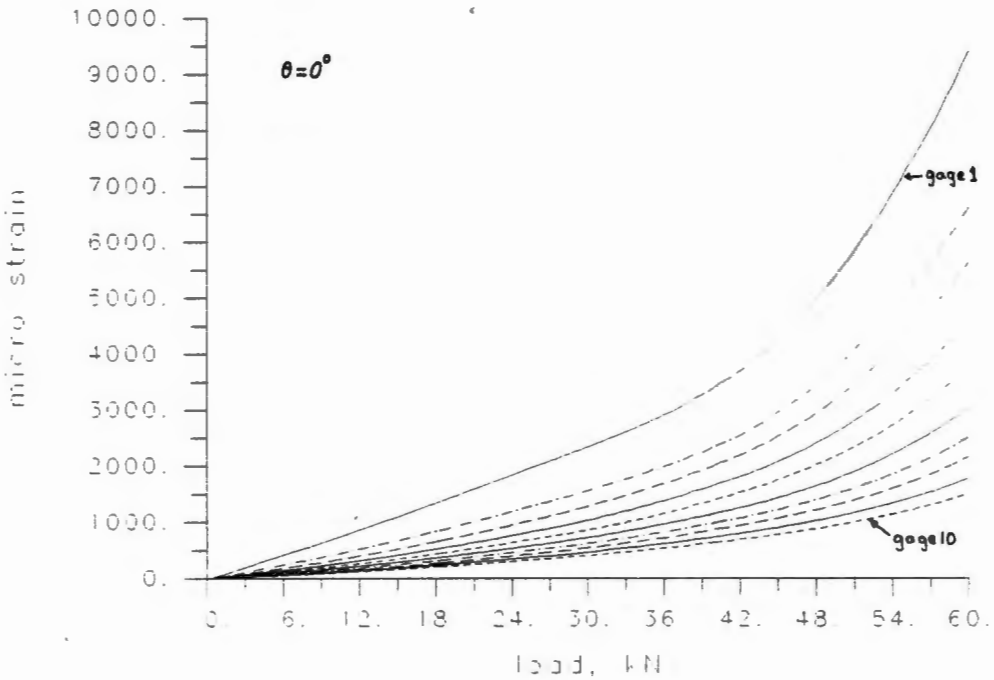

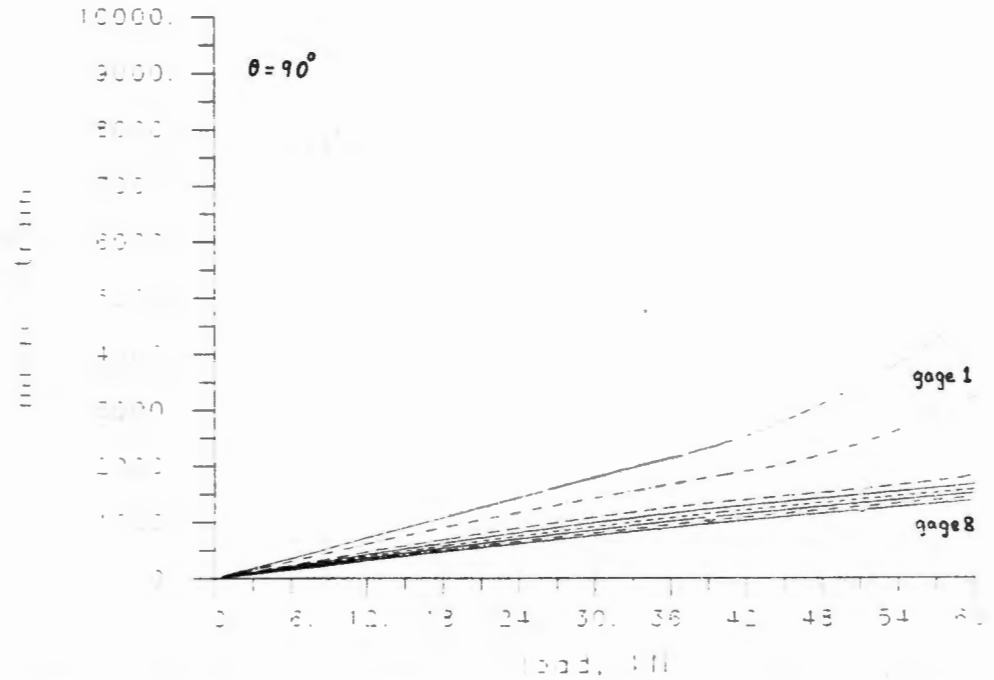

Figure 7.9 **Strain profiles obtained from gages in experiment 1.**

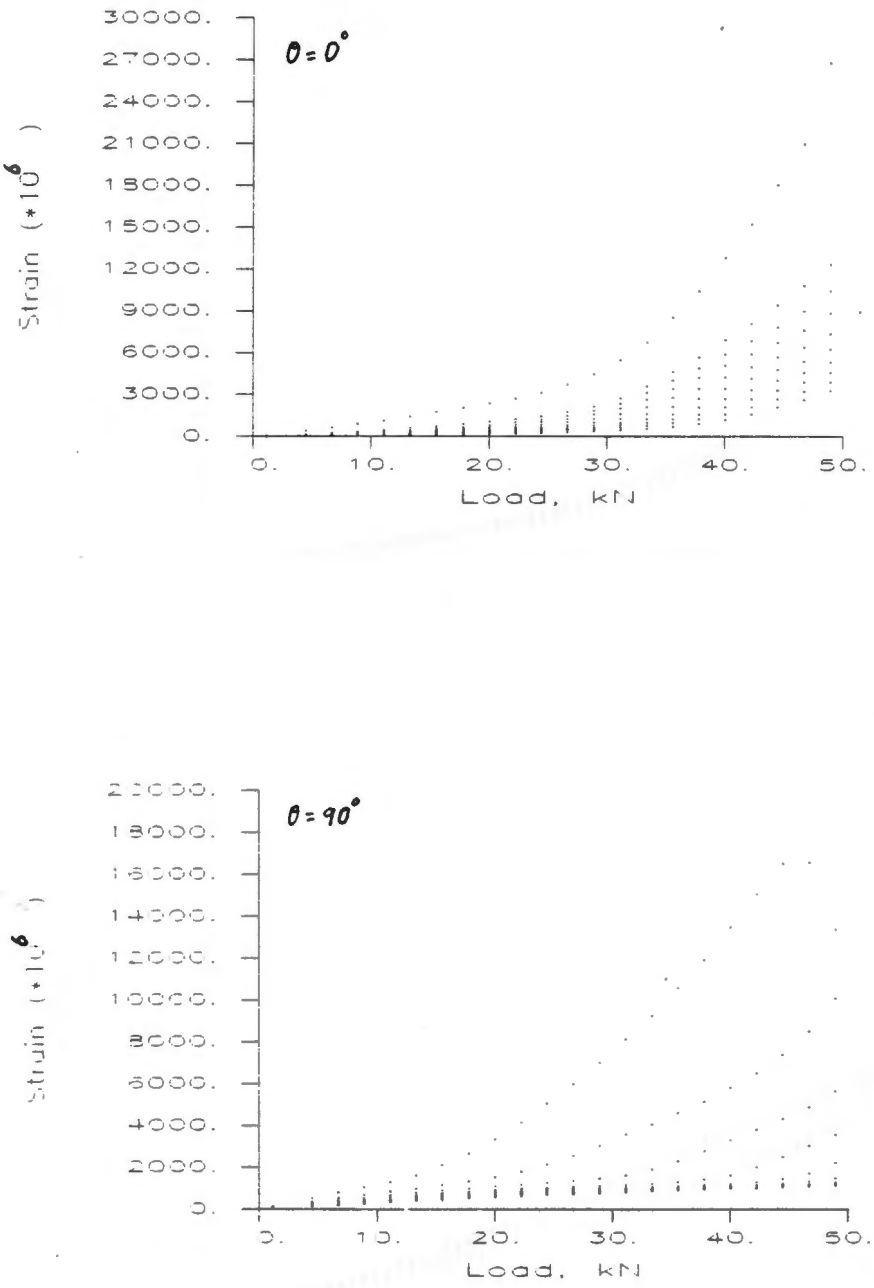

Figure 7.10 Strain profiles obtained from gages in experiment 2.

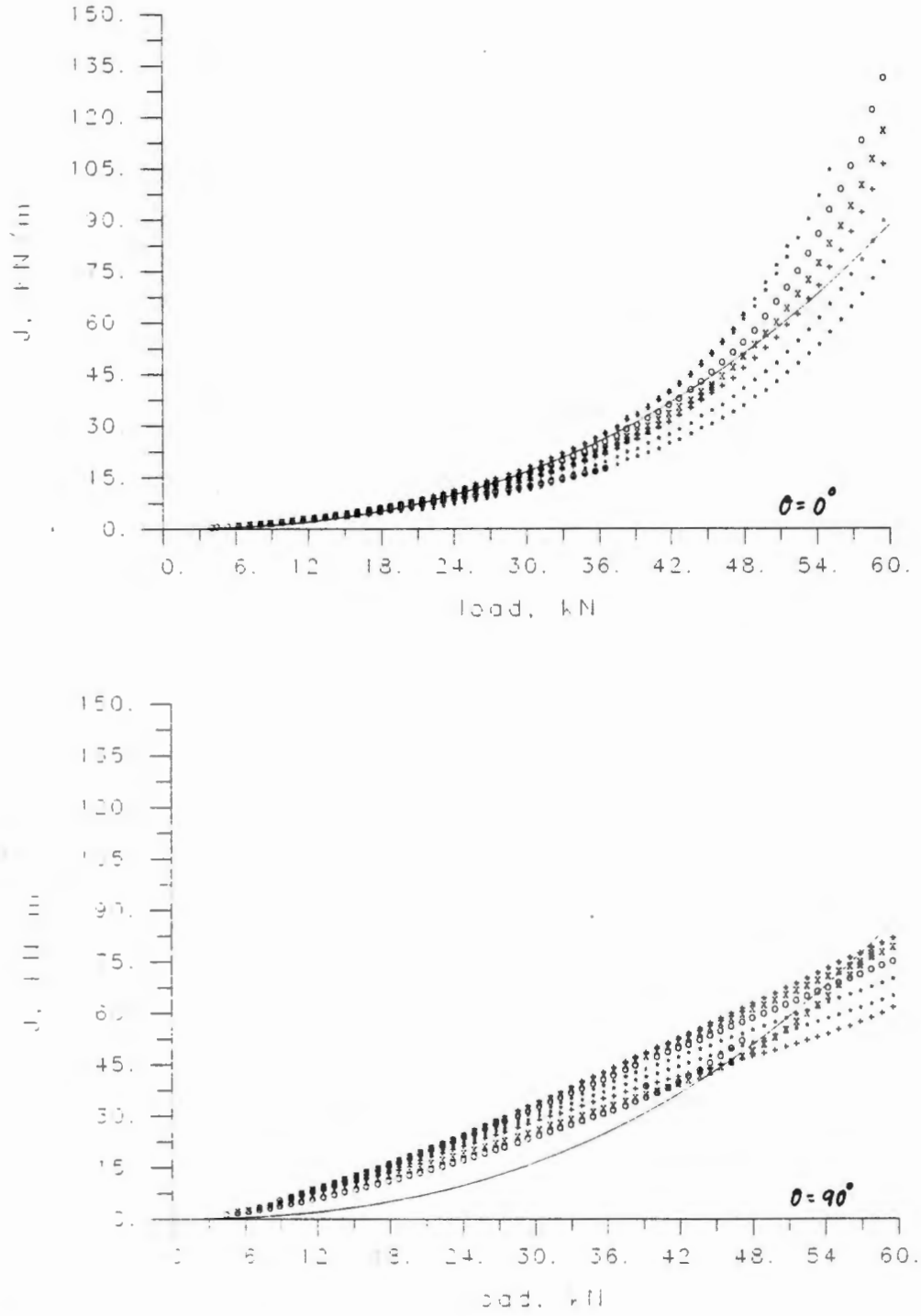

Figure 7.11 Experimental and theoretical J values obtained from the gages in experiment 1.

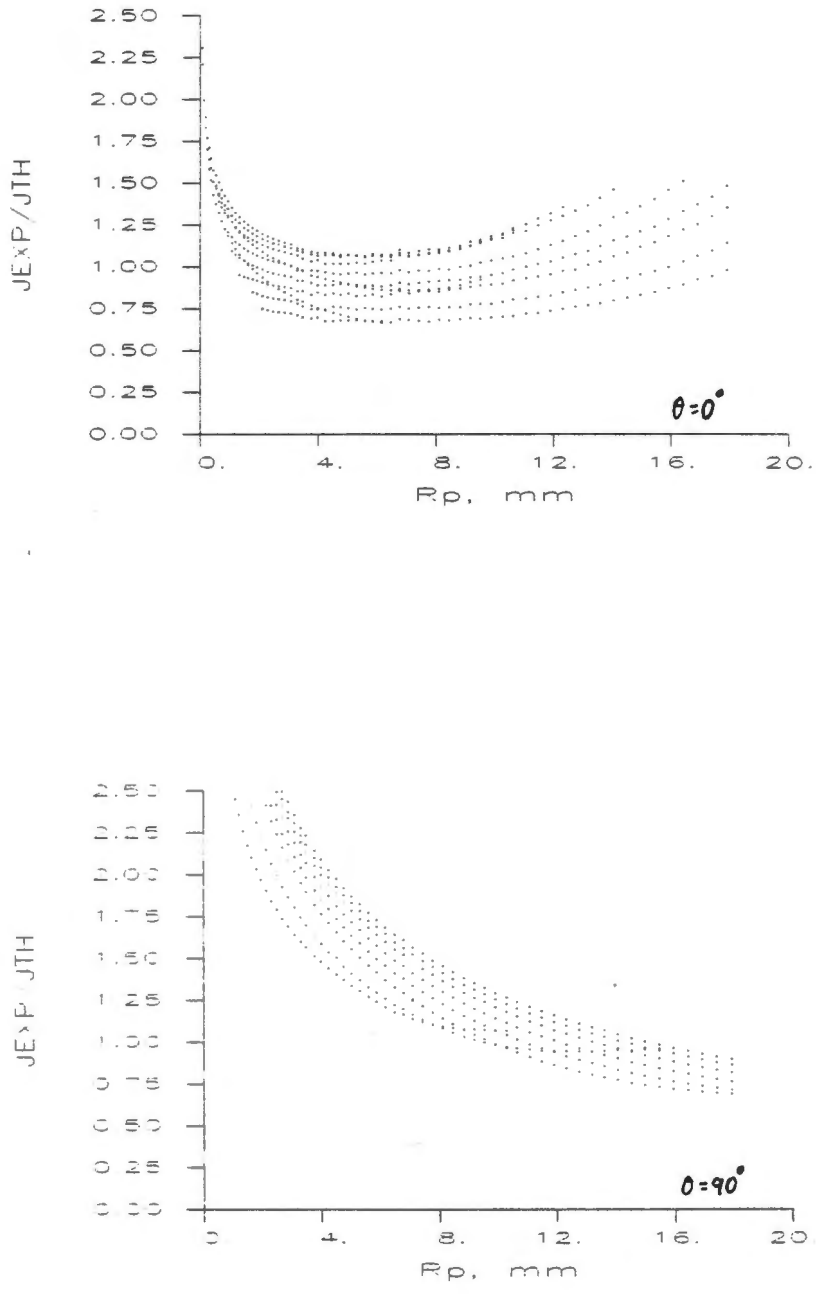

Figure 7.12 Variation of J/J_{th} with r_p for $\theta = 0°$ & $\theta = 90°$ direction.(expt. 1)

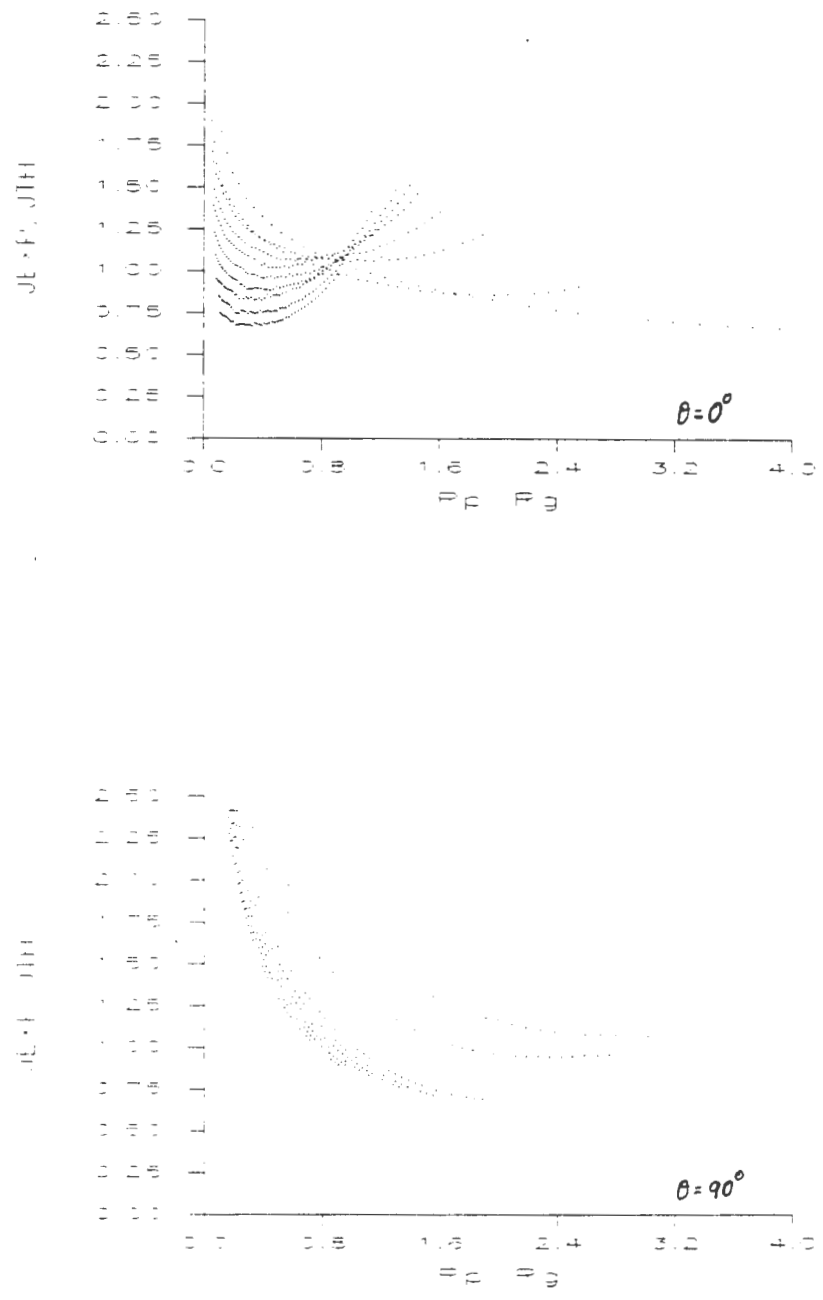

Figure 7.13 Variation of J/J_{th} with r_p/r_g for $\theta = 0°$ & $\theta = 90°$ direction.(expt. 1)

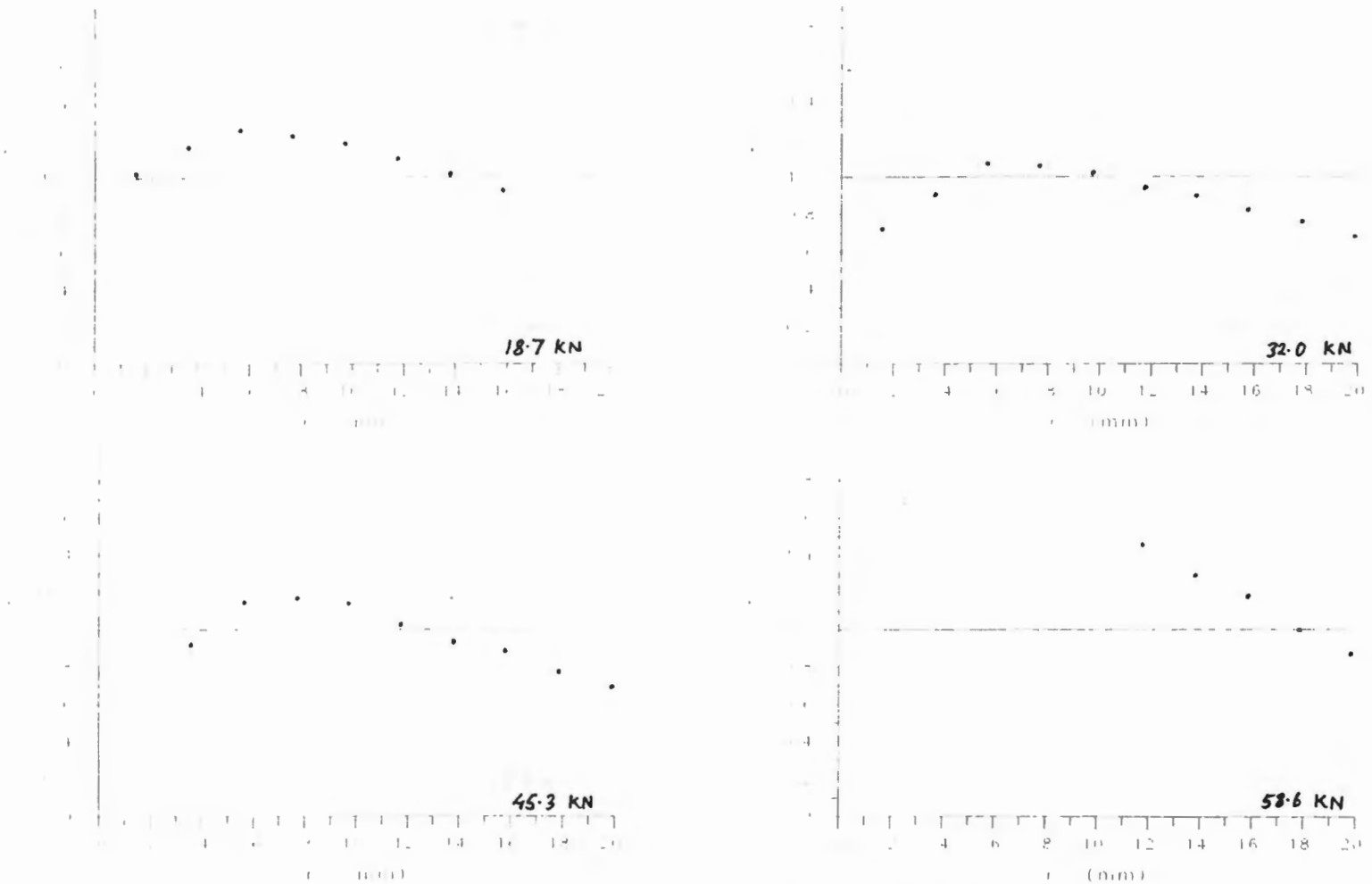

Figure 7.14a Plots of J/J_{th} variation with gage location for various load values ($\theta = 0°$, expt.1).

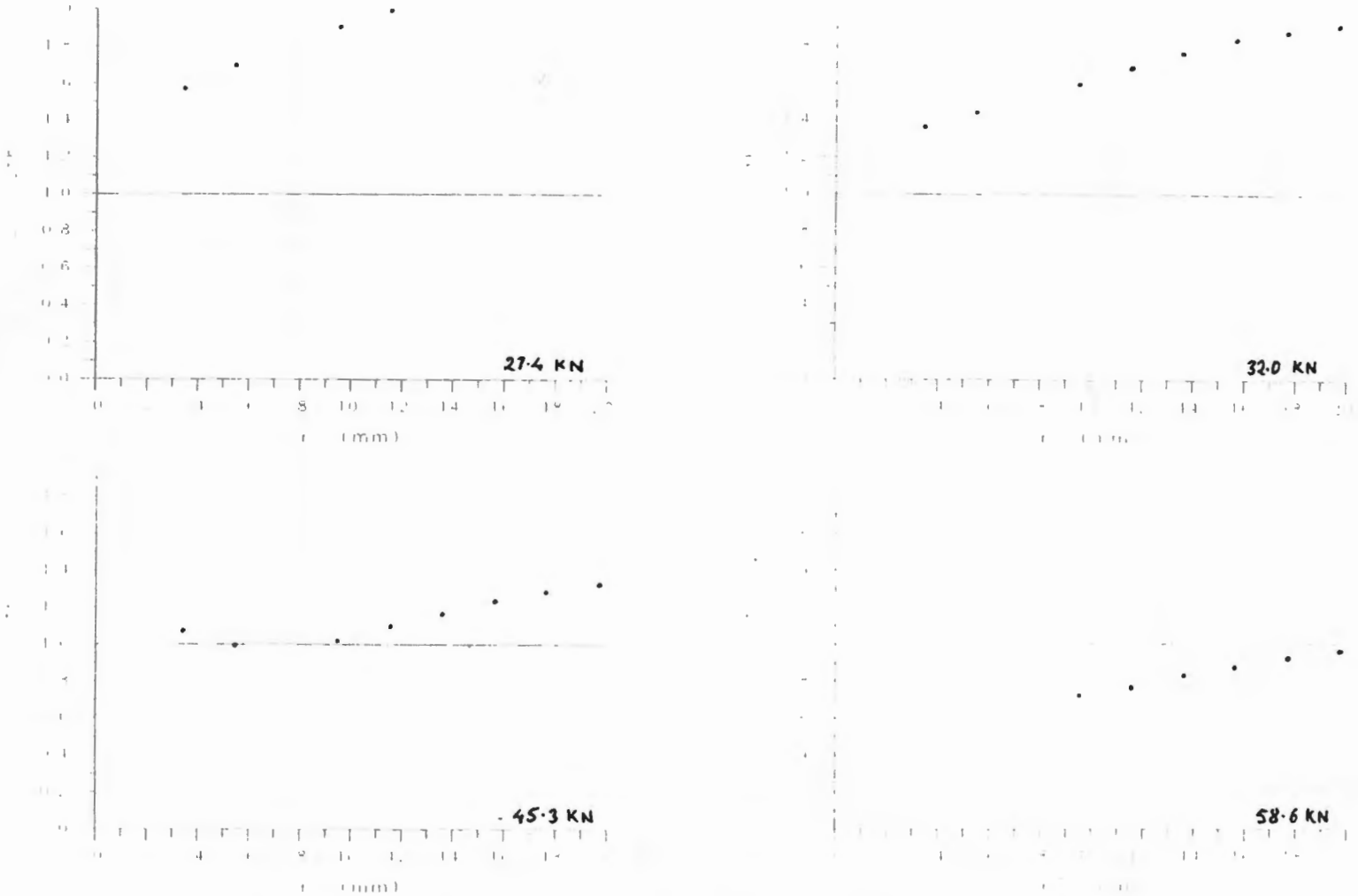

Figure 7.14b Plots of J/J_{th} variation with gage location for various load values ($\theta = 90°$, expt. 1).

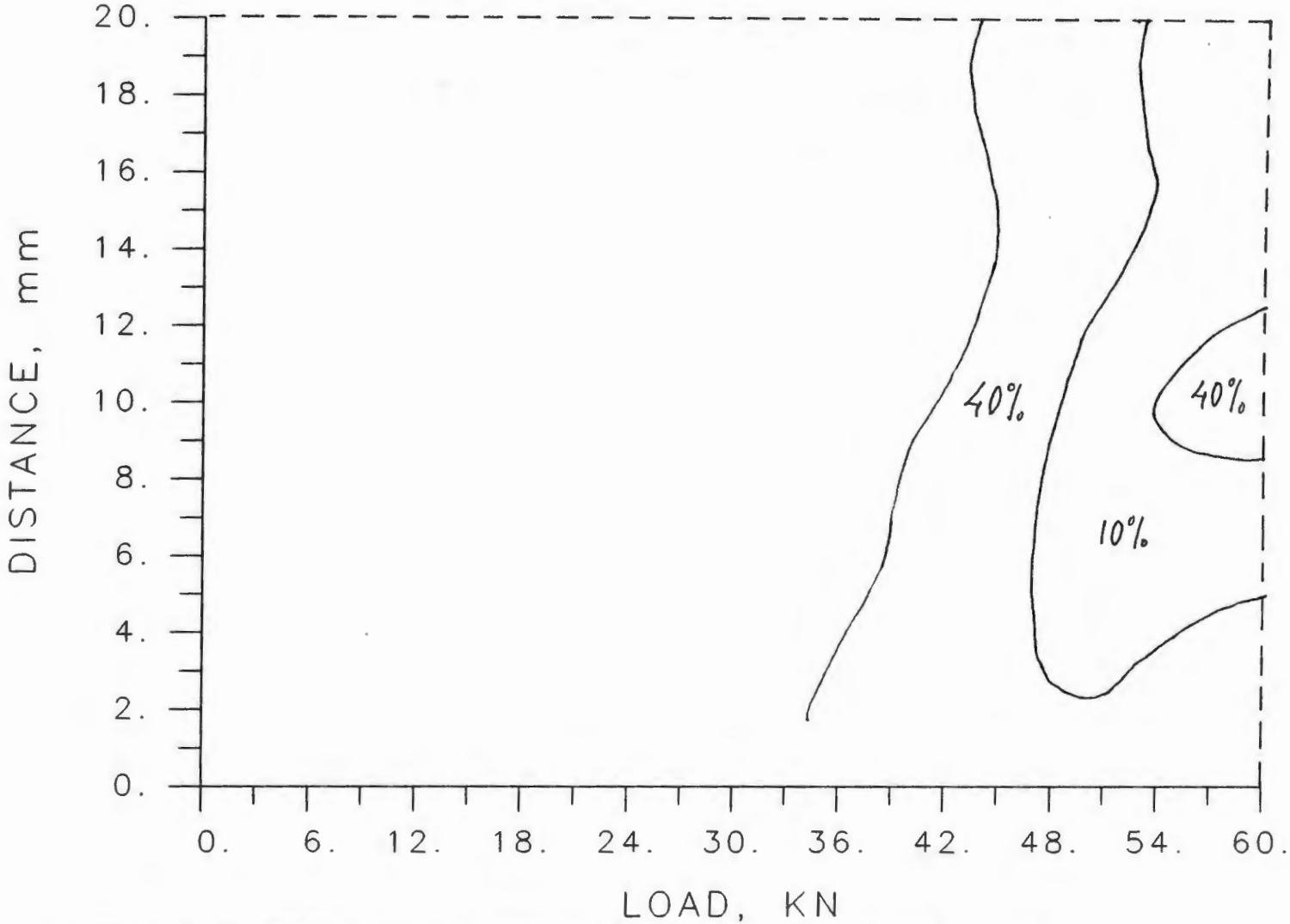

Figure 7.15a Regions where the gages can be placed to ach eve desired accuracy for a given load ($\theta = 0°$, expt.1).

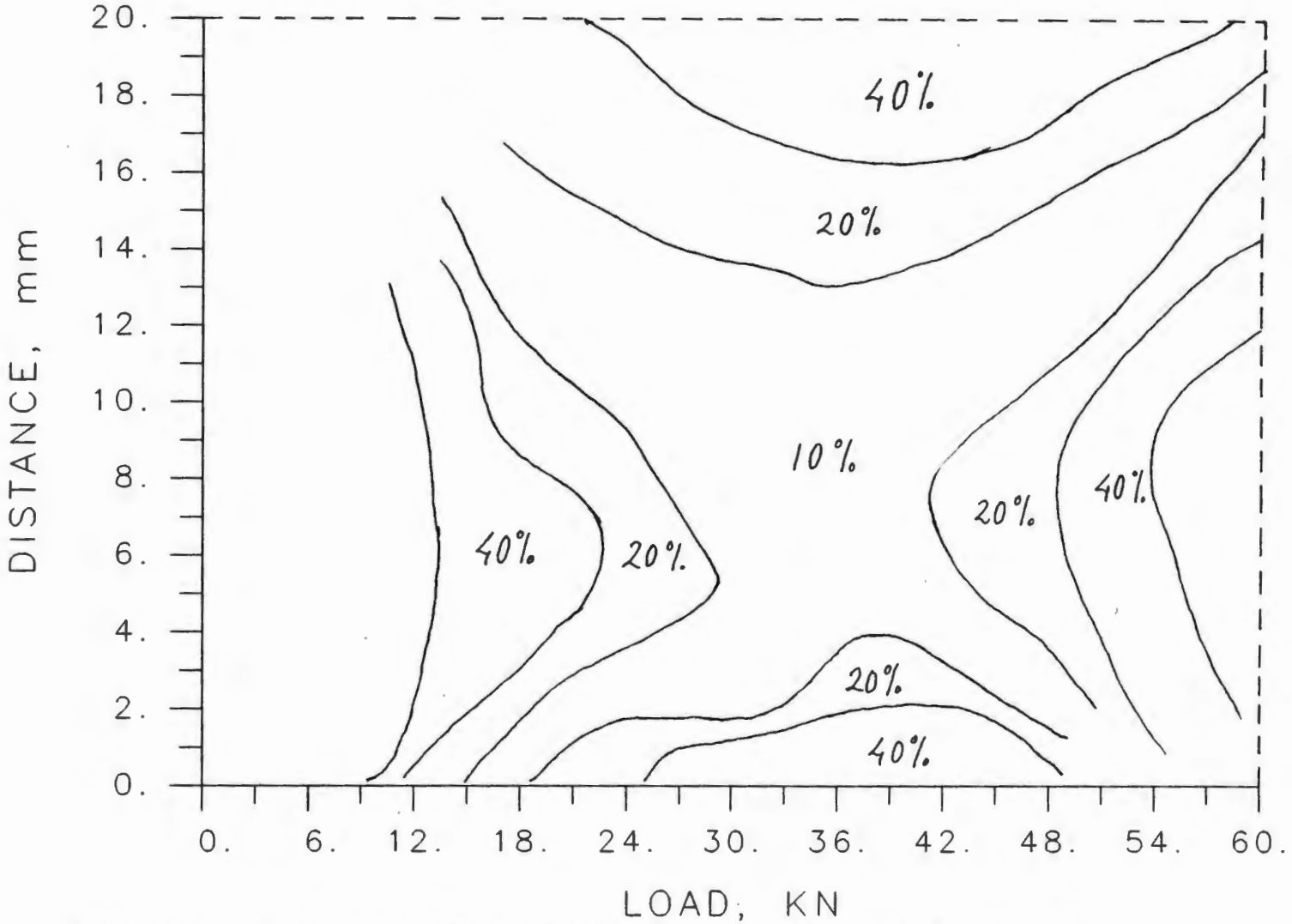

Figure 7.15b Regions where the gages can be placed to achieve desired accuracy for a given load ($\theta = 90°$, expt.1).

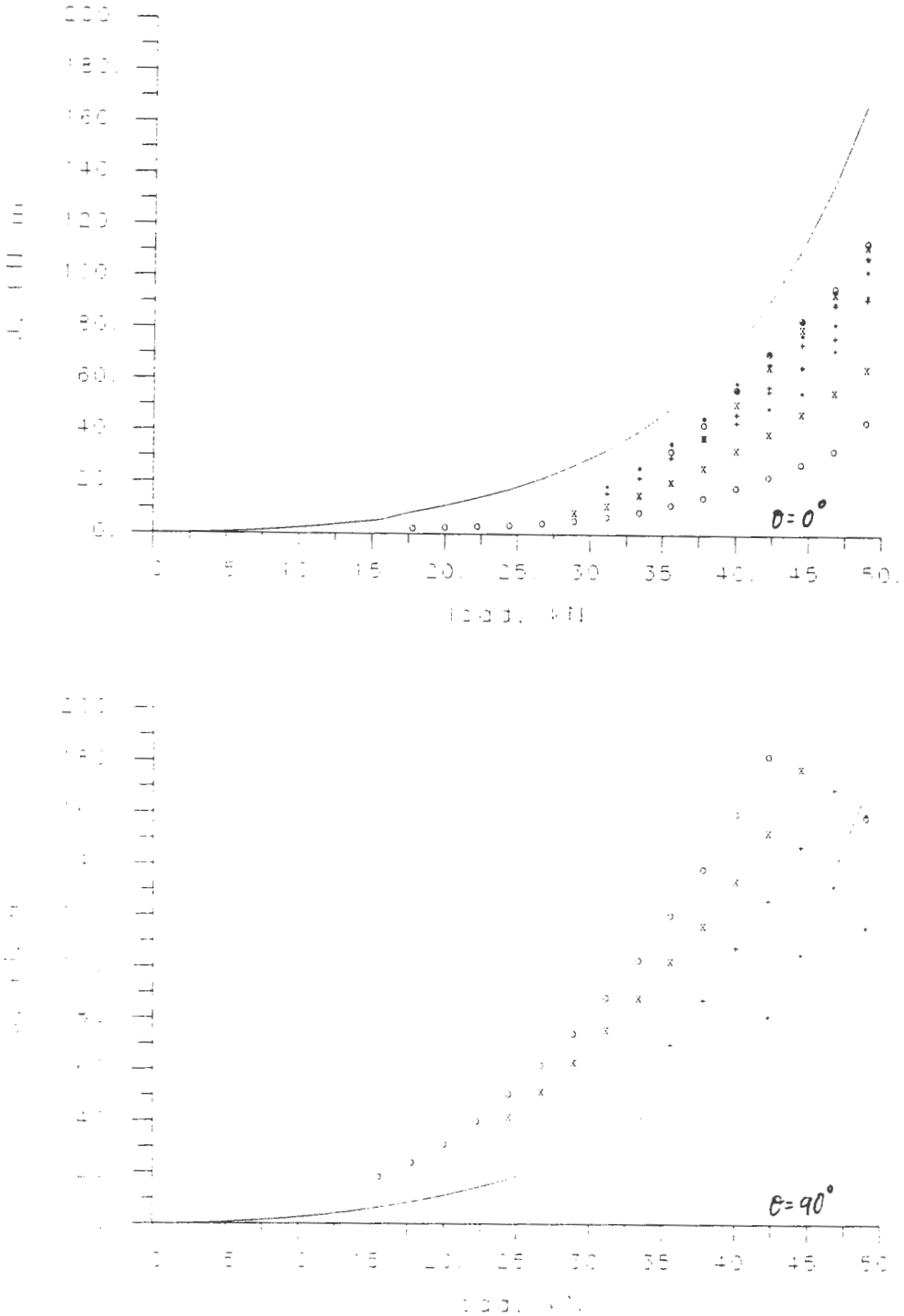

Figure 7.16 Experimental and theoretical J values obtained from the gages in experiment 2.

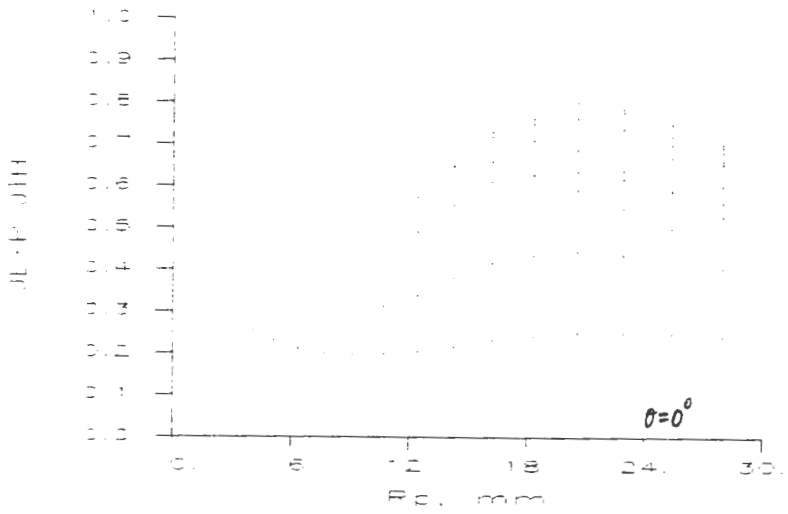

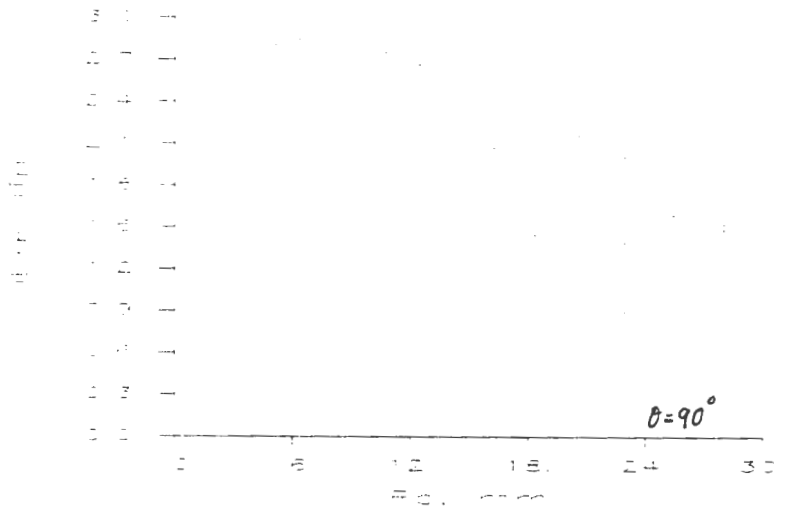

Figure 7.17 Variation of J/J_{th} with r_p for $\theta = 0^\circ$ & $\theta = 90^\circ$ direction.(expt. 2)

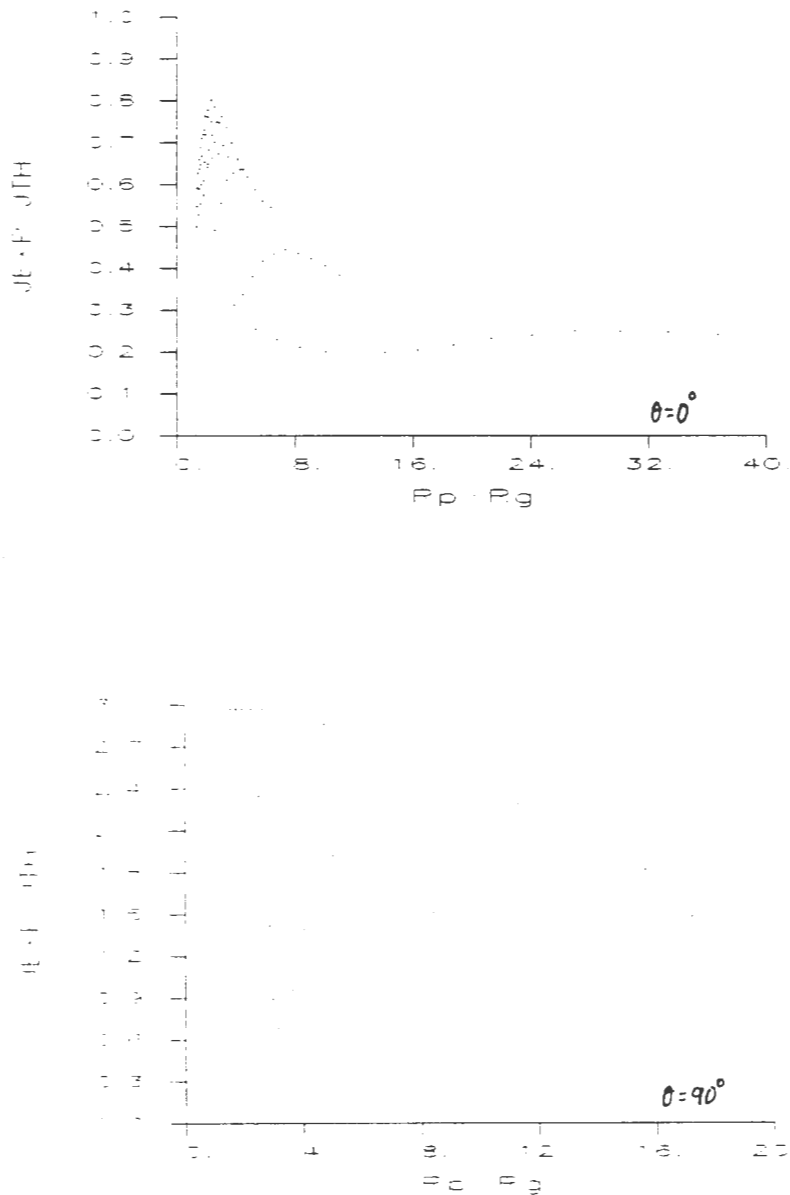

Figure 7.18 Variation of J/J_{th} with r_p/r_g for $\theta = 0°$ & $\theta = 90°$ direction.(expt. 2)

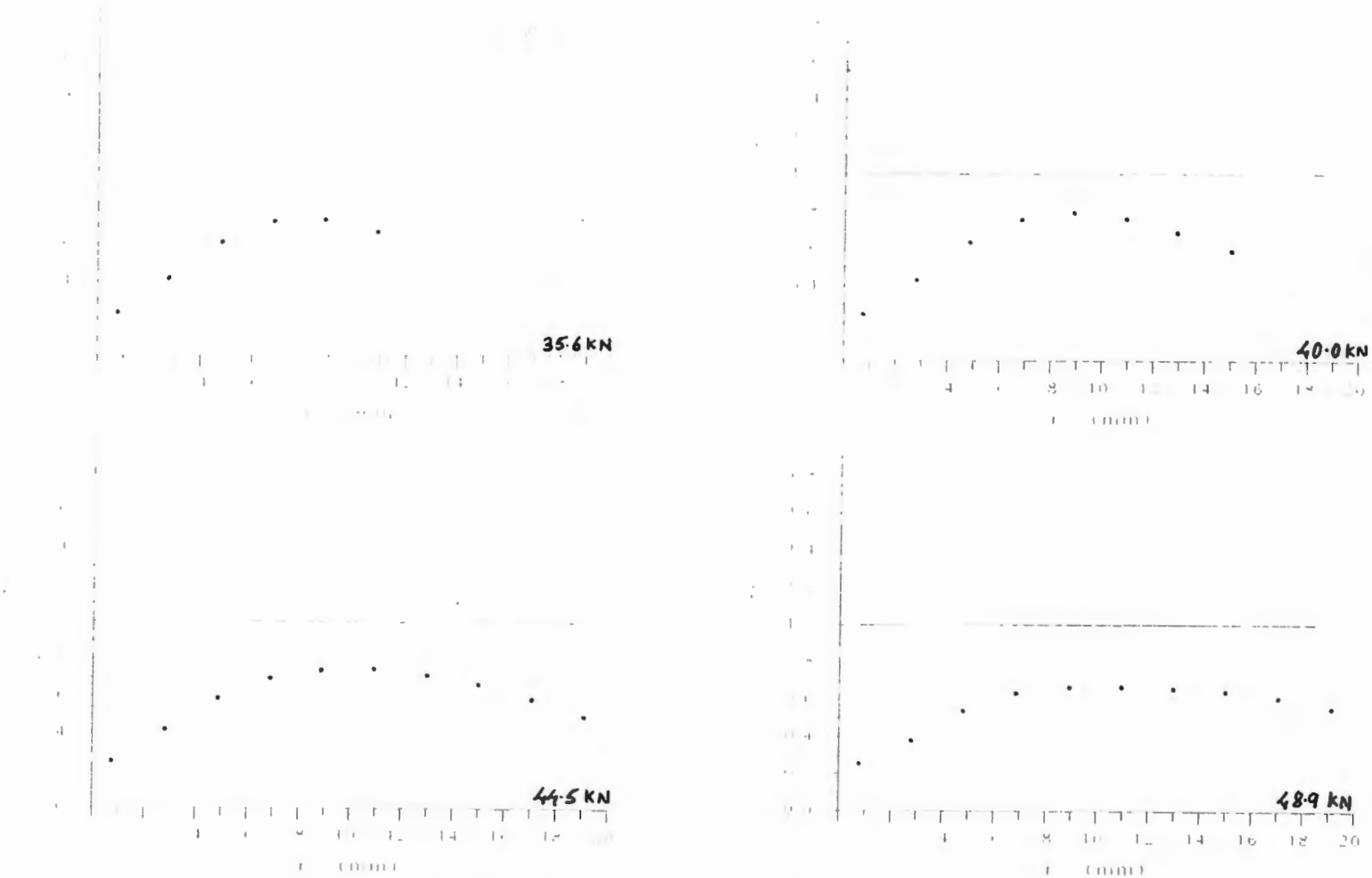

Figure 7.19a Plots of J/J_{th} variation with gage location for various load values ($\theta = 0°$, expt.2).

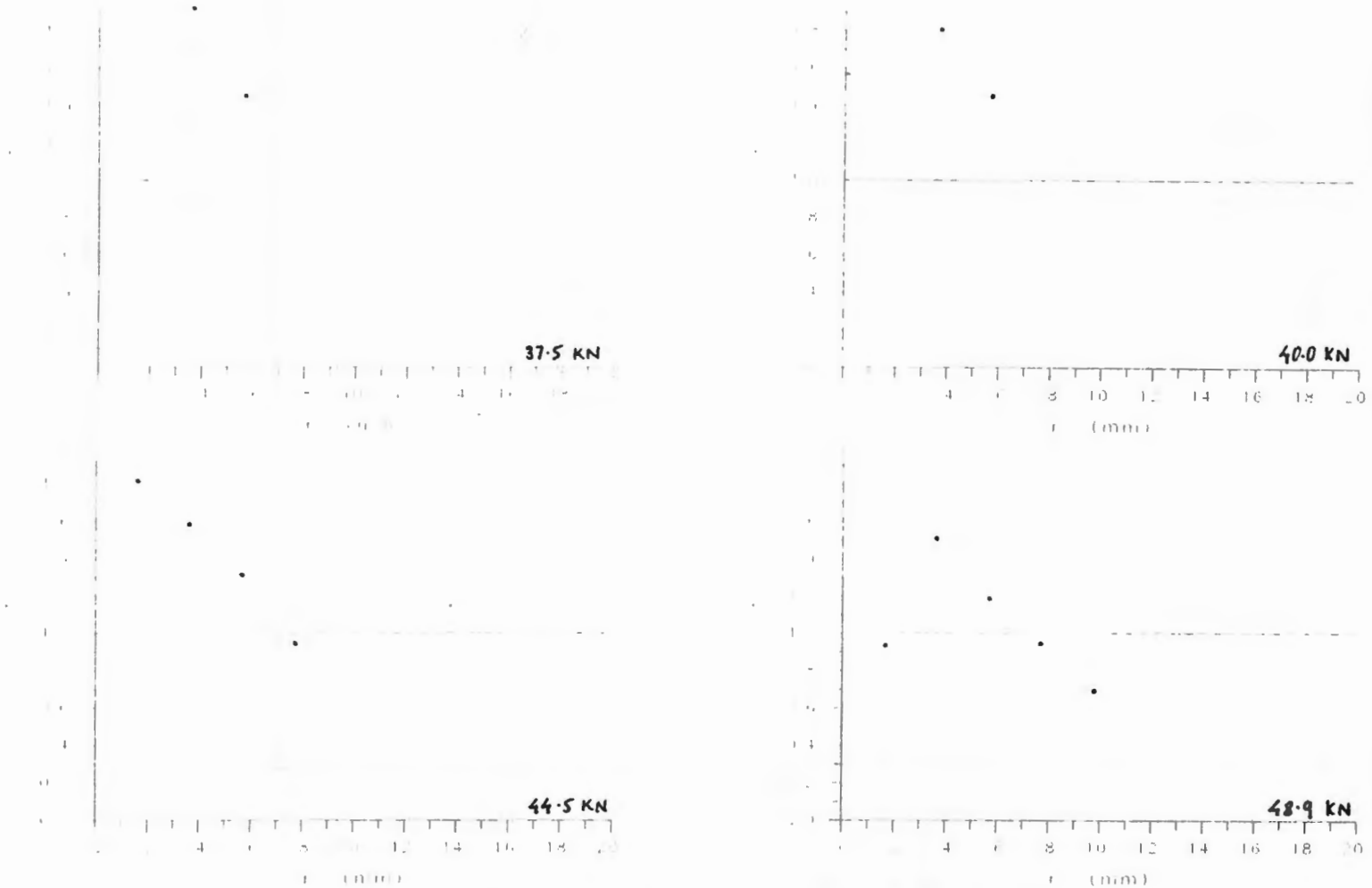

Figure 7.19b Plots of J/J_{th} variation with gage location for various load values ($\theta = 90°$, expt. 2).

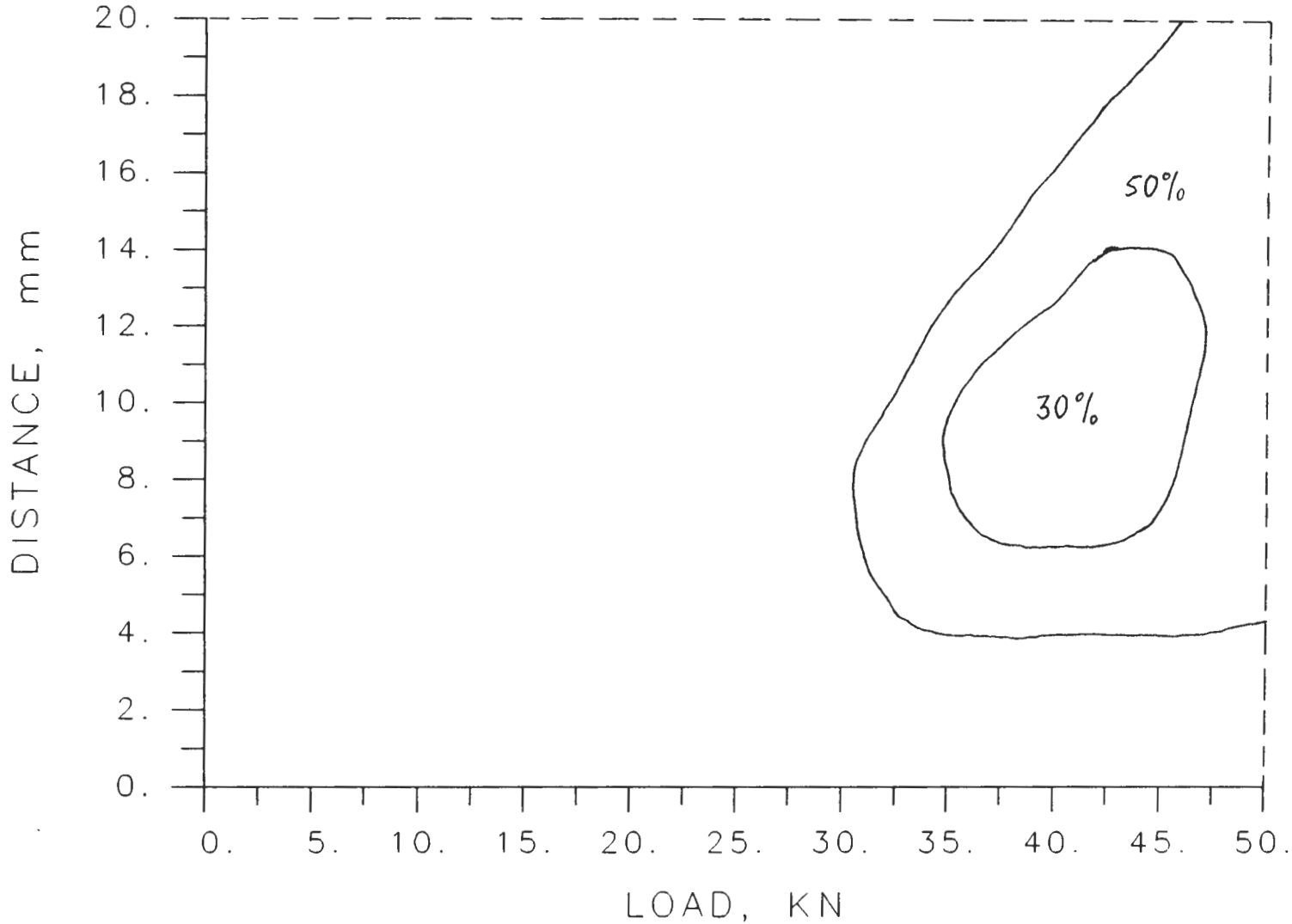

Figure 7.20a Regions where the gages can be placed to achieve desired accuracy for a given load ($\theta = 0°$, expt.2).

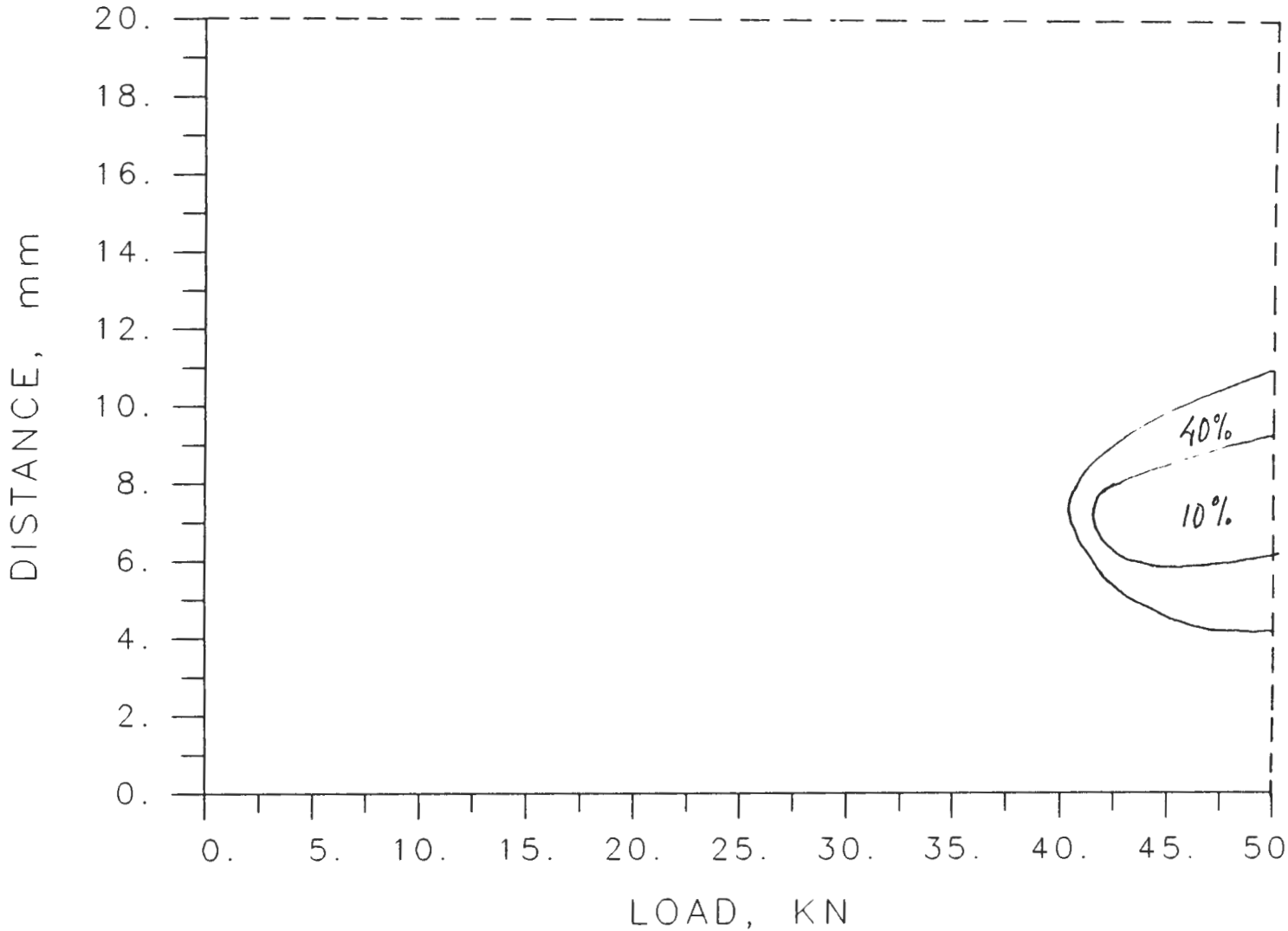

Figure 7.20b Regions where the gages can be placed to achi ve desired accuracy for a given load ($\theta = 90°$, expt.2).

CLOSURE

This dissertation presented an experimental study of the final propagation stage of a growing crack in polymers and metals. It also presented the development of a new technique to measure J integral values using strain gages in materials exhibiting elastic plastic behavior.

As a part of this work facilities were developed to perform caustic experiments on transparent and opaque materials. Also, the technique of strain gages was used for the first time for dynamic fracture studies of metals.

From the comparison of techniques work presented in chapter 4 for Homalite 100 it is found that caustic technique gives considerably lower values of the stress intensity factor as compared to the values obtained using the technique of photoelasticity. Further investigation into the effect of strain rate dependence of the material properties effecting caustics is suggested to determine the possible cause for the difference.

From the work done with the technique of photoelasticity it was found that merely increasing the number of parameters in the stress field solution does not necessarily increase the accuracy of the technique. Fringe re-plots should be used to find the best solution from this technique.

The newly developed technique of using strain gages to evaluate J integral has been studied in detail. This technique has been used to obtain an engineering estimate of the size of HRR singularity field. The regions around the crack tip which give accurate values have been outlined.

BIBLIOGRAPHY

[1] Beinert,J. and Kalthoff,J.F., "Experimental determination of dynamic stress intensity factors by shadow patterns," Mechanics of Fracture, vol. VII, G.C.Sih, ed., Noordhoff Int. Publishing, London, The Netherlands, 1981.

[2] Chao,Y.J., Lee,C., Sutton,M.A. and Peters,W.H., "Spread of Plastic Deformation in Cracked Plate," Proceedings of the 1987 SEM Spring Conference on Experimental Mechanics, Houston, Texas, June 14-19, 1987, pp. 438-445.

[3] Chona,R., Irwin,G.R. and Sanford,R.J., "Influence of Specimen Size and Shape on the Singularity-Dominated Zone," Fracture Mechanics: Fourteenth Symposium, vol. 1: Theory and Analysis, ASTM STP 791, J.C.Lewis and G.Sines eds., ASTM, 1983, pp. I-3-I-23.

[4] Dally,J.W., "Dynamic Photoelastic Studies of Fracture," Experimental Mechanics, vol. 19, No. 10, October 1979. pp. 349-361.

[5] Dally,J.W. and Berger,J.R., "A Strain Gage Method for Determining KI and KII in a Mixed Mode Stress Field," Proceedings of the 1986 SEM Spring Conference on Experimental Mechanics, New Orleans, June 8-13, 1986, pp. 603-612.

[6] Dally,J.W. and Riley,W.F., Experimental Stress Analysis, Mc Graw- Hill, (1978).

[7] Dally,J.W. and Sanford,R.J., "Strain Gage Methods for Measuring the Opening Mode Stress Intensity Factor," SEM Spring Conference Proceedings 1985, Las Vegas, pp. 851-860.

[8] Hutchinson,J.W., "Singular Behavior at the End of a Tensile Crack in a Hardening Material," J Mech. Phys. Solids, vol. 16, 1968, pp. 13-31.

[9] Hutchinson,J.W., "Plastic Stress and Strain Fields at a Crack Tip," Journal of the Mechanics and Physics of Solids, vol. 16, 1968, pp. 337-347.

[10] Irwin,G.R., "Series Representation of the Stress Field Around Constant Speed Cracks," Univ. of Maryland Lecture Notes, 1980.

[11] Irwin,G.R., Dally,J.W. and Fourney,W.L., "On the Uniqueness of the Stress Intensity Factor-Crack Velocity Relationship," International Journal of Fracture, 27, 1985, pp. 159-168.

[12] Irwin,G.R., Dally,J.W, Kobayashi,T., Fourney,W.L., Etheridge,M.J. and Rossmanith,H.P., "On he Determination of the $\dot{a}$-K Relationship for Birefringent Polymers," Experimental Mechanics, vol. 19, No. 4, April 1979, pp. 121-128.

[13] Kalthoff,J.F., "On some Current problems in Experimental Fracture Dynamics," Workshop on Dynamic Fracture, Caltech, Feb. 11-25, 1983.

[14] Kalthoff,J.F., "Stress Intensity Factor Determination by Caustics," Intl. Conf. Experimental Mechanics, Society for Exptl. Stress Analysis and Japan Society of Mech. Engrs., Honolulu, Hawaii, USA, May 23-28, 1982.

[15] Kalthoff,J.F. et al, "Experimental Analysis of Dynamic Effects in Different Crack Arrest Test Specimens," ASTM STP 711 - Crack Arrest Methodology and Applications, American Society for Testing and Materials, Philadelphia, USA, 1980, 109-127.

[16] Kamath,S.M. and Kim,K.S., "Coherent-Light-Shadow Spot of a Crack Under Mode I Loading: Theory and Experiment," Experimental Mechanics, vol. 26, No. 4, December 1986, pp.386-393.

[17] Kang,B.S.-J. and Kobayashi,A.S., "J-Resistance Curves in Aluminum SEN Specimens," Proceedings of the 1987 SEM Spring Conference on Experimental Mechanics, Houston, Texas, June 14-19, 1987, pp. 243-249.

[18] Knauss,W.G. and Ravi-Chander,K., "Some Basic Problems in Stress Wave Dominated Fracture," International Journal of Fracture, Vol. 27, 1985, pp. 127-143.

[19] Kobayashi,A.S., et al., "Dynamic Fracture Toughness," International Journal of Fracture, vol. 30, 1986, pp. 275-286.

[20] Kobayashi,T., and Dally,J.W., "Dynamic Photoelastic Determination of the $\dot{a}$-K Relation for 4340 Alloy Steel," Crack Arrest Methodology and Applications, ASTM STP 711, G.T.Hahn and M.F.Kanninen, Eds., American Society for Testing Materials, 1980, pp. 189-210.

[21] Lam,P.S., and Freund,L.B., "Analysis of Dynamic Crack Growth of a Tensile Crack in an Elastic Plastic Material," Journal of Mechanics and Physics of Solids, vol. 33, 1985, pp. 153-167.

[22] Marchand,A., Freund,L.B., Ma,C.C. and Duffy,J., "Use of the Shadow Spot Method in Evaluating J for Ductile Steels," Brown University Technical Report ONR 0597/1 MRL E-160, February, 1986.

[23] Nigam,H., "Comparison of the Optical Techniques of Caustic and Photoelasticity as applied to Fracture," M.S. Thesis, University of Rhode Island, 1985.

[24] Ravi-Chandar,K., "An Experimental Investigation into the Mechanics of Dynamic Fracture," PhD Thesis, California Institute of Technology, 1982.

[25] Ravi-Chander,K. and Knauss,W.G., "An Experimental Investigation into Dynamic Fracture: I Crack Initiation and Arrest," International Journal of Fracture, 25, 1984, 247-262.

[26] Ravi-Chander,K. and Knauss,W.G., "An Experimental Investigation into Dynamic Fracture: III On Steady-State Crack Propagation and Crack Branching," International Journal of Fracture, 26, 1984, 141-154.

[27] Ravi-Chander,K. and Knauss,W.G., "An Experimental Investigation into Dynamic Fracture: IV On the Interaction of Stress Waves with propagating Cracks," International Journal of Fracture, 26, 1984, 189-200.

[28] Ravi-Chander,K. and Knauss,W.G., "Process Controlling the Dynamic Frac-

ture of Brittle Solids," Workshop on Dynamic Fracture, Calif. Inst. of Tech., February 1983, pp. 119-128.

[29] Rice,J.R., "A Path Independent Integral and the Approximate Analysis of Strain Concentration by Notches and Cracks," Journal of Applied Mechanics, vol. 35, 1968, pp. 379-386.

[30] Rice,J.R., "Mathematical Analysis in the Mechanics of Fracture," in Fracture: An Advanced Treatise (ed. H. Liebowitz), vol. 2, Academic Press, 1968, pp. 191-311.

[31] Rice,J.R. and Rosengren,G.F., "Plane Strain Deformation Near a Crack Tip in a Power Law Hardening Material," J of the Mech. and Phy. of Solids, vol. 16, 1968, pp. 1-12.

[32] Rosakis,A.J., "Experimental Determination of the Fracture Initiation and Dynamic Crack Propagation Resistance of Structural Steels by the Optical Method of Caustics," PhD Thesis, Brown University, June 1982.

[33] Rosakis,A.J., "Analysis of the Optical Method of Caustics for Dynamic Crack Propagation," Report ONR-79-1 Division of Engineering Brown Univ., Mar.1979, Engineering Fracture Mechanics, vol.13, 1980, pp. 331-347.

[34] Rosakis,A.J. and Freund,L.B., "Optical Measurement of the Plastic Strain Concentration at a Crack Tip in a Ductile Steel Plate," Journal of Engineering Materials and Technology, vol. 104, April 1982, pp. 115-120.

[35] Rosakis,A.J. and Freund,L.B., "The Effect of Crack Tip Plasticity on the Determination of Dynamic Stress Intensity Factors by the Optical Method of Caustics," Trans. ASME, J Appl. Mech., vol. 48, June 1981, pp. 302-308.

[36] Rosakis,A.J., Ma,C.C. and Freund,L.B., "Analysis of the Optical Shadow Spot Method for a Tensile Crack in a Power-Law Hardening Material," Journal of Applied Mechanics, vol. 105, December 1983, pp. 777-782.

[37] Rosakis,A.J. and Ravi Chander,K., "On Crack Tip Stress State: An Experimental Evaluation of Three Dimensional Effects," Caltech Report, SM84-2, March 1984.

[38] Rosakis,A.J., and Zehnder,A.T., "On the Method of Caustics: An Exact Analysis Based on Geometrical Optics," Journal of Elasticity, vol. 15, 1985, pp. 347-367.

[39] Sanford,R.J. and Dally,J.W., "A General Method for Determining Mixed-mode Stress Intensity Factor from Isochromatic Fringe Patterns, Journal of Engineering Fracture Mechanics, 11, 1979, pp. 621-633.

[40] Shukla,A., Agarwal,R.K., and Nigam,H., "Dynamic Fracture studies on 7075-T6 Aluminum and 4340 Steel Using Strain Gages And Photoelastic Coatings," To appear in Journal of Engineering Fracture Mrchanics.

[41] Shukla,A., Chona,R., and Agarwal,R.K., "Investigation of Dynamic Fracture Using Strain Gages," Society for Experimental Mechanics, Fall meeting, Houston 1987.

[42] Shih,C.F., "Tables of Hutchinson-Rice-Rosengren Singular Field Quantities," Brown University Report MRL E-147, Materials Research Laboratory, Brown University, June 1983.

[43] Theocaris,P.S., "Elastic Stress Intensity Factors Evaluated by Caustics," Mechanics of Fracture, vol. VII, G.C.Sih, ed., Noordhoff Int. Publishing, London, The Netherlands, 1981.

[44] Zehnder,A.T., "Dynamic Fracture Initiation and Propagation in Metals: Experimental Results and Techniques," Ph.D. Thesis, California Institute of Technology, 1987.